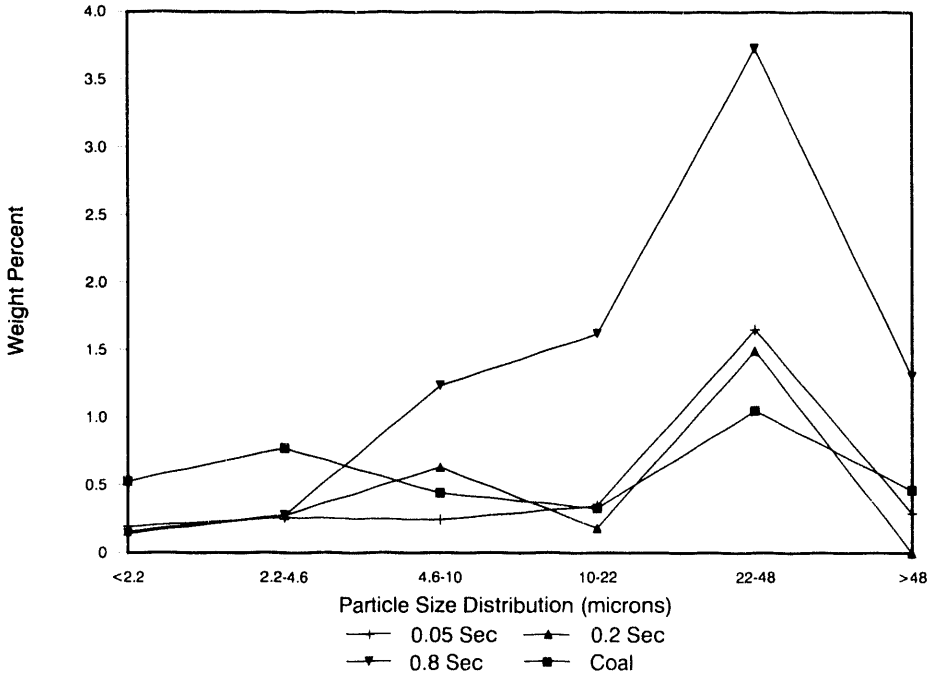

Figure 55. Distribution of Fe-aluminosilicate in Upper Freeport coal and char during combustion.

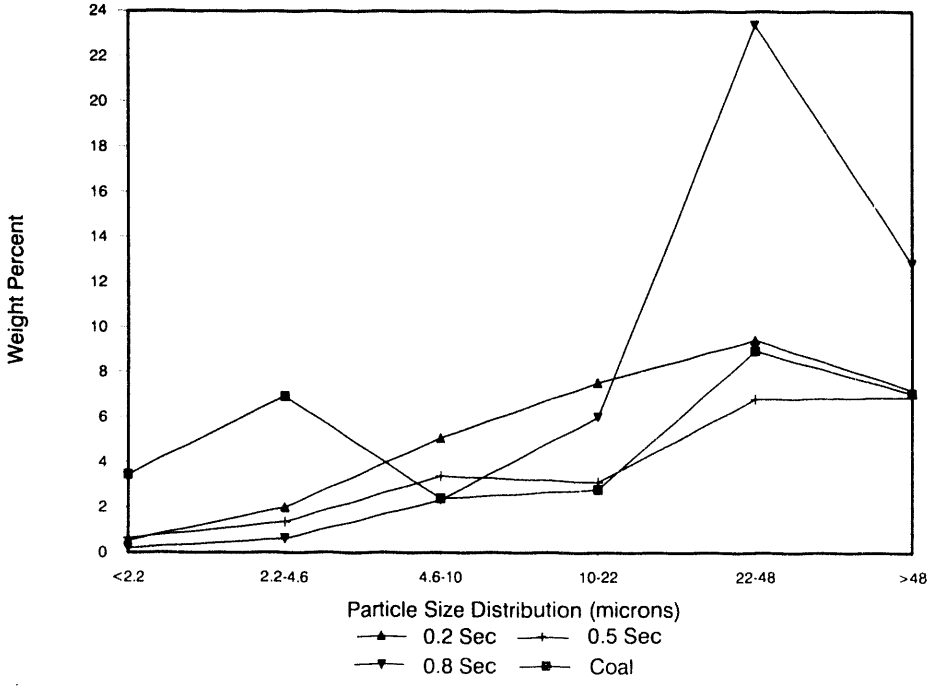

Figure 56. Distribution of illite or K-aluminosilicate in Upper Freeport coal and char during combustion.

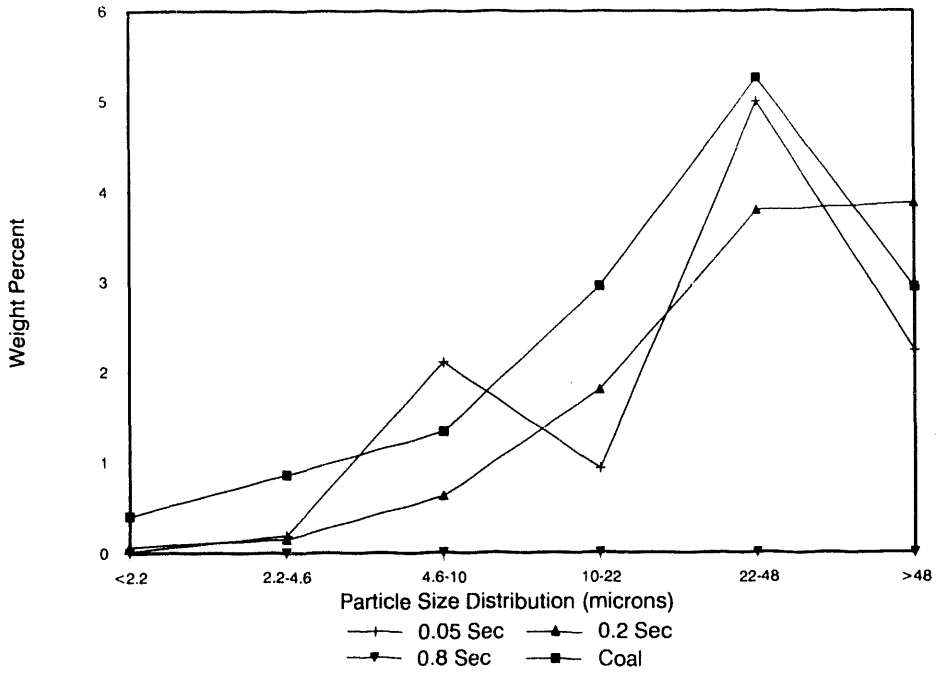

Figure 57. Distribution of pyrite in Upper Freeport coal and char during combustion.

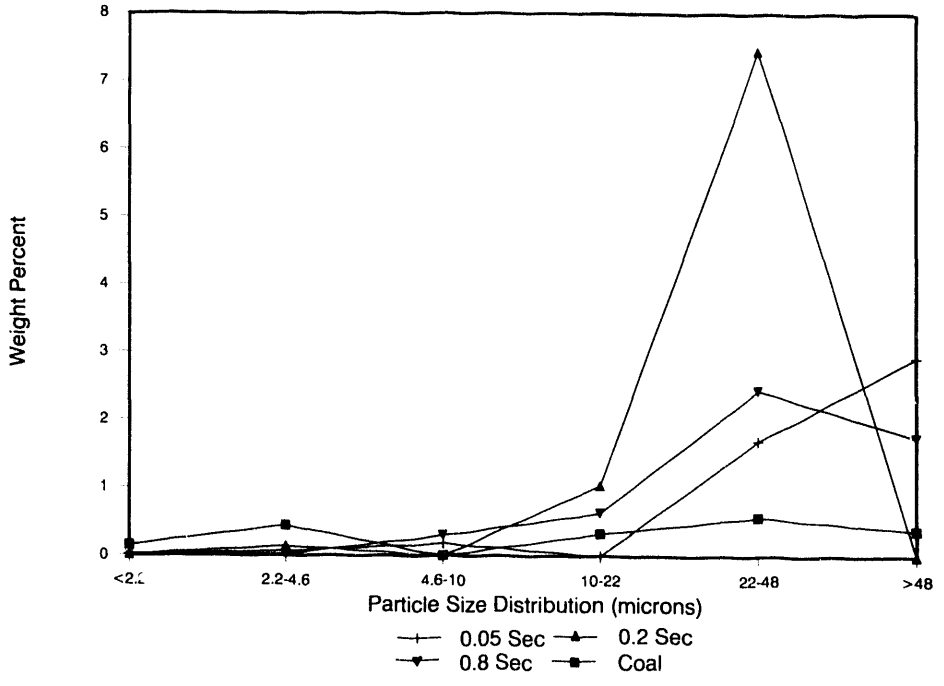

Figure 58. Distribution of iron oxide Upper Freeport coal and char during combustion.

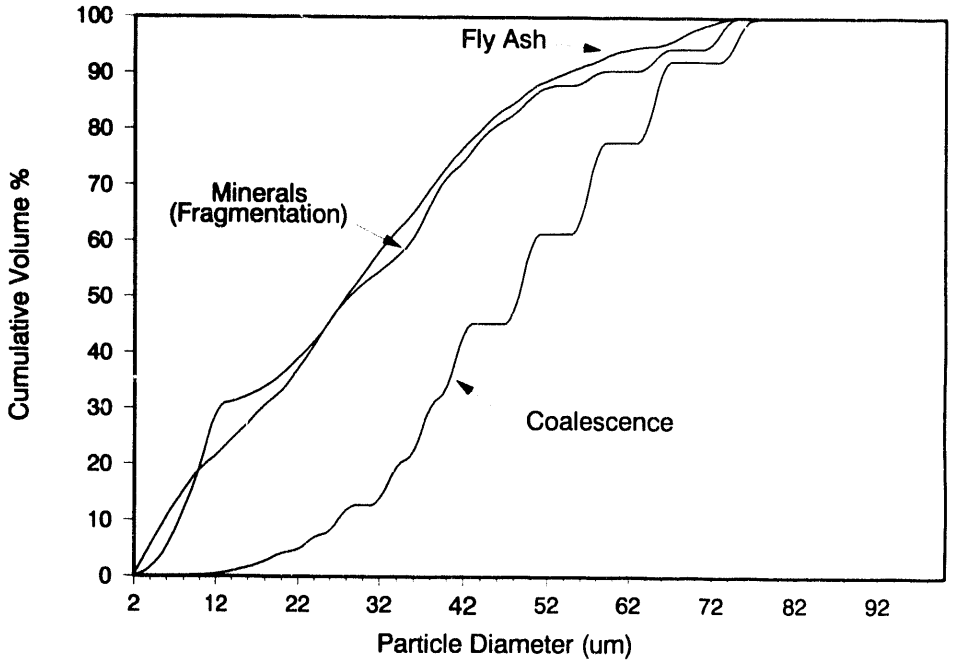

Figure 59. Kentucky #9 particle-size distributions.

be distributed homogeneously throughout the coal. The mineral and coalescence distribution curves should act as the two limiting ends of the actual particle-size distribution after combustion, if coal fragmentation and coalescence are the dominating combustion processes. In Figure 59, the fly ash distribution lies outside this zone. This could be explained by the fact that both the fly ash and mineral PSD's are measured with the CCSEM routine which analyses a cross section of a sample. The minerals have a random orientation and shape, and thus a true average is achieved. The fly ash is generally spherical in nature, and thus the average measured diameter is actually smaller by a factor of $\pi/4$ than the true average diameter. Figure 60 shows the corrected fly ash PSD also falling between the two limiting distributions. The fly ash curve approaches the fragmentation regime even more so than the uncorrected curve and exceeds it slightly. The fragmentation of a few of the larger minerals may explain the area where the fly ash distribution exceeds the coal fragmentation limit.

Figures 61 and 62 show the uncorrected and corrected San Miguel PSD's, respectively. From Figure 62, the fly ash PSD of San Miguel (at 1500°C) lies between the two limits, corresponding more toward the fragmentation regime. This implies that partial fragmentation followed by coalescence takes place.

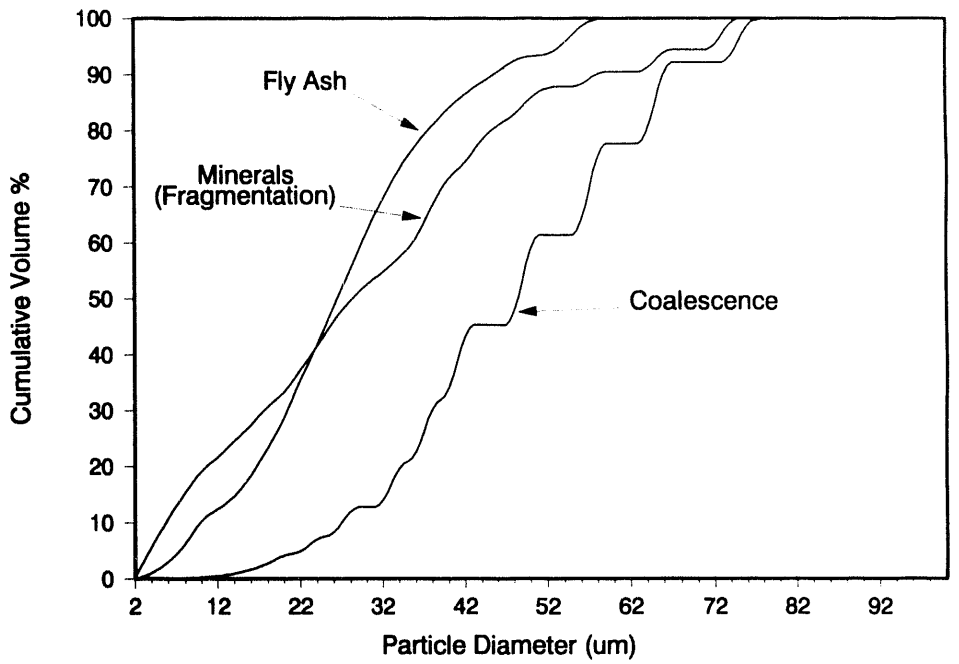

Figure 60. Kentucky #9 particle-size distributions, corrected.

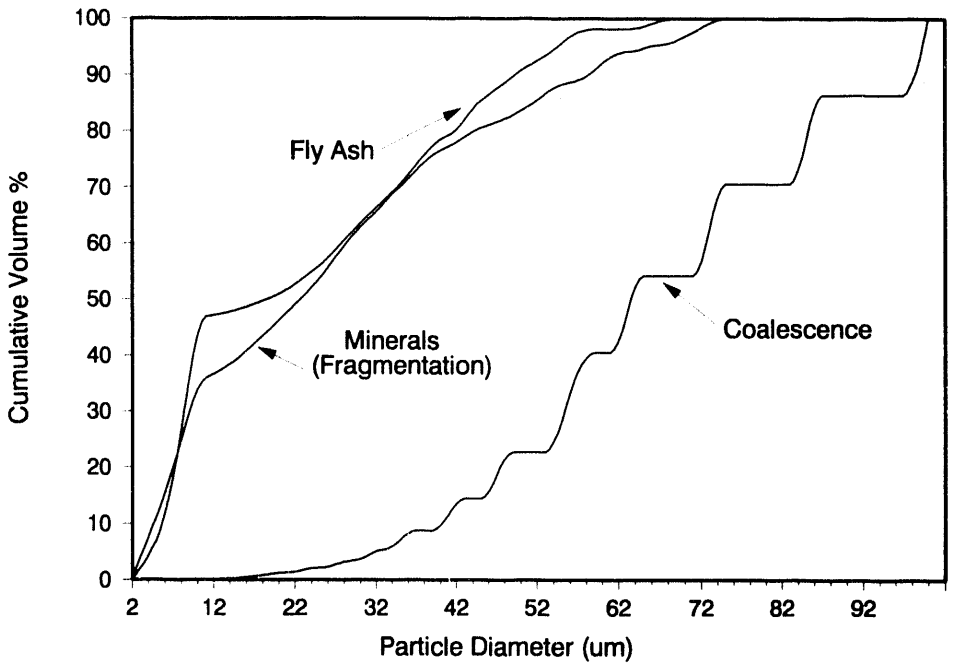

Figure 61. San Miguel particle-size distributions.

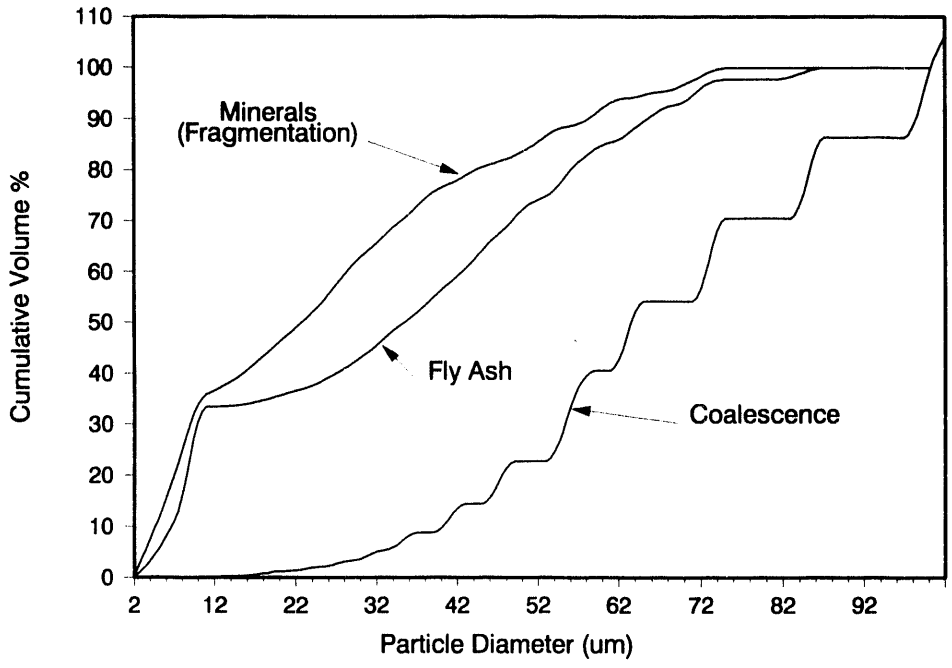

Figure 62. San Miguel particle-size distributions, corrected.

3.14.1 Conclusions

The combustion of Kentucky #9 is highly dominated by the fragmentation process, with overall coalescence and some fragmentation of a few of the larger mineral particles. The combustion of San Miguel may also demonstrate partial fragmentation followed by coalescence.

4.0 TASK 3: LABORATORY-SCALE COMBUSTION TESTING

4.1 Introduction

Coals contain a complex suite of inorganic species that include significant quantities of both organically associated cations and discrete minerals. Problems associated with inorganic constituents in coal combustion systems include ash deposition, fine particulate formation, and corrosion and erosion of boiler parts. Of specific interest are the interactions between those inorganic constituents that result in the formation of low melting point phases during combustion and gas cooling. These phases are often the cause of ash deposition problems on boiler heat transfer surfaces. The formation of these low melting point phases is a result of a combination of complex physical and chemical transformations of inorganic components of coals during combustion studied in a drop-tube furnace designed to simulate the time-temperature profile of a pulverized coal-fired utility boiler. The chemical and physical transformations of the inorganic constituents depend upon their

association in the coal and upon combustion conditions. Volatilization and condensation of sodium is one of the key transformations that the drop-tube furnace project is investigating to gain insight into the formation of liquid phases in and on the surfaces of entrained ash particles. The primary objectives of the drop-tube furnace task are to determine the factors that affect the size and composition of the fly ash.

4.2 Equipment and Procedures

4.2.1 Drop-Tube Furnace System

The drop-tube furnace is a laboratory-scale, entrained flow, tube furnace with the ability to combust coal and produce ash under closely controlled conditions. Combustion parameters such as initial hot zone temperature, residence time, and gas cooling rate can be closely controlled and monitored.

The furnace system is housed in a three-floor laboratory specifically designed for clean and efficient operation of the system, as shown in Figure 63. The furnaces are mounted on furnace bars extending through all three levels and can be moved to accommodate specific applications. The adjoining control room provides a clean, climate-controlled environment for the electronic equipment associated with the drop-tube system.

The furnace assembly consists of a series of vertically oriented tube furnaces illustrated in Figure 64. These furnaces possess a total of four independently controlled, electrically heated zones. Each of these furnaces can be used separately or in conjunction with the other furnaces. This allows for maximum flexibility and precise control over combustion conditions.

Coal, primary air, and secondary air are introduced into the furnace system by means of a preheat injector. This system injects ambient temperature primary air and coal into the furnace from a water-cooled probe assembly at the center of the tube. Secondary air is typically heated to 1000°C and introduced into the furnace through a mullite flow straightener. Thus the material to be combusted is introduced into the top of the furnace, along with preheated secondary air, and travels down the length of the furnace in a laminar flow regime.

The coal feed system is designed to feed particles of various sizes in the pulverized coal range at rates of 0.05 to 0.5 grams per minute and at primary carrier gas rates of approximately one liter per minute. The basic apparatus shown in Figure 65 consists of a pressurized cylinder in which a container filled with coal is placed. A rotating brush and stirrer attached to a variable speed motor feeds the coal from the container into a funnel where it is transported through the feed tubing into the furnace injector by the carrier gas.

Fly ash is cooled by means of a fly ash quenching probe shown in Figure 66. This system is reliable and versatile. Several collection devices can be added to the probe to collect the fly ash.

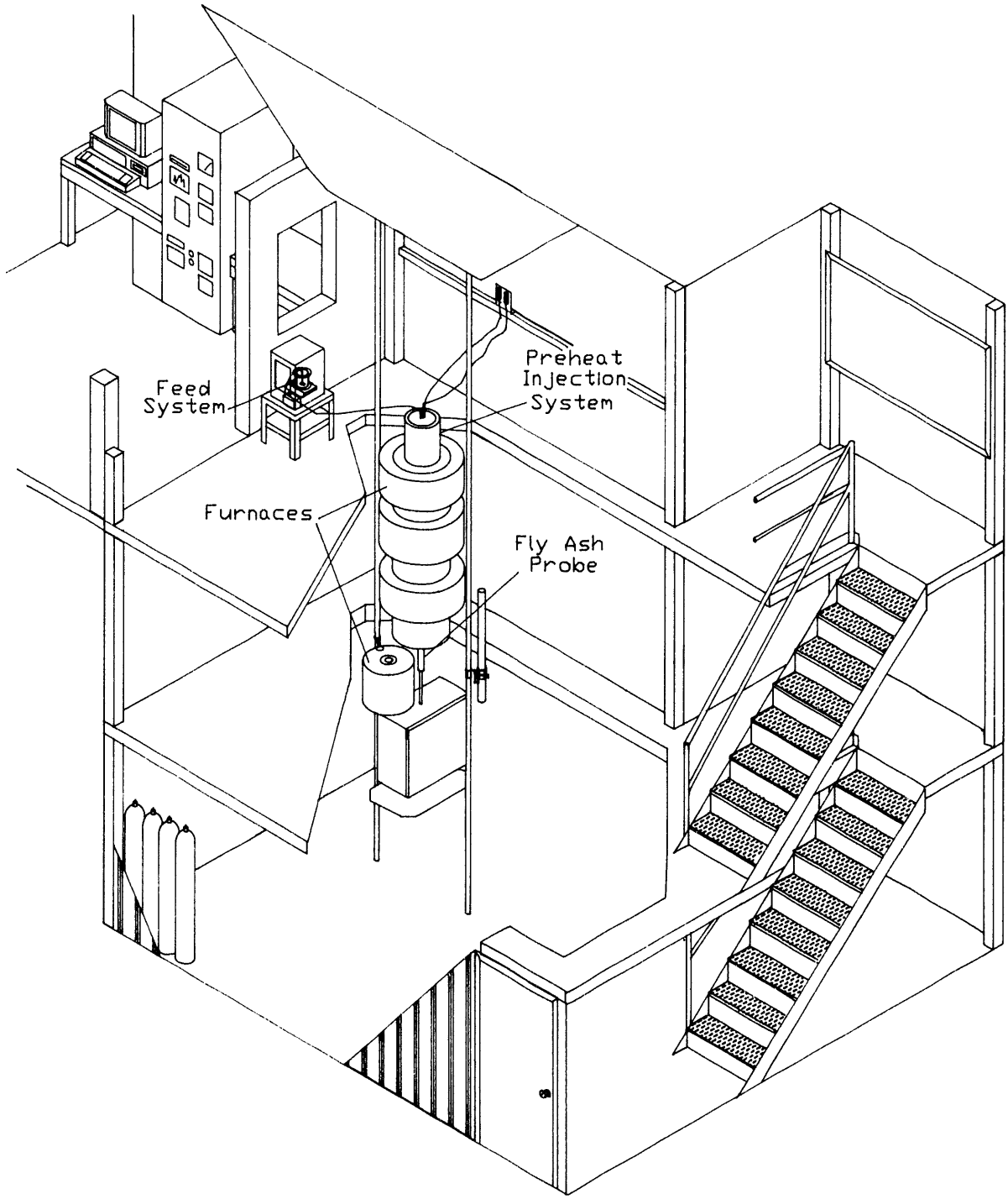

Figure 63. Drop-tube furnace laboratory.

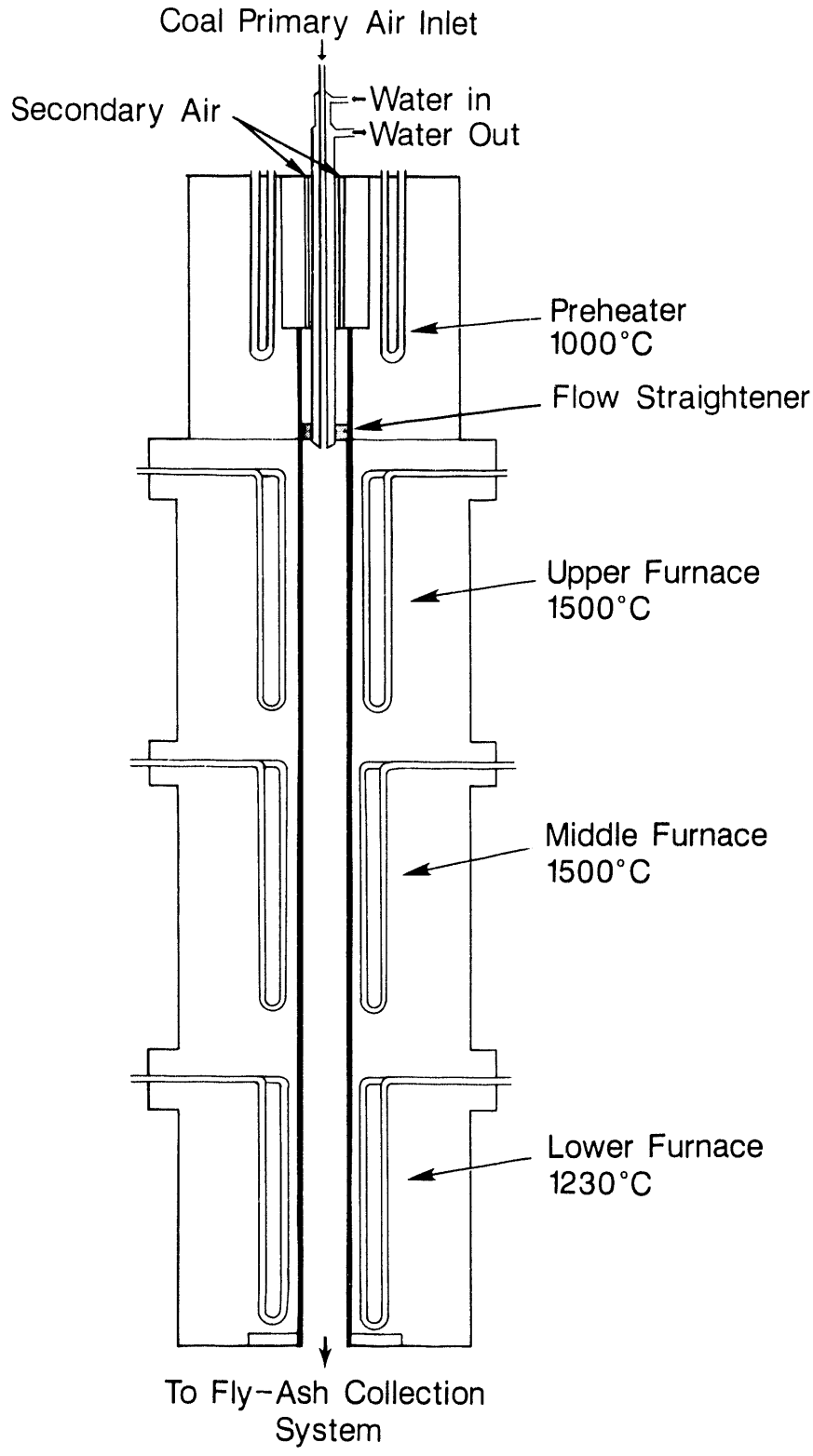

Figure 64. Cross-sectional diagram of the drop-tube furnace.

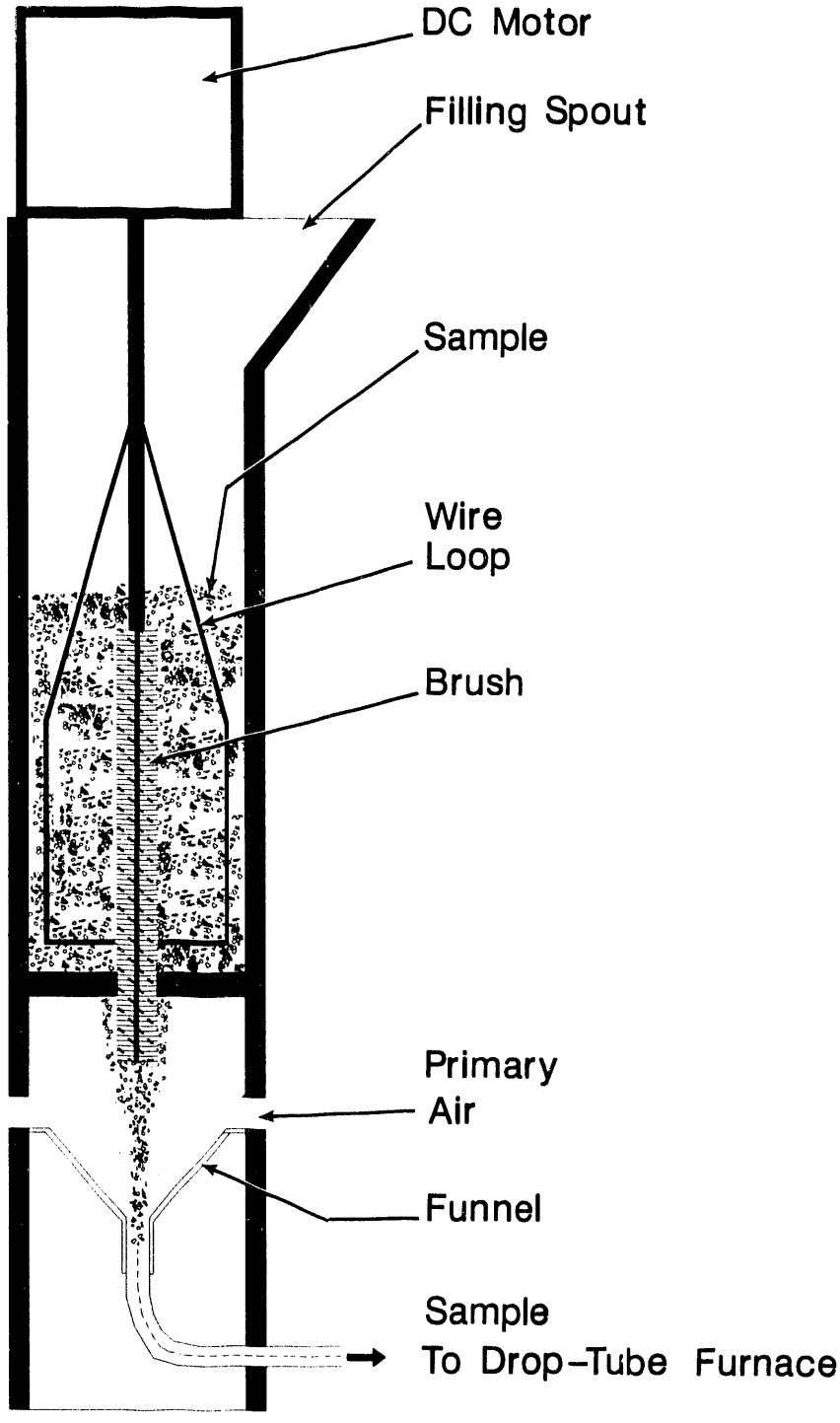

Figure 65. Coal feeder for the drop-tube furnace.

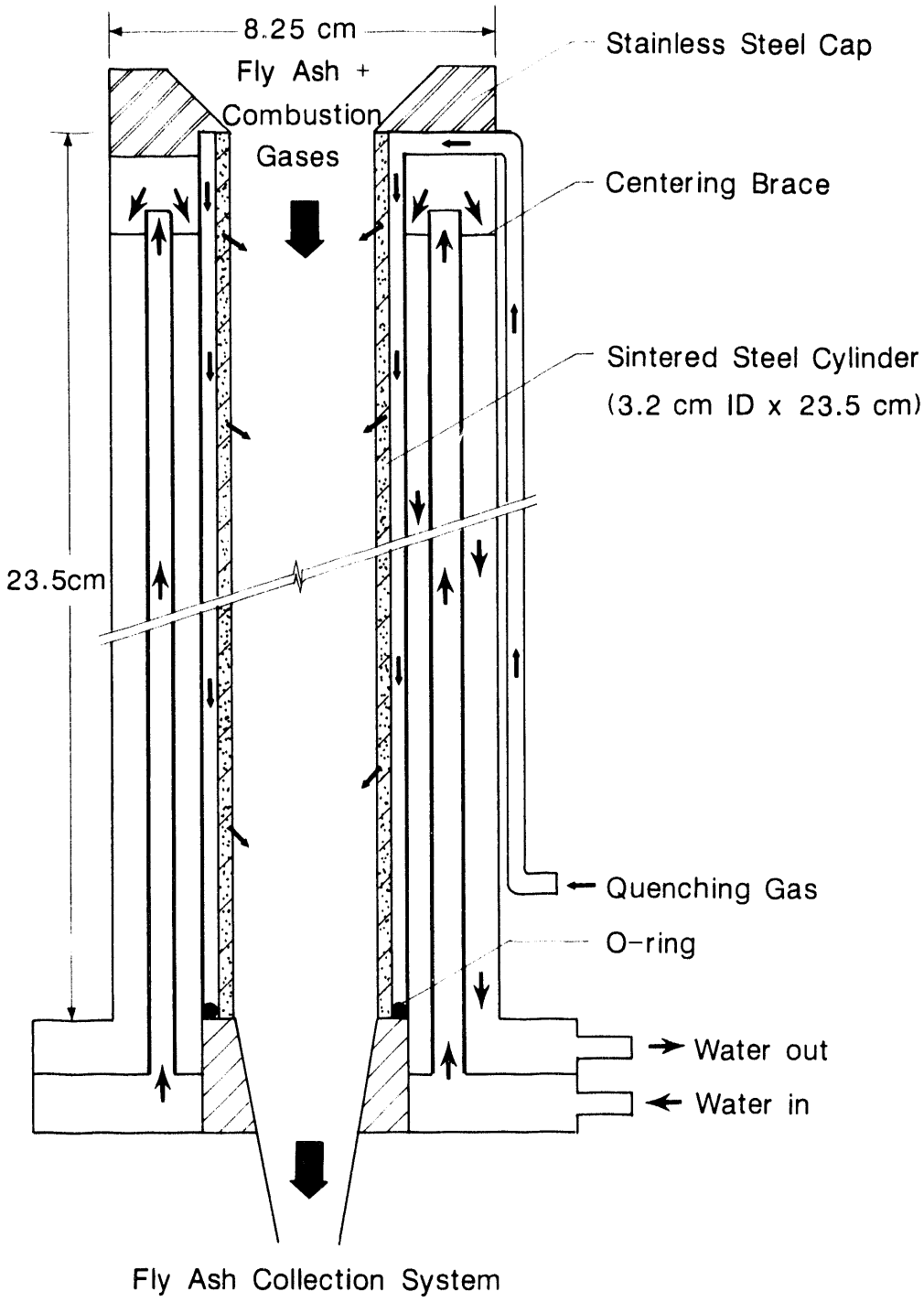

Figure 66. Fly ash quenching probe assembly for the drop-tube furnace.

Size-segregating methods of fly ash collection are being employed. The Environmental Protection Agency Southern Research Institute five-stage cyclone (EPAFSC) is being used on a routine basis to collect fly ash. The EPAFSC is designed to make five equally spaced particle-size cuts (D_{50}) on a logarithmic scale within the range of 0.1-10 millimeters. The advantage of this system is its capability of collecting the relatively large sample amounts needed for subsequent chemical and morphological analyses.

In addition to the EPAFSC, the University of Washington Mark 5 source test cascade impactor (STCI) is used during selected combustion tests. The STCI was developed as a means of measuring the size distribution of particles in stacks and ducts at air pollution emission sources. The Mark 5 impactor produces size cuts of fly ash particles by inertial separation. These data will be used for comparison with the EPAFSC data and to provide more detailed information concerning the effects of combustion conditions on the size distribution of the fly ashes.

A short residence time probe was designed and constructed to collect ash samples at any residence time. The probe consists of a series of four concentric, water-cooled, steel tubes. The outer shell is for introducing the quench gas at the top of the probe. The innermost shell removes the combustion gases, and the remaining shells carry the cooling water. The probe is covered with an alumina-insulating cylinder two inches in outside diameter (Figure 67). The probe is inserted in the bottom of the furnace a set distance calculated from the desired residence time. The quench gas and the vacuum are turned on. The coal is fed through the preheat injector and collected on a filter or with an impactor or multicyclone. The samples collected are analyzed by standard techniques such as XRFA and also advanced SEM techniques.

4.2.2 Preparation and Characterization of Kentucky #9 and San Miguel Coal, Char, and Fly Ash

This report details the initial characterization of two test coals chosen for combustion testing for this year. Kentucky #9 bituminous coal and San Miguel lignite were chosen based on characteristics unique from the five test coals studied thus far under CIT. These coals were also chosen because they are currently being used as test coals by PSI Technology for the study of inorganic transformations. Both coals were obtained from PSIT.

Kentucky #9 coal retains a relatively high amount of mineral matter with carbon after grinding and contains significant quantities of calcite (28). The San Miguel coal is a Texas lignite that is very high in ash, alkali elements, and clay minerals and has a reputation for severe fouling (28).

Coal sieve fractions were prepared for the Kentucky #9 and San Miguel test coals using a sonic-sieving technique. The sonic-sieving equipment consists of a sieve stack of stainless steel sieves that segregate the sample into <38, 38-53, 53-74, 74-106, and >106-micron fractions. The principle of operation is that the material on the sieves is agitated with an air column driven by a sonic source, the amplitude of which can be controlled. In addition, a pulse generator imparts a tap at intervals to the sieve stack to dislodge sticking particles and improve the sieving effectiveness.

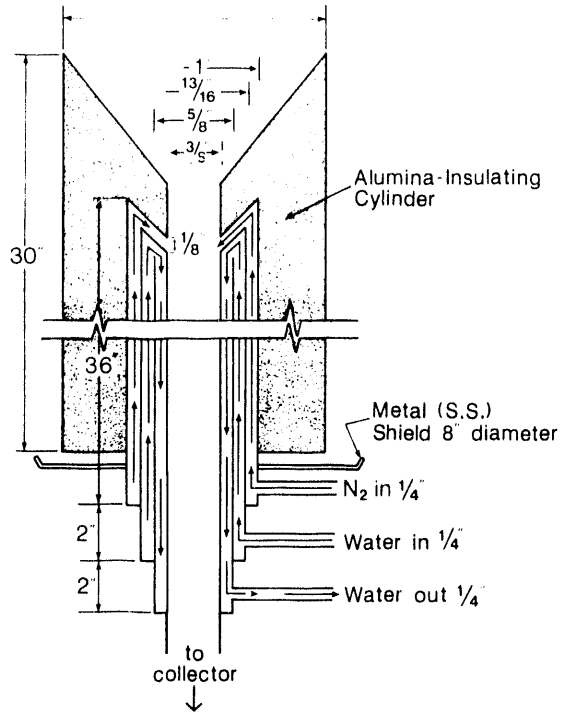

Figure 67. Short residence time probe for the drop-tube furnace.

Approximately 1-2 grams of sample is placed on the top (largest size) sieve, and the sieve stack is placed into the sonic sieve. The sonic amplitude is increased until the sample on the top sieve is bouncing 1-2 cm high, nominally corresponding to an amplitude of 4-5 on the dial scale. The "bouncing" will subsequently decrease as finer material falls through the upper sieve. The pulse amplitude is set to a dial scale reading of 9-10, nearly the maximum for the pulse unit. The sieve timer is set to sieve the sample for five minutes.

When the sieving cycle is completed, the sample retained on each sieve is transferred to a separate container. The material adhering to the bottom of each screen is removed by tapping on the side of the screen and included in the next smaller sample size container. The sieve stack is reassembled and the sieve cycle repeated until sufficient samples of each size cut (approximately 100-200 grams) have been processed. The size cuts obtained are >106 microns, 106-74 microns, 74-53 microns, 53-38 microns, and <38 microns. A thorough cleaning of the sieve stack is done after the entire sample has been sieved.

The 38-53, 53-74, 74-106-μm fractions and a bulk unsized sample of the Kentucky #9 and San Miguel coals were submitted for proximate/ultimate and ASTM ash composition analysis. Chemical fractionation analysis was performed on the 53-74-μm size fraction for the San Miguel. Chemical fractionation (29) is used to selectively extract elements from the coals based on how they are associated in the coal. Briefly, the technique involves extracting the coal with water to remove water soluble elements, followed by extraction with 1M ammonium acetate to remove elements that are associated as salts of organic

acid groups. The residue from the ammonium acetate extraction is extracted with 1M HCl to remove acid soluble species in the form of organic coordination complexes, hydroxides, oxides, and carbonates. The inorganic components in the residue after all three extractions are assumed to be associated in the coal with insoluble minerals such as clays, quartz, and pyrite.

Computer-controlled scanning electron microscopy (CCSEM) is being used to characterize coal, char, and ash samples and inorganic combustion products. In addition to the CCSEM analysis of coals to determine size and type of minerals, the technique is used to determine the juxtaposition of minerals; i.e., how minerals are associated with each other, and whether mineral grains are associated within coal particles (included) or are excluded from coal particles. Another SEM technique used to analyze the fly ash samples was SEMPC. These techniques have already been described in the methods sections of Tasks 2 and 3.

4.3 Char and Fly Ash Production for Kentucky #9 and San Miguel Coals and for Synthetic Coal-Model Mixture Studies

Drop-tube furnace multicyclone and impactor tests were performed using 38-53-μm, 53-74-μm, and 74-106-μm size fractions of Kentucky #9 and San Miguel coals at combustion temperatures of 1300°C, 1400°C, and 1500°C. Bulk filter tests using the 53-74-μm and bulk coal size fractions of both coals were run at combustion temperatures of 1500°C. Char production of both coals at 0.05, 0.1, 0.2, 0.5, and 0.8 second residence times also was performed at combustion temperatures of 1500°C. Run conditions for the various tests are listed in Tables 35-50. The upper and lower temperatures of Furnace #1 recorded in Tables 35-50 are gas temperatures derived from temperatures taken from the wall of the furnace tube. The gas temperatures have been found to be approximately 30°C lower than the wall temperatures by tests performed with a suction pyrometer.

Drop-tube furnace tests were performed using 38-106-μm synthetic coal at combustion temperatures of 900 and 1500°C. Run conditions for the various tests are listed in Tables 51-55. Synthetic coal containing 11% SiO_2, 4% Na, and 1% S was burned to form fly ash at 900 and 1500°C at normal residence times of 2.08 and 2.46 seconds, respectively, and at shorter residence times of 0.5 and 0.1 seconds (Tables 51 and 52). An additional run was made at 1500°C under a nitrogen atmosphere (Table 53). A synthetic coal sample that was S- and Na-free was combusted at 900 and 1500°C (Table 54) and a 10-20-μm pure silica sample was fired in the combustor at 1500°C (Table 55).

4.4 Results and Discussion

4.4.1 Characterization of Kentucky #9 Coal

The proximate/ultimate and coal ash composition data for the Kentucky #9 coal are given in Table 56. The relatively high calculated calorific values of the coal fractions verify the bituminous rank of this coal. Ash content decreases with increasing size fraction, which is probably the result of the size distribution of the minerals. The SiO_2 and Al_2O_3 contents also decrease

TABLE 35

DROP-TUBE FURNACE RUN CONDITIONS FOR MULTICYCLONE COLLECTION OF FLY ASH USING KENTUCKY #9 COAL (38-53 μm)

Run #	2290	2690	2890
Gas Flow Rates (L\min):			
Primary air	0.8	0.8	0.8
Secondary air	3.2	3.2	3.2
Quench Gas (N_2)	3.0	3.0	3.0
Vacuum	7.5	7.5	7.5
Temperatures (°C):			
Injector	867	898	928
Preheat	1050	1090	1130
Furnace #1 Upper	1292	1392	1488
Furnace #1 Lower	1312	1413	1512
Coal Burned (g)	6.75	6.37	5.92
Coal Feed Rate (g/min)	0.08	0.09	0.06
Ash Collected (g)	0.91	0.85	0.77
Residence Time (sec)	2.7	2.6	2.5

TABLE 36

DROP-TUBE FURNACE RUN CONDITIONS FOR MULTICYCLONE COLLECTION OF FLY ASH USING KENTUCKY #9 COAL (53-74 μm)

Run #	2090	2490	1290
Gas Flow Rates (L\min):			
Primary air	0.8	0.8	0.8
Secondary air	3.2	3.2	3.2
Quench Gas (N_2)	3.0	3.0	3.0
Vacuum	7.5	7.5	7.76
Temperatures (°C):			
Injector	871	837	932
Preheat	1050	1090	1130
Furnace #1 Upper	1292	1385	1482
Furnace #1 Lower	1312	1410	1511
Coal Burned (g)	3.83	6.48	10.49
Coal Feed Rate (g/min)	0.06	0.09	0.14
Ash Collected (g)	0.41	0.75	1.14
Residence Time (sec)	2.5	2.4	2.3

TABLE 37

DROP-TUBE FURNACE RUN CONDITIONS FOR MULTICYCLONE COLLECTION OF FLY ASH USING KENTUCKY #9 COAL (74-106 μm)

Run #	3290	3090	3490
Gas Flow Rates (L\min):			
Primary air	0.8	0.8	0.8
Secondary air	3.2	3.2	3.2
Quench Gas (N_2)	3.0	3.0	3.0
Vacuum	7.5	7.5	7.5
Temperatures (°C):			
Injector	860	899	931
Preheat	1050	1090	1130
Furnace #1 Upper	1291	1388	1490
Furnace #1 Lower	1313	1410	1515
Coal Burned (g)	4.05	4.73	4.67
Coal Feed Rate (g/min)	0.09	0.1	0.16
Ash Collected (g)	0.35	0.49	0.47
Residence Time (sec)	2.0	2.0	1.9

TABLE 38

DROP-TUBE FURNACE RUN CONDITIONS FOR IMPACTOR COLLECTION OF FLY ASH USING KENTUCKY #9 COAL (38-53 μm)

Run #	1990	2590	2990
Gas Flow Rates (L\min):			
Primary air	0.8	0.8	0.8
Secondary air	3.2	3.2	3.2
Quench Gas (N_2)	3.0	3.0	3.0
Vacuum	7.76	7.5	7.5
Temperatures (°C):			
Injector	860	833	923
Preheat	1050	1090	1130
Furnace #1 Upper	1292	1384	1489
Furnace #1 Lower	1313	1409	1514
Coal Burned (g)	6.43	6.22	4.71
Coal Feed Rate (g/min)	0.11	0.08	0.12
Ash Collected (g)	0.84	0.82	0.64
Residence Time (sec)	2.7	2.6	2.5

TABLE 39

DROP-TUBE FURNACE RUN CONDITIONS FOR IMPACTOR COLLECTION OF FLY ASH USING KENTUCKY #9 COAL (53-74 μm)

Run #	1090	2190	1390
Gas Flow Rates (L\min):			
Primary air	0.8	0.8	0.8
Secondary air	3.2	3.2	3.2
Quench Gas (N_2)	3.0	3.0	3.0
Vacuum	7.76	7.5	7.76
Temperatures (°C):			
Injector	865	898	937
Preheat	1050	1090	1130
Furnace #1 Upper	1308	1392	1482
Furnace #1 Lower	1329	1414	1506
Coal Burned (g)	5.28	4.51	6.46
Coal Feed Rate (g/min)	0.06	0.05	0.16
Ash Collected (g)	0.57	0.50	0.72
Residence Time (sec)	2.5	2.4	2.3

TABLE 40

DROP-TUBE FURNACE RUN CONDITIONS FOR IMPACTOR COLLECTION OF FLY ASH USING KENTUCKY #9 COAL (74-106 μm)

Run #	3390	3190	3590
Gas Flow Rates (L\min):			
Primary air	0.8	0.8	0.8
Secondary air	3.2	3.2	3.2
Quench Gas (N_2)	3.0	3.0	3.0
Vacuum	7.5	7.76	7.76
Temperatures (°C):			
Injector	861	900	928
Preheat	1050	1090	1130
Furnace #1 Upper	1288	1389	1489
Furnace #1 Lower	1309	1415	1517
Coal Burned (g)	3.4	4.8	4.58
Coal Feed Rate (g/min)	0.1	0.08	0.09
Ash Collected (g)	0.30	0.51	0.42
Residence Time (sec)	2.0	2.0	1.9

TABLE 41

DROP-TUBE FURNACE RUN CONDITIONS FOR BULK FILTER COLLECTION OF FLY ASH USING KENTUCKY #9 COAL

Run #	0889	0990
Description	53-74 μm	Bulk
Gas Flow Rates (L\min):		
Primary air	0.8	0.8
Secondary air	3.2	3.2
Quench Gas (N_2)	3.0	3.0
Vacuum	7.76	7.76
Temperatures (°C):		
Injector	935	939
Preheat	1130	1130
Furnace #1 Upper	1491	1476
Furnace #1 Lower	1518	1503
Coal Burned (g)	2.96	3.07
Coal Feed Rate (g/min)	0.05	0.1
Ash Collected (g)	0.23	0.30
Residence Time (sec)	2.3	2.3

TABLE 42

DROP-TUBE FURNACE RUN CONDITIONS FOR CHAR PRODUCTION USING KENTUCKY #9 COAL (53-74 μm)

Run #	0789	0689	0589	3790	3690
Gas Flow Rates (L\min):					
Primary air	0.8	0.8	0.8	0.8	0.8
Secondary air	3.2	3.2	3.2	3.2	3.2
Quench Gas (N_2)	3.0	3.0	3.0	3.0	3.0
Vacuum	7.76	7.76	7.76	7.5	7.5
Temperatures (°C):					
Injector	933	932	930	928	928
Preheat	1130	1130	1130	1130	1130
Furnace #1 Upper	1480	1481	1484	1497	1499
Furnace #1 Lower	1493	1494	1495	1499	1483
Coal Burned (g)	3.38	2.74	2.75	2.08	2.36
Coal Feed Rate (g/min)	0.11	0.06	0.07	0.04	0.05
Ash Collected (g)	0.37	0.39	0.47	0.23	0.26
Residence Time (sec)	0.05	0.1	0.2	0.5	0.8

TABLE 43

DROP-TUBE FURNACE RUN CONDITIONS FOR MULTICYCLONE COLLECTION OF FLY ASH USING SAN MIGUEL COAL (38-53 μm)

Run #	0590	0390	0190
Gas Flow Rates (L\min):			
Primary air	0.8	0.8	0.8
Secondary air	3.2	3.2	3.2
Quench Gas (N_2)	3.0	3.0	3.0
Vacuum	7.5	7.5	7.5
Temperatures (°C):			
Injector	858	897	929
Preheat	1050	1090	1130
Furnace #1 Upper	1290	1389	1492
Furnace #1 Lower	1313	1413	1519
Coal Burned (g)	5.1	4.75	4.69
Coal Feed Rate (g/min)	0.19	0.19	0.19
Ash Collected (g)	2.01	1.50	0.89
Residence Time (sec)	2.7	2.6	2.5

TABLE 44

DROP-TUBE FURNACE RUN CONDITIONS FOR MULTICYCLONE COLLECTION OF FLY ASH USING SAN MIGUEL COAL (53-74 μm)

Run #	1290	1590	1890
Gas Flow Rates (L\min):			
Primary air	0.8	0.8	0.8
Secondary air	3.2	3.2	3.2
Quench Gas (N_2)	3.0	3.0	3.0
Vacuum	7.5	7.5	7.5
Temperatures (°C):			
Injector	835	893	925
Preheat	1050	1090	1130
Furnace #1 Upper	1297	1400	1486
Furnace #1 Lower	1305	1410	1500
Coal Burned (g)	5.07	4.29	4.84
Coal Feed Rate (g/min)	0.2	0.17	0.19
Ash Collected (g)	1.89	1.78	2.14
Residence Time (sec)	2.5	2.4	2.3

TABLE 45

DROP-TUBE FURNACE RUN CONDITIONS FOR MULTICYCLONE COLLECTION OF FLY ASH USING SAN MIGUEL COAL (74-106 μm)

Run #	1790	1090	0890
Gas Flow Rates (L\min):			
Primary air	0.8	0.8	0.8
Secondary air	3.2	3.2	3.2
Quench Gas (N_2)	3.0	3.0	3.0
Vacuum	7.5	7.5	7.5
Temperatures (°C):			
Injector	860	886	922
Preheat	1050	1090	1130
Furnace #1 Upper	1290	1407	1492
Furnace #1 Lower	1305	1417	1519
Coal Burned (g)	4.69	3.57	4.64
Coal Feed Rate (g/min)	0.24	0.19	0.19
Ash Collected (g)	0.28	0.06	0.49
Residence Time (sec)	2.0	2.0	1.9

TABLE 46

DROP-TUBE FURNACE RUN CONDITIONS FOR IMPACTOR COLLECTION OF FLY ASH USING SAN MIGUEL COAL (38-53 μm)

Run #	0690	0490	0290
Gas Flow Rates (L\min):			
Primary air	0.8	0.8	0.8
Secondary air	3.2	3.2	3.2
Quench Gas (N_2)	3.0	3.0	3.0
Vacuum	7.5	7.5	7.5
Temperatures (°C):			
Injector	854	893	925
Preheat	1050	1090	1130
Furnace #1 Upper	1292	1389	1490
Furnace #1 Lower	1315	1414	1517
Coal Burned (g)	0.85	0.84	1.52
Coal Feed Rate (g/min)	0.14	0.17	0.15
Ash Collected (g)	0.28	0.28	0.57
Residence Time (sec)	2.7	2.6	2.5

TABLE 47

DROP-TUBE FURNACE RUN CONDITIONS FOR IMPACTOR COLLECTION OF FLY ASH USING SAN MIGUEL COAL (53-74 μm)

Run #	1390	1490	1990
Gas Flow Rates (L\min):			
Primary air	0.8	0.8	0.8
Secondary air	3.2	3.2	3.2
Quench Gas (N_2)	3.0	3.0	3.0
Vacuum	7.5	7.5	7.5
Temperatures (°C):			
Injector	834	892	923
Preheat	1050	1090	1130
Furnace #1 Upper	1298	1394	1487
Furnace #1 Lower	1308	1406	1500
Coal Burned (g)	0.78	0.89	0.9
Coal Feed Rate (g/min)	0.2	0.25	0.23
Ash Collected (g)	0.28	0.32	0.40
Residence Time (sec)	2.5	2.4	1.9

TABLE 48

DROP-TUBE FURNACE RUN CONDITIONS FOR IMPACTOR COLLECTION OF FLY ASH USING SAN MIGUEL COAL (74-106 μm)

Run #	1690	0990	1790
Gas Flow Rates (L\min):			
Primary air	0.8	0.8	0.8
Secondary air	3.2	3.2	3.2
Quench Gas (N_2)	3.0	3.0	3.0
Vacuum	7.5	7.5	7.5
Temperatures (°C):			
Injector	865	881	926
Preheat	1050	1090	1130
Furnace #1 Upper	1290	1392	1492
Furnace #1 Lower	1303	1416	1518
Coal Burned (g)	0.95	0.83	0.91
Coal Feed Rate (g/min)	0.24	0.21	0.18
Ash Collected (g)	0.18	0.08	0.11
Residence Time (sec)	2.0	2.0	1.9

TABLE 49

DROP-TUBE FURNACE RUN CONDITIONS FOR BULK FILTER COLLECTION OF FLY ASH USING SAN MIGUEL COAL

Run #	2090	2190
Description	53-74 μm	Bulk
Gas Flow Rates (L\min):		
Primary air	0.8	0.8
Secondary air	3.2	3.2
Quench Gas (N_2)	3.0	3.0
Vacuum	7.5	7.5
Temperatures (°C):		
Injector	927	923
Preheat	1130	1130
Furnace #1 Upper	1483	1486
Furnace #1 Lower	1497	1500
Coal Burned (g)	0.85	1.79
Coal Feed Rate (g/min)	0.17	0.18
Ash Collected (g)	0.31	0.69
Residence Time (sec)	2.4	2.4

TABLE 50

DROP-TUBE FURNACE RUN CONDITIONS FOR CHAR PRODUCTION USING SAN MIGUEL COAL (53-74 μm)

Run #	2290	2390	2690	2790	2890
Gas Flow Rates (L/min):					
Primary air	0.8	0.8	0.8	0.8	0.8
Secondary air	3.2	3.2	3.2	3.2	3.2
Quench Gas (N_2)	3.0	3.0	3.0	3.0	3.0
Vacuum	7.5	7.5	7.5	7.5	7.5
Temperatures (°C):					
Injector	910	926	910	910	910
Preheat	1134	1131	1130	1130	1130
Secondary air	1091	1095	1090	1090	1090
Furnace #1 Upper	1510	1507	1505	1505	1501
Furnace #1 Lower	1480	1487	1499	1501	1496
Coal Burned (g)	0.99	1.12	1.17	1.82	1.2
Coal Feed Rate (g/min)	0.14	0.14	0.15	0.14	0.15
Ash Collected (g)	0.38	0.45	0.22	0.08	0.05
Residence Time (sec)	0.8	0.5	0.2	0.1	0.05

TABLE 51

DROP-TUBE FURNACE RUN CONDITIONS FOR PRODUCTION OF FLY ASH USING SYNTHETIC COAL

Test No.	1	6
Gas Flow Rates (L/min):		
Primary Air	0.8	0.8
Secondary Air	3.2	3.2
Quench Gas (N_2)	3.0	3.0
Vacuum	7.06	7.06
Temperatures (°C):		
Injector	677	937
Preheat	800	1130
Furnace #1 Upper	871	1464
Furnace #1 Lower	896	1499
Coal Burned (g)	5.14	3.05
Coal Feed Rate (g/min)	0.17	0.15
Ash Collected (g)	0.75	0.38
Residence Time (s)	2.46	2.08

TABLE 52

DROP-TUBE FURNACE RUN CONDITIONS FOR CHAR PRODUCTION USING SYNTHETIC COALS

	0.1-Second Char		0.5-Second Char	
Test No.	4	11	3	10
Gas Flow Rates (L/min)				
Primary Air	0.8	0.8	0.8	0.8
Secondary Air	3.2	3.2	3.2	3.2
Quench Gas (N_2)	3.0	3.0	3.0	3.0
Vacuum	7.06	7.06	7.06	7.06
Temperatures (°C)				
Injector	675	933	680	933
Preheat	800	1130	800	1130
Furnace #1 Upper	866	1471	871	1470
Furnace #1 Lower	874	1486	869	1483
Coal Burned (g)	3.04	2.58	3.11	2.13
Coal Feed Rate (g/min)	0.1	0.09	0.10	0.04
Ash Collected (g)	0.78	0.49	0.32	0.10
Residence Time (sec)	0.1	0.1	0.5	0.5

TABLE 53

DROP-TUBE FURNACE RUN CONDITIONS FOR FLY ASH PRODUCTION USING SYNTHETIC COAL AND NITROGEN ATMOSPHERE

	Test No. 7
Gas Flow Rates (L/min)	
Primary (N_2)	0.8
Secondary (N_2)	3.2
Quench Gas (N_2)	3.0
Vacuum	7.06
Temperatures (°C)	
Injector	937
Preheat	1130
Furnace #1 Upper	1469
Furnace #1 Lower	1505
Coal Burned (g)	2.97
Coal Feed Rate (g/min)	0.15
Ash Collected (g)	1.72
Residence Time (sec)	2.08

TABLE 54

DROP-TUBE FURNACE RUN CONDITIONS FOR FLY ASH PRODUCTION USING NA- AND S-FREE SYNTHETIC COAL

Test No.	5	8
Gas Flow Rates (L/min)		
Primary Air	0.8	0.8
Secondary Air	3.2	3.2
Quench Gas (N_2)	3	3
Vacuum	7.06	7.06
Temperatures (°C)		
Injector	684	941
Preheat	800	1130
Furnace #1 Upper	872	1470
Furnace #1 Lower	892	1506
Coal Burned (g)	3.09	2.9
Coal Feed Rate (g/min)	0.09	0.09
Ash Collected (g)	0.31	0.88
Residence Time (sec)	2.46	2.08

TABLE 55

DROP-TUBE FURNACE RUN CONDITIONS FOR COMBUSTION OF PURE SILICA

	Test No. 9
Gas Flow Rates (L/min)	
Primary Air	0.8
Secondary Air	3.2
Quench Gas (N_2)	3.0
Vacuum	7.06
Temperatures (°C)	
Injector	933
Preheat	1130
Furnace #1 Upper	1460
Furnace #1 Lower	1490
Coal Burned (g)	1.31
Coal Feed Rate (g/min)	0.01
Ash Collected (g)	0.06
Residence Time (sec)	2.08

with increasing coal particle size. This observation may indicate more quartz and/or aluminosilicate clay such as kaolinite in the smaller coal size fraction. The Fe_2O_3 content increases by over 10% with increasing coal particle size probably due to larger-sized pyrite. Other elements listed in Table 56 do not show any significant trends.

Kentucky #9 coal contained about 15% total ash (Table 56). The most abundant minerals in the ash were quartz, aluminosilicate (degraded illite or mineral clay), illite, pyrite, and for the 74-106 and unsized fraction, siderite (Table 57). Ash content decreased with increasing coal size, but mineral size increased. Variability in mineral content was noted for these different coal sizes analyzed by CCSEM. An increase in pyrite with coal size corresponded with an increase in iron oxide in the coal ashes (Tables 56 and 57). Table 58 lists the detailed CCSEM mineral content distributions for the three sized fractions and unsized or bulk fraction of Kentucky #9.

4.4.2 Characterization of Kentucky #9 Char and Fly Ash

Time resolved combustion studies of Kentucky #9 coal produced chars at 0.05, 0.1, 0.2, 0.5, and 0.8 seconds residence time. The CCSEM analyses of inorganic phases in these chars are given in Table 59. Particle distribution for Kentucky #9 inorganic phases produced at different residence times were plotted in Figure 68. The amount of ash decreased in the smaller size bins (22-10 μm) and increased in the larger size bins (10-46 μm) with time. This is evidence of coalescence of the smaller mineral grains.

TABLE 56

RESULTS OF KENTUCKY #9 COAL AND ASH ANALYSIS[a]

Proximate, Wt%	Bulk Coal	38-53 μm	53-74 μm	74-106 μm
Moisture	7.9	7.0	7.5	7.5
Volatile Matter	35.24	35.36	36.13	36.61
Fixed Carbon	49.32	48.37	49.27	49.56
Ash	15.44	16.27	14.60	13.83
Ultimate, Wt%				
Carbon	64.74	64.14	65.79	65.77
Hydrogen	4.56	4.27	4.37	4.39
Nitrogen	1.35	1.30	1.34	1.33
Oxygen (diff.)	9.73	10.33	9.91	9.9
Sulfur	4.16	3.66	3.97	4.76
Ash Analysis, Wt%				
SiO_2	46.1	47.4	45.3	40.6
Al_2O_3	21.1	21.0	20.8	19.3
Fe_2O_3	19.7	17.6	21.4	29.0
TiO_2	1.1	1.2	1.2	1.1
P_2O_5	0.1	0.2	0.1	0.0
CaO	3.4	3.8	3.9	3.4
MgO	1.6	1.5	1.3	1.2
Na_2O	0.6	0.0	0.0	0.0
K_2O	3.0	3.4	2.3	2.6
SO_3	3.3	3.9	3.9	2.9
Heating Valve, Btu/lb				
Calc. Calorific Value	10,758	10,570	10,837	10,866

[a] Results reported on a dry basis except for the moisture determination.

TABLE 57

MINERAL CONTENT FOR KENTUCKY #9 COAL SIZE FRACTIONS
(WT% MINERAL BASIS)

Wt% Mineral Basis	Bulk Coal	38-53 μm	53-74 μm	74-106 μm
Quartz	31.92	14.47	9.04	31.25
Iron Oxide	8.42	0.65	0.41	4.63
Aluminosilicate	4.48	20.08	16.67	4.00
Ca-aluminosilicate	0.18	0.25	0.50	0.12
Fe-aluminosilicate	0.79	0.31	1.17	0.43
K-aluminosilicate	11.63	24.49	32.40	6.52
Ankerite	0.00	0.00	0.00	0.00
Pyrite	27.64	25.75	26.11	43.74
Gypsum	0.99	1.82	0.56	0.06
Barite	0.00	0.00	0.00	0.00
Gypsum/Barite	0.00	0.00	0.00	0.00
Apatite	0.00	0.03	0.07	0.57
Ca-Silicate	0.02	0.04	0.14	0.01
Aluminosil./Gypsum	0.00	0.08	0.41	0.00
Ca-Aluminate	0.00	0.00	0.00	0.00
Spinel	0.01	0.04	0.00	0.00
Alumina	0.23	0.02	0.00	0.05
Calcite	0.90	2.76	1.99	1.89
Rutile	0.10	0.19	0.79	0.00
Dolomite	0.00	0.00	0.05	0.00
Pyrrhotite	1.67	0.98	0.73	2.96
Ca-Rich	0.00	0.05	0.00	0.00
Si-Rich	0.45	0.92	2.08	0.18
Periclase	0.00	0.00	0.00	0.00
Unknown	0.59	7.10	6.87	3.61
Wt% Total Minerals (Coal Basis)	19.08	5.78	11.60	7.58

TABLE 58

MINERAL-SIZE DISTRIBUTION IN KENTUCKY #9 BULK AND SIZED FRACTIONS (WT% MINERAL BASIS)

	Kentucky #9 Bulk Coal Particle-Size Categories (μm)							COAL
							TOTAL	BASIS
Mineral/Phase	1-2.2	2.2-4.6	4.6-10	10-22	22-46	>46	WT%	WT%
Quartz	6.2	11.8	11.9	1.5	0.5	0.0	31.9	6.10
Iron Oxide	3.8	4.6	0.0	0.0	0.0	0.0	8.4	1.61
Aluminosilicate	0.3	1.7	1.5	0.7	0.4	0.0	4.5	0.85
Ca-aluminosilicate	0.0	0.1	0.0	0.0	0.0	0.0	0.2	0.03
Fe-aluminosilicate	0.1	0.6	0.0	0.0	0.1	0.0	0.8	0.15
K-aluminosilicate	0.5	1.9	4.2	2.3	2.6	0.2	11.6	2.22
Pyrite	1.0	2.5	6.6	3.9	8.2	5.4	27.6	5.26
Gypsum	0.0	0.0	0.8	0.1	0.1	0.0	1.0	0.19
Alumina	0.0	0.2	0.0	0.0	0.0	0.0	0.2	0.04
Calcite	0.0	0.0	0.3	0.2	0.5	0.0	0.9	0.17
Rutile	0.0	0.1	0.0	0.0	0.0	0.0	0.1	0.02
Pyrrhotite	0.0	0.4	1.0	0.2	0.1	0.0	1.7	0.32
Si-Rich	0.1	0.3	0.0	0.1	0.0	0.0	0.4	0.09
Unknown	3.3	4.0	2.1	0.6	0.3	0.2	10.6	2.02
TOTAL (and PSD)	15.4	28.2	28.3	9.5	12.8	5.9	100.0	19.08

	Kentucky #9 38-53-μm Coal Particle-Size Categories (μm)							COAL
							TOTAL	BASIS
Mineral/Phase	1-2.2	2.2-4.6	4.6-10	10-22	22-46	>46	WT%	WT%
Quartz	2.7	6.4	3.9	0.4	0.8	0.2	14.5	0.84
Iron Oxide	0.2	0.3	0.0	0.0	0.2	0.0	0.7	0.04
Aluminosilicate	2.7	6.7	7.5	1.5	1.7	0.0	20.1	1.16
Ca-aluminosilicate	0.1	0.2	0.0	0.0	0.0	0.0	0.3	0.02
Fe-aluminosilicate	0.1	0.2	0.0	0.0	0.0	0.0	0.3	0.02
K-aluminosilicate	2.2	6.9	9.6	2.9	2.4	0.4	24.5	1.42
Pyrite	1.3	3.1	11.7	5.9	3.7	0.0	25.7	1.49
Gypsum	0.1	0.2	1.2	0.1	0.2	0.0	1.8	0.11
Aluminosil./Gypsum	0.1	0.0	0.0	0.0	0.0	0.0	0.1	0.00
Calcite	0.1	0.0	0.3	0.7	1.7	0.0	2.8	0.16
Rutile	0.1	0.0	0.0	0.0	0.1	0.0	0.2	0.01
Pyrrhotite	0.3	0.3	0.0	0.4	0.0	0.0	1.0	0.06
Si-Rich	0.1	0.3	0.4	0.1	0.0	0.0	0.9	0.05
Unknown	1.2	2.9	2.3	0.6	0.1	0.0	7.1	0.41
TOTAL (and PSD)	11.3	27.6	36.9	12.8	10.8	0.7	100.0	5.78

	Kentucky #9 53-74-μm Coal Particle-Size Categories (μm)							COAL
							TOTAL	BASIS
Mineral/Phase	1-2.2	2.2-4.6	4.6-10	10-22	22-46	>46	WT%	WT%
Quartz	2.3	2.0	2.7	0.8	1.0	0.2	9.0	1.05
Iron Oxide	0.1	0.0	0.0	0.0	0.2	0.0	0.4	0.05
Aluminosilicate	3.0	5.4	5.3	1.2	1.5	0.3	16.7	1.94
Ca-Al-Silicate	0.4	0.1	0.0	0.0	0.0	0.0	0.5	0.06
Fe-Al-Silicate	0.4	0.2	0.4	0.0	0.2	0.0	1.2	0.14
K-Al-Silicate	3.6	7.5	7.2	3.3	5.0	5.7	32.4	3.76
Pyrite	0.7	2.0	4.1	7.3	12.0	0.0	26.1	3.02
Gypsum	0.0	0.2	0.2	0.1	0.0	0.0	0.6	0.07
Ca-Silicate	0.1	0.1	0.0	0.0	0.0	0.0	0.1	0.02
Gyp/Al-Silicate	0.1	0.3	0.0	0.1	0.0	0.0	0.4	0.05
Calcite	0.1	0.1	0.0	0.3	1.3	0.2	2.0	0.23
Rutile	0.0	0.1	0.6	0.0	0.0	0.0	0.1	0.09
Dolomite	0.0	0.1	0.0	0.0	0.0	0.0	0.5	0.01
Pyrrhotite/Fe-Sulfate	0.1	0.5	0.0	0.2	0.0	0.0	0.7	0.09
Si-Rich	0.3	0.4	1.3	0.2	0.0	0.0	2.1	0.24
Unknown	2.0	2.3	0.9	0.6	1.0	0.0	6.9	0.80
Total	13.2	21.1	22.9	14.1	22.3	6.4	100.0	11.6

continued . . .

TABLE 58 (Continued)

MINERAL-SIZE DISTRIBUTION IN KENTUCKY #9 BULK AND SIZED FRACTIONS (WT% MINERAL BASIS)

Mineral/Phase	Kentucky #9 74-106-μm Coal Particle-Size Categories (μm) 1-2.2	2.2-4.6	4.6-10	10-22	22-46	>46	TOTAL WT%	COAL BASIS WT%
Quartz	7.7	11.3	10.2	1.4	0.7	0.0	31.2	2.39
Iron Oxide	2.7	1.4	0.4	0.1	0.0	0.0	4.6	0.35
Aluminosilicate	1.0	1.0	0.6	0.9	0.6	0.0	4.0	0.30
Ca-aluminosilicate	0.1	0.0	0.0	0.0	0.0	0.0	0.1	0.01
Fe-aluminosilicate	0.1	0.2	0.0	0.1	0.1	0.0	0.4	0.03
K-aluminosilicate	0.5	0.9	1.2	1.7	2.2	0.0	6.5	0.49
Pyrite	0.8	1.2	2.3	12.9	22.0	4.5	43.7	3.30
Gypsum	0.0	0.0	0.0	0.0	0.0	0.0	0.1	0.00
Apatite	0.0	0.0	0.0	0.0	0.6	0.0	0.6	0.04
Alumina	0.1	0.0	0.0	0.0	0.0	0.0	0.1	0.00
Calcite	0.0	0.0	0.0	0.2	1.0	0.7	1.9	0.14
Pyrrhotite	0.3	0.4	0.0	0.7	1.5	0.0	3.0	0.22
Si-Rich	0.1	0.0	0.0	0.1	0.0	0.0	0.2	0.01
Unknown	0.7	0.8	0.2	0.8	0.8	0.4	3.6	0.27
TOTAL (and PSD)	14.1	17.1	14.8	19.0	29.4	5.5	100.0	7.58

PSD = Particle-Size Distribution

TABLE 59

PARTICLE-SIZE DISTRIBUTION FOR INDIVIDUAL INORGANIC PHASES IN KENTUCKY #9 CHARS AT DIFFERENT RESIDENCE TIMES (MINERAL WEIGHT%)

Mineral/Phase	A. Kentucky #9 0.05-Second Char Particle-Size Categories (microns) 1-2.2	2.2-4.6	4.6-10	10-22	22-46	>46	TOTAL WT%
Quartz	0.11	1.00	2.44	2.68	1.07	0.96	8.26
Iron Oxide	0.12	1.19	2.20	4.87	10.23	0.00	18.60
Aluminosilicate	0.00	0.05	0.04	1.32	0.62	0.85	2.88
Ca-aluminosilicate	0.01	0.05	0.16	0.00	0.00	0.00	0.22
Fe-aluminosilicate	0.09	0.48	0.74	0.81	0.92	0.00	3.05
K-aluminosilicate	0.16	2.27	5.33	8.05	10.55	3.32	29.68
Ankerite	0.00	0.02	0.00	0.00	0.00	0.00	0.02
Pyrite	0.00	0.02	0.00	0.81	1.42	3.55	5.79
Gypsum	0.01	0.07	0.06	0.03	0.00	0.00	0.17
Apatite	0.00	0.00	0.00	0.14	0.00	0.00	0.14
Ca-Silicate	0.02	0.00	0.00	0.06	0.00	0.00	0.07
Aluminosil./Gypsum	0.00	0.00	0.03	0.00	0.00	0.00	0.03
Calcite	0.02	0.03	0.44	0.51	3.80	0.95	5.75
Rutile	0.03	0.00	0.00	0.00	0.00	0.00	0.03
Pyrrhotite/Fe-Sulfate	0.05	0.39	1.37	4.26	6.42	1.20	13.68
Ca-Rich	0.01	0.05	0.05	0.04	0.56	0.00	0.69
Si-Rich	0.06	0.43	0.08	0.22	0.37	0.00	1.17
Unknown	0.41	1.91	2.20	1.68	2.61	0.96	9.77
TOTAL (and PSD)	1.08	7.94	15.13	25.47	38.59	11.79	100.0

continued . . .

TABLE 59 (Continued)

PARTICLE-SIZE DISTRIBUTION FOR INDIVIDUAL INORGANIC PHASES
IN KENTUCKY #9 CHARS AT DIFFERENT RESIDENCE TIMES (MINERAL WEIGHT%)

	B. Kentucky #9 0.1-Second Char Particle-Size Categories (microns)						
Mineral/Phase	<2.2	2.2-4.6	4.6-10	10-22	22-46	>46	TOTAL WT%
Quartz	0.05	0.21	0.81	5.60	3.75	0.00	10.41
Iron Oxide	0.00	0.16	0.26	0.18	0.77	0.00	1.36
Aluminosilicate	0.00	0.04	0.13	0.66	0.69	0.00	1.53
Ca-aluminosilicate	0.05	0.50	3.15	8.20	2.85	0.44	15.20
Fe-aluminosilicate	0.00	0.04	0.00	0.08	0.00	0.00	0.12
K-aluminosilicate	0.01	0.02	0.19	0.26	0.64	0.00	1.10
Ankerite	0.05	0.10	0.15	0.10	0.00	0.00	0.40
Gypsum	0.08	0.31	1.50	2.33	1.89	1.06	7.15
Gypsum/Barite	0.01	0.00	0.00	0.00	0.00	0.00	0.01
Apatite	0.00	0.00	0.00	0.03	0.00	0.00	0.03
Ca-Silicate	0.16	0.76	5.56	12.03	4.29	1.77	24.56
Aluminosil./Gypsum	0.01	0.04	0.08	0.00	0.21	0.00	0.34
Ca-Aluminate	0.02	0.12	0.46	0.63	0.00	0.00	4.03
Calcite	0.04	0.30	0.98	2.05	0.67	0.00	4.03
Rutile	0.00	0.00	0.00	0.10	0.00	0.00	0.10
Dolomite	0.00	0.00	0.14	0.21	0.00	0.00	0.35
Pyrrhotite/Fe-Sulfate	0.00	0.04	0.00	0.00	0.00	0.00	0.04
Ca-Rich	0.09	0.48	2.14	3.64	0.57	0.00	6.93
Si-Rich	0.01	0.01	0.46	0.41	0.00	0.00	0.88
Unknown	0.36	1.48	6.28	10.14	4.71	1.29	24.25
TOTAL (and PSD)	0.94	4.59	22.26	46.62	21.03	4.56	100.00

	C. Kentucky #9 0.2-Second Char Particle-Size Categories (microns)						
Mineral/Phase	<2.2	2.2-4.6	4.6-10	10-22	22-46	>46	TOTAL WT%
Quartz	0.86	1.55	2.64	2.76	2.27	0.97	11.05
Iron Oxide	0.14	0.88	1.24	3.89	9.30	1.09	16.54
Aluminosilicate	0.79	1.12	0.71	1.19	0.89	0.32	5.02
Ca-aluminosilicate	0.20	0.15	0.00	0.16	0.11	0.00	0.62
Fe-aluminosilicate	1.45	1.82	2.35	1.33	2.72	0.62	10.29
K-aluminosilicate	1.75	3.71	4.29	8.05	16.51	3.11	37.42
Pyrite	0.00	0.00	0.00	0.06	0.00	0.00	0.06
Gypsum	0.00	0.00	0.00	0.06	0.00	0.00	0.06
Ca-Silicate	0.15	0.06	0.00	0.07	0.27	0.00	0.55
Ca-Aluminate	0.02	0.00	0.00	0.00	0.00	0.00	0.02
Spinel	0.03	0.00	0.00	0.00	0.00	0.00	0.03
Calcite	0.02	0.00	0.00	0.68	1.68	1.80	4.17
Rutile	0.00	0.00	0.00	0.00	0.18	0.00	0.18
Pyrrhotite/Fe-Sulfate	0.20	0.49	0.18	1.37	2.89	0.46	5.59
Ca-Rich	0.02	0.02	0.00	0.00	0.00	0.00	0.04
Si-Rich	0.11	0.04	0.29	0.08	0.24	0.00	0.75
Unknown	0.50	0.85	0.42	1.77	2.79	1.29	7.61
TOTAL (and PSD)	6.22	10.69	12.11	21.46	39.86	9.66	100.00

continued . . .

TABLE 59 (Continued)

PARTICLE-SIZE DISTRIBUTION FOR INDIVIDUAL INORGANIC PHASES
IN KENTUCKY #9 CHARS AT DIFFERENT RESIDENCE TIMES (MINERAL WEIGHT%)

D. Kentucky #9 0.5-Second Char
Particle-Size Categories (microns)

Mineral/Phase	<2.2	2.2-4.6	4.6-10	10-22	22-46	>46	TOTAL WT%
Quartz	0.11	0.51	1.42	3.06	2.68	0.29	8.07
Iron Oxide	0.12	0.18	0.95	8.39	13.78	1.60	25.01
Aluminosilicate	0.05	0.50	0.88	1.64	1.19	0.00	4.26
Ca-aluminosilicate	0.05	0.14	0.17	0.12	0.07	0.00	0.54
Fe-aluminosilicate	0.46	1.56	1.15	3.41	4.31	0.27	11.16
K-aluminosilicate	0.28	1.41	3.61	11.90	17.12	3.14	37.46
Gypsum	0.00	0.00	0.00	0.04	0.00	0.00	0.04
Ca-Silicate	0.01	0.04	0.00	0.00	0.27	0.00	0.32
Calcite	0.01	0.01	0.05	2.30	1.81	0.33	4.51
Pyrrhotite/Fe-Sulfate	0.00	0.01	0.00	0.12	0.64	0.00	0.76
Ca-Rich	0.01	0.01	0.00	0.03	0.08	0.00	0.12
Si-Rich	0.01	0.05	0.08	0.22	0.18	0.00	0.54
Unknown	0.21	0.45	0.46	1.84	3.36	0.89	7.21
TOTAL (and PSD)	1.32	4.87	8.77	33.04	45.48	6.52	100.00

E. Kentucky #9 0.8-Second Char
Particle-Size Categories (microns)

Mineral/Phase	<2.2	2.2-4.6	4.6-10	10-22	22-46	>46	TOTAL WT%
Quartz	0.02	0.18	0.34	1.57	1.79	0.44	4.35
Iron Oxide	0.03	0.10	0.36	10.63	22.10	2.33	35.54
Aluminosilicate	0.01	0.09	0.22	0.11	0.00	0.00	0.44
Ca-aluminosilicate	0.01	0.03	0.03	0.02	0.00	0.00	0.08
Fe-aluminosilicate	0.13	0.45	0.53	1.02	1.43	0.37	3.92
K-aluminosilicate	0.05	0.35	0.83	4.08	7.99	20.99	34.29
Ankerite	0.00	0.00	0.02	0.00	0.00	0.00	0.02
Ca-Silicate	0.01	0.01	0.00	0.02	0.27	0.00	0.31
Calcite	0.00	0.02	0.06	2.32	1.89	0.00	4.27
Si-Rich	0.01	0.03	0.05	0.62	0.86	0.00	1.56
Unknown	0.05	0.17	0.14	2.89	10.71	1.26	15.21
TOTAL (and PSD)	0.30	1.42	2.57	23.28	47.04	25.39	100.00

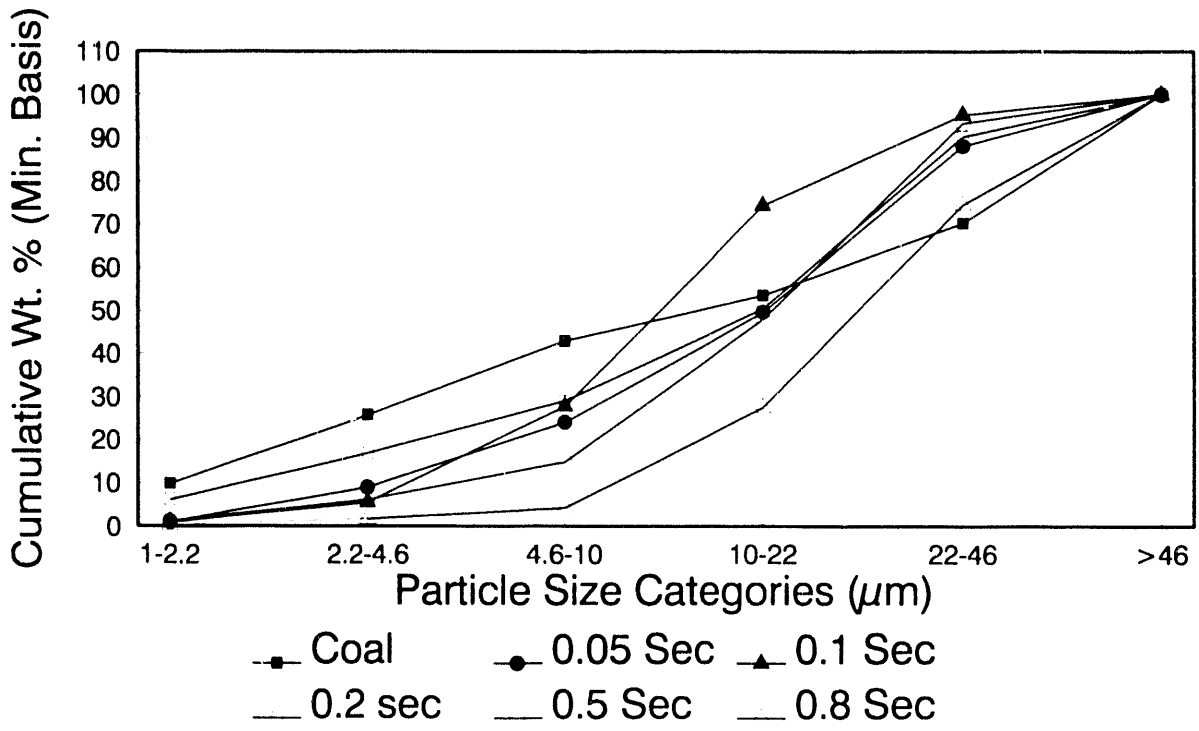

Figure 68. Kentucky #9 coal and char mineral/phase particle-size distribution.

K-aluminosilicate and iron oxide increased with time while quartz remained fairly consistent in quantity from coal to 0.8 seconds residence time. Pyrite disappeared from the CCSEM analysis after 0.05 seconds combustion because it decomposes to iron oxide and SO_2. New phases that are formed include calcium silicate, iron oxide, calcium oxide, and iron aluminosilicate. Thermal gravimetric analysis of the Kentucky #9 chars revealed near 100% carbon burnout by 0.5 seconds combustion (Figure 69).

At about 2-seconds residence time, a fly ash sample was collected which had virtually 100% carbon burnout. This fly ash was similar in inorganic phase content to the 0.8-second char with major potassium aluminosilicate, iron oxide, calcium oxide, and iron aluminosilicate (Table 60). If iron oxide is derived from pyrite and K-aluminosilicate is derived from illite, then the large amounts of these phases in char imply relatively limited reaction with other inorganics. Possibly these minerals were originally mostly excluded from coal particles and remained as separate unreactive particles throughout the combustion process. Fly ash was also collected on a bulk filter at 1500°C using unsized coal. CCSEM results from this fly ash are given in Table 61. The results are very similar to those of the 53-74-μm coal fraction fly ash.

Fly ash was also produced and collected using the multicyclone for the 53-74-μm Kentucky #9 coal. The five stages and the filters were analyzed using SEMPC. Table 62 gives the SEMPC results of the fly ash. Interaction between iron in the pyrite with aluminosilicate to form Fe-aluminosilicate was

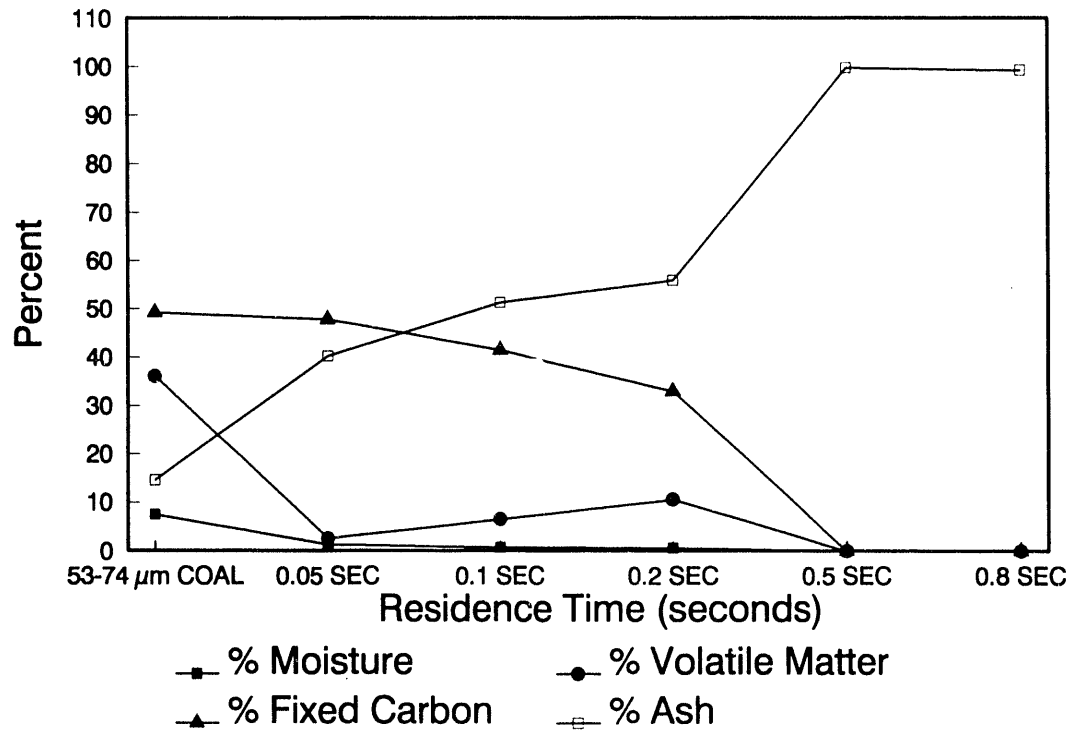

Figure 69. TGA analysis of Kentucky #9 coal and chars.

TABLE 60

MINERAL-SIZE DISTRIBUTION IN KENTUCKY #9 53-74 μm COAL BULK FILTER FLY ASH
(WT% MINERAL BASIS)

	Particle-Size Categories (μm)						
Mineral/Phase	1-2.2	2.2-4.6	4.6-10	10-22	22-46	>46	TOTAL WT%
Quartz	0.09	0.36	1.57	3.13	2.43	1.17	8.75
Iron Oxide	0.12	0.42	1.04	9.25	15.15	0.61	26.58
Aluminosilicate	0.04	0.16	0.45	1.79	2.28	0.00	4.72
Ca-aluminosilicate	0.02	0.03	0.08	0.09	0.12	0.00	0.33
Fe-aluminosilicate	0.52	1.89	2.17	3.45	4.69	0.55	13.26
K-aluminosilicate	0.20	1.18	4.06	9.38	17.65	2.88	35.35
Ankerite	0.00	0.00	0.00	0.00	0.28	0.00	0.28
Pyrite	0.00	0.00	0.00	0.00	0.23	0.00	0.23
Gypsum	0.00	0.00	0.00	0.00	0.00	0.00	0.00
Barite	0.00	0.00	0.00	0.00	0.00	0.00	0.00
Gypsum/Barite	0.00	0.00	0.00	0.00	0.00	0.00	0.00
Apatite	0.00	0.00	0.00	0.00	0.10	0.27	0.37
Ca-Silicate	0.01	0.04	0.00	0.03	0.29	0.00	0.37
Aluminosil./Gypsum	0.00	0.00	0.00	0.02	0.00	0.00	0.02
Ca-Aluminate	0.00	0.00	0.00	0.00	0.00	0.00	0.00
Spinel	0.01	0.00	0.00	0.00	0.00	0.00	0.01
Alumina	0.00	0.00	0.00	0.00	0.00	0.00	0.00

continued . . .

TABLE 60 (Continued)

MINERAL-SIZE DISTRIBUTION IN KENTUCKY #9 53-74 μm COAL BULK FILTER FLY ASH (WT% MINERAL BASIS)

	Particle-Size Categories (μm)						
Mineral/Phase	1-2.2	2.2-4.6	4.6-10	10-22	22-46	>46	TOTAL WT%
Calcite	0.00	0.02	0.26	1.47	1.09	0.25	3.10
Rutile	0.00	0.00	0.00	0.00	0.00	0.00	0.00
Dolomite	0.00	0.00	0.00	0.00	0.00	0.00	0.00
Pyrrhotite/Fe-Sulfate	0.00	0.00	0.00	0.12	0.18	0.00	0.31
Ca-Rich	0.00	0.01	0.02	0.05	0.05	0.00	0.13
Si-Rich	0.02	0.05	0.09	0.27	0.53	0.00	0.96
Periclase	0.00	0.00	0.00	0.00	0.00	0.00	0.00
Unknown	0.17	0.34	0.66	1.07	2.53	0.47	5.23
TOTAL (and PSD)	1.20	4.49	10.39	30.11	47.62	6.20	100.00

TABLE 61

CCSEM ANALYSIS OF INORGANIC PHASES IN KENTUCKY #9 BULK FILTER FLY ASH FROM UNSIZED COAL (WT%)

Mineral/Phase	<2.2	2.2-4.6	4.6-10	10-22	22-46	>46	TOTAL
Quartz	.052	.212	1.259	4.341	3.025	.000	8.890
Iron Oxide	.037	.119	1.296	7.470	11.663	1.887	22.473
Aluminosilicate	.005	.008	.197	1.000	1.425	.000	2.635
Ca-Al-Silicate	.006	.017	.042	.046	.000	.000	.112
Fe-Al-Silicate	.211	1.395	2.957	3.925	6.339	.353	15.175
K-Al-Silicate	.113	.755	4.723	15.196	15.273	1.225	37.286
Ankerite	.000	.000	.000	.044	.067	.000	.111
Pyrite	.000	.000	.000	.000	.000	.000	.000
Gypsum	.003	.000	.031	.034	.072	.000	.141
Barite	.000	.000	.000	.000	.000	.000	.000
Gypsum/Barite	.000	.000	.000	.000	.000	.000	.000
Apatite	.000	.000	.000	.000	.189	.000	.189
Ca-Silicate	.004	.021	.061	.104	.110	.000	.299
Gyp/Al-Silicate	.000	.010	.000	.000	.000	.000	.010
Ca-Aluminate	.000	.000	.000	.000	.000	.000	.000
Spinel	.000	.000	.000	.000	.000	.000	.000
Alumina	.000	.000	.000	.000	.000	.000	.000
Calcite	.013	.021	.252	.936	1.381	.388	2.992
Rutile	.007	.000	.000	.081	.000	.000	.089
Dolomite	.000	.000	.000	.000	.000	.000	.000
Pyrrhotite/Fe-Sulfate	.000	.000	.000	.050	.107	.000	.157
Ca-Rich	.002	.008	.030	.000	.000	.000	.039
Si-Rich	.022	.064	.273	.685	.441	.000	1.486
Periclase	.000	.000	.000	.000	.000	.000	.000
Unknown	.130	.406	.487	2.445	3.828	.620	7.916
Total	.606	3.034	11.608	36.356	43.922	4.473	100.000

TABLE 62

COMPOSITION OF KENTUCKY #9 FLY ASH UNDER SLAGGING CONDITIONS - SEMPC ANALYSIS (WEIGHT%)

%Mass	0.24	3.90	3.00	5.19	2.71	84.96	
Cutpoints	<2.4	2.4-6.4	6.4-10.7	10.7-17.1	17.1-18.1	>18.1	
Mean Diameter (μm)	1.0	2.4	5.1	8.2	10.7	22.3	
Phase Composition	FILTER	MC5	MC4	MC3	MC2	MC1	Weighted Average
Gehlenite	0.0	0.0	0.0	0.0	0.0	0.4	0.3
Quartz	0.4	0.4	4.1	4.9	6.6	7.0	6.5
Iron Oxide	0.8	0.0	1.0	2.5	4.9	7.7	6.9
Calcium Oxide	0.0	0.0	0.0	0.0	0.8	1.6	1.4
Ankerite (Ca, Mg, Fe CO_3)	0.0	0.0	0.0	0.0	0.0	0.8	0.0
Pure Kaolinite (amorp.)	0.0	0.0	0.0	0.0	0.0	0.8	0.7
Kaolinite Derived	0.0	3.3	8.1	7.8	7.0	2.9	3.4
Illite (amorp.)	0.0	0.0	1.0	1.2	0.4	4.9	4.3
Unclassified	98.8	96.3	85.8	83.5	79.4	74.5	76.3
Bulk Oxide Composition							
SiO_2	39.5	44.6	49.8	50.8	51.2	51.9	51.4
Al_2O_3	11.6	24.1	22.4	21.7	19.0	18.0	18.6
Fe_2O_3	20.9	18.2	17.4	17.0	19.5	19.6	19.3
TiO_2	7.0	3.4	1.5	1.8	1.0	1.0	1.2
P_2O_5	0.4	0.2	0.1	0.1	0.1	0.3	0.3
CaO	8.0	3.4	2.3	2.4	3.2	3.4	3.3
MgO	0.7	1.3	1.0	1.0	0.8	0.9	0.9
Na_2O	0.4	1.0	0.7	0.6	0.5	0.5	0.5
K_2O	2.9	2.2	2.8	3.0	3.7	3.5	3.4
SO_3	8.0	0.9	0.6	0.4	0.4	0.2	0.3
BaO	0.1	0.2	0.1	0.1	0.1	0.1	0.1
Mn_2O_7	0.2	0.2	0.1	0.2	0.3	0.2	0.2
ClO	0.4	0.3	1.0	0.9	0.2	0.4	0.4
Amorphous Oxide Composition							
SiO_2	43.7	45.0	49.3	49.3	49.8	55.9	54.7
Al_2O_3	12.8	24.5	24.4	23.7	21.4	22.5	22.6
Fe_2O_3	22.0	18.4	16.8	16.0	18.0	11.8	12.6
TiO_2	7.0	3.4	1.5	1.8	1.0	1.0	1.2
P_2O_5	0.4	0.2	0.2	0.1	0.1	0.9	0.8
CaO	8.9	3.5	2.6	3.6	3.7	1.3	1.6
MgO	0.8	1.3	1.1	1.1	0.9	1.1	1.1
Na_2O	0.4	1.0	0.7	0.7	0.6	0.6	0.6
K_2O	3.2	2.3	3.0	3.2	4.1	4.4	4.2
SO_3	0.0	0.0	0.0	0.0	0.0	0.0	0.0
BaO	0.1	0.1	0.1	0.1	0.1	0.1	0.1
Mn_2O_7	0.2	0.2	0.1	0.2	0.2	0.1	0.1
ClO	0.0	0.0	0.0	0.0	0.0	0.0	0.0

evident, by comparing this fly ash with the original unsized coal CCSEM analysis (Table 58). The iron content remained nearly the same in all size fractions. Calcium and sulfur were enriched and aluminum and silicon depleted in the smallest fraction of the multicyclone. Most of the fly ash mass (85%) was greater than 22.3 μm (Table 62).

4.5 Characterization of San Miguel Coal

San Miguel lignite was characterized for inorganic constituents using proximate/ultimate analysis, x-ray diffusion, x-ray fluorescence, chemical fractionation, and CCSEM analysis. San Miguel had about 53% ash on a dry basis and was very low in iron (1.9%) and calcium (3.5%) (Table 63). The total ash contents and elemental oxide chemistries were similar for the different coal size fractions. Sodium content was moderately low at 2.5% of the ash. Sodium and calcium were 65% and 72% organically bound, respectively in the 53-74-μm fraction, as shown in Table 64. The major minerals in the San Miguel lignite, as determined by CCSEM, were quartz, clinoptilolite, and an unknown aluminosilicate that was probably mixed clay or montmorillonite (Table 65). Mineralogic compositions on a mineral basis were similar for 38-53, 53-74, and 74-106-μm coal fractions; however, larger minerals were observed with increased coal size (Table 66). Detailed results of coal mineral particle-size distributions for the three coal sized fractions and the unsized coal are given in Table 66.

4.5.1 Characterization of San Miguel Char and Fly Ash

Table 67 contains the compositions for San Miguel short residence time char and coal as derived from CCSEM analysis. Quartz and K-aluminosilicate content remained fairly consistent through the combustion process, relative to their content in the original coal. Aluminosilicate was slightly reduced, and Fe-aluminosilicate and calcium silicate were slightly increased. Table 68 gives CCSEM results for each char. Results from thermal gravimetric analysis on each char showed 100% carbon burnout by 0.5 seconds (Figure 70).

The particle-size distributions of the char inorganic phases showed coalescence with increased residence time (Figure 71). Smaller minerals between 1 and 10 μm decreased in abundance, and large inorganic phases 22-46 μm increased in abundance progressively until 0.5 seconds into combustion. The 0.5 and 0.8-second chars were nearly identical in particle size and composition: the result of near 100% carbon burnout by 0.5 seconds of combustion (Figure 70).

Fly ash was produced at a residence time of about 2.6 seconds and collected on bulk filters for the San Miguel 53-74 μm and unsized coals. Table 69 compares the original mineral contents and the inorganic phase composition of the fly ash for these coals. In general, these San Miguel fly ashes were similarly composed. Aluminosilicate and K-aluminosilicate decreased during combustion, probably through interaction with the other mineral or organically bound components. The unsized coal fly ash had much more aluminosilicate and quartz in the >46-μm category, as observed in the particle-size distribution (Table 70). This shows the effect of removing larger-sized minerals during the sieving of the coal.

TABLE 63

RESULTS OF SAN MIGUEL COAL AND ASH ANALYSIS[a]

Proximate, Wt%	Bulk Coal	38-53 μm	53-74 μm	74-106 μm
Moisture	12.90	12.80	11.30	13.40
Volatile Matter	28.26	28.36	28.83	29.54
Fixed Carbon	18.46	17.67	16.85	17.01
Ash	53.28	53.97	54.32	53.45
Ultimate, Wt%				
Carbon	29.14	28.82	28.62	28.94
Hydrogen	2.39	2.34	2.41	2.39
Nitrogen	0.59	0.65	0.65	0.63
Oxygen (diff.)	12.58	12.27	12.05	12.38
Sulfur	2.00	1.93	1.93	2.19
Ash Analysis, Wt%				
SiO_2	66.3	66.7	66.2	66.2
Al_2O_3	19.1	19.5	19.3	19.4
Fe_2O_3	1.9	2.0	2.3	1.7
TiO_2	1.1	1.1	1.1	1.1
P_2O_5	0.1	0.0	0.1	0.1
CaO	3.5	3.5	3.3	3.7
MgO	0.9	1.0	1.0	1.0
Na_2O	2.5	2.1	2.1	2.5
K_2O	2.2	2.1	2.2	2.2
SO_3	2.6	1.8	2.4	2.2
Heating Valve, Btu/lb				
Calc. Calorific Value	4284	4231	4287	4256

[a] Results reported on a dry basis except for the moisture determination.

TABLE 64

CHEMICAL FRACTIONATION RESULTS FOR SAN MIGUEL 53-74-μm COAL

	Initial μg/g dry coal	% Removed by H_2O	% Removed by NH_4OAc	% Removed by HCl	% Remaining
Na	19,700	28	72	0	0
Mg	6,220	0	16	0	84
Al	11,030	2	0	7	91
Si	348,800	0	2	0	98
Ca	26,300	0	65	25	10
Fe	12,700	6	0	49	45

TABLE 65

MINERAL CONTENT FOR SAN MIGUEL COAL SIZE FRACTIONS
(Wt% Mineral Basis)

Wt% Mineral Basis	Unsized	38-53 μm	53-74 μm	74-106 μm
Quartz	16.27	16.40	15.47	16.67
Iron Oxide	0.12	0.06	0.22	0.00
Aluminosilicate	21.75	14.21	16.02	21.27
Ca-aluminosilicate	0.28	0.14	20.7	0.57
Fe-aluminosilicate	0.03	0.10	0.52	0.03
K-aluminosilicate	45.76	52.48	29.20	37.44
Ankerite	0.00	0.00	0.00	0.00
Pyrite	0.93	1.91	1.14	0.63
Gypsum	1.01	1.47	0.70	1.91
Barite	0.08	0.00	0.00	0.12
Gypsum/Barite	0.00	0.00	0.00	0.00
Apatite	0.00	0.00	0.00	0.00
Ca-Silicate	0.02	0.00	0.25	0.05
Aluminosil./Gypsum	0.09	0.00	0.67	0.42
Ca-Aluminate	0.00	0.00	0.02	0.01
Spinel	0.00	0.01	0.00	0.00
Alumina	0.00	0.00	0.02	0.01
Calcite	0.00	0.00	0.00	0.03
Rutile	0.05	0.52	0.00	0.03
Dolomite	0.00	0.00	0.00	0.00
Pyrrhotite	0.21	0.00	0.13	0.08
Ca-Rich	0.00	0.00	0.00	0.00
Si-Rich	5.83	6.80	10.33	7.45
Periclase	0.00	0.00	0.00	0.01
Unknown	7.59	5.90	13.26	13.28
Wt% Total Minerals (Coal Basis)	44.9	17.7	24.7	43.8

TABLE 66

MINERAL-SIZE DISTRIBUTION IN SAN MIGUEL BULK AND SIZED FRACTIONS (WT% MINERAL BASIS)

	San Miguel Bulk Coal Particle-Size Categories (μm)							COAL
							TOTAL	BASIS
Mineral/Phase	1-2.2	2.2-4.6	4.6-10	10-22	22-46	>46	WT%	WT%
Quartz	1.5	3.5	3.4	3.5	3.8	0.6	16.3	7.45
Iron Oxide	0.0	0.0	0.0	0.0	0.1	0.0	0.1	0.05
Aluminosilicate	1.8	4.7	5.0	3.1	4.1	3.2	21.8	9.98
Ca-aluminosilicate	0.1	0.0	0.0	0.0	0.1	0.0	0.3	0.13
Fe-aluminosilicate	0.0	0.0	0.0	0.0	0.0	0.0	0.0	0.01
K-aluminosilicate	1.2	3.6	10.4	12.5	14.8	3.3	45.8	20.00
Pyrite	0.0	0.2	0.2	0.1	0.4	0.0	0.9	0.42
Gypsum	0.0	0.2	0.2	0.3	0.2	0.0	1.0	0.45
Barite	0.0	0.0	0.0	0.0	0.0	0.0	0.1	0.04
Ca-Silicate	0.0	0.0	0.0	0.0	0.0	0.0	0.0	0.01
Aluminosil./Gypsum	0.0	0.0	0.0	0.0	0.0	0.0	0.1	0.04
Rutile	0.0	0.0	0.0	0.1	0.0	0.0	0.1	0.02
Pyrrhotite	0.0	0.0	0.1	0.1	0.0	0.0	0.2	0.10
Si-Rich	0.8	1.1	2.3	0.8	0.4	0.3	5.8	2.81
Unknown	0.7	1.3	1.4	1.9	2.3	0.0	7.6	3.42
TOTAL (and PSD)	6.2	14.7	23.0	22.4	26.2	7.4	100.0	44.92

	San Miguel 38-53-μm Coal Particle-Size Categories (μm)							COAL
							TOTAL	BASIS
Mineral/Phase	1-2.2	2.2-4.6	4.6-10	10-22	22-46	>46	WT%	WT%
Quartz	2.4	5.8	5.1	2.7	0.5	0.0	16.4	2.90
Iron Oxide	0.1	0.0	0.0	0.0	0.0	0.0	0.1	0.01
Aluminosilicate	2.1	5.8	4.8	1.1	0.5	0.0	14.2	2.52
Ca-aluminosilicate	0.1	0.0	0.0	0.0	0.0	0.0	0.1	0.03
Fe-aluminosilicate	0.1	0.0	0.0	0.0	0.0	0.0	0.1	0.02
K-aluminosilicate	2.3	9.2	27.2	11.1	2.7	0.0	52.5	9.28
Pyrite	0.1	0.0	0.6	0.5	0.7	0.0	1.9	0.34
Gypsum	0.1	0.6	0.4	0.3	0.1	0.0	1.5	0.26
Spinel	0.0	0.0	0.0	0.0	0.0	0.0	0.0	0.00
Rutile	0.1	0.0	0.4	0.0	0.0	0.0	0.5	0.09
Si-Rich	1.2	2.0	3.0	0.5	0.1	0.0	6.8	1.21
Unknown	1.4	1.3	2.1	0.8	0.2	0.0	5.9	1.04
TOTAL (and PSD)	9.9	24.8	43.5	17.1	4.7	0.0	100.0	17.70

	San Miguel 53-74-μm Coal Particle-Size Categories (μm)							COAL
							TOTAL	BASIS
Mineral/Phase	1-2.2	2.2-4.6	4.6-10	10-22	22-46	>46	WT%	WT%
Quartz	1.7	5.7	2.7	2.9	2.5	0.0	15.5	3.80
Iron Oxide	0.2	0.0	0.0	0.0	0.0	0.0	0.2	0.06
Aluminosilicate	2.0	5.6	5.3	1.3	1.6	0.1	16.0	3.97
Ca-aluminosilicate	0.5	0.6	1.0	0.0	0.0	0.0	2.1	0.52
Fe-aluminosilicate	0.2	0.3	0.0	0.0	0.0	0.0	0.5	0.13
K-aluminosilicate	2.2	6.9	12.3	9.2	8.3	0.4	39.2	9.59
Pyrite	0.0	0.0	0.0	0.2	0.9	0.0	1.1	0.27
Gypsum	0.1	0.2	0.0	0.2	0.2	0.0	0.7	0.17
Ca-Silicate	0.1	0.2	0.0	0.0	0.0	0.0	0.3	0.06
Aluminosil./Gypsum	0.2	0.2	0.3	0.0	0.0	0.0	0.7	0.17
Alumina	0.0	0.0	0.0	0.0	0.0	0.0	0.0	0.00
Pyrrhotite	0.0	0.0	0.0	0.0	0.1	0.0	0.1	0.03
Si-Rich	1.6	3.8	4.3	0.5	0.2	0.0	10.3	2.57
Unknown	3.0	4.2	5.2	0.5	0.4	0.0	13.3	3.30
TOTAL (and PSD)	12.0	27.6	31.0	14.8	14.2	0.5	100.0	24.65

continued . . .

TABLE 66 (Continued)

MINERAL-SIZE DISTRIBUTION IN SAN MIGUEL BULK AND SIZED FRACTIONS
(WT% MINERAL BASIS)

	San Miguel 74-106-μm Coal Particle-Size Categories (μm)							COAL
							TOTAL	BASIS
Mineral/Phase	1-2.2	2.2-4.6	4.6-10	10-22	22-46	>46	WT%	WT%
Quartz	2.2	3.9	5.0	2.0	3.0	0.7	16.7	7.54
Aluminosilicate	1.5	3.6	5.0	1.5	5.1	4.5	21.3	9.31
Ca-aluminosilicate	0.2	0.2	0.2	0.0	0.0	0.0	0.6	0.27
Fe-aluminosilicate	0.0	0.0	0.0	0.0	0.0	0.0	0.0	0.01
K-aluminosilicate	1.2	2.6	8.0	6.5	15.4	3.8	37.4	15.89
Pyrite	0.0	0.0	0.0	0.0	0.6	0.0	0.6	0.25
Gypsum	0.1	0.1	0.1	0.7	1.0	0.0	1.9	0.78
Barite	0.0	0.1	0.0	0.0	0.0	0.0	0.3	0.06
Ca-Silicate	0.0	0.0	0.0	0.0	0.0	0.0	0.1	0.02
Aluminosil./Gypsum	0.2	0.1	0.1	0.0	0.0	0.0	0.4	0.20
Alumina	0.0	0.0	0.0	0.0	0.0	0.0	0.0	0.01
Calcite	0.0	0.0	0.0	0.0	0.0	0.0	0.0	0.01
Rutile	0.0	0.0	0.0	0.0	0.0	0.0	0.0	0.01
Pyrrhotite	0.0	0.0	0.0	0.1	0.0	0.0	0.1	0.03
Si-Rich	1.7	2.8	1.5	0.5	0.6	0.3	7.4	3.45
Periclase	0.0	0.0	0.0	0.0	0.0	0.0	0.0	0.01
Unknown	1.9	4.0	2.7	1.6	1.8	1.3	13.3	5.99
TOTAL (and PSD*)	9.0	17.4	22.6	12.9	27.5	10.6	100.0	43.83

* Particle-Size Distribution

TABLE 67

COMPARISON OF SAN MIGUEL COAL AND CHARS
(TOTAL WT% - CCSEM ANALYSIS)

	Coal	0.05 Sec	0.1 Sec	0.2 Sec	0.5 Sec	0.8 Sec
Quartz	15.47	22.48	23.59	25.06	25.67	21.94
Iron Oxide	0.22	0.39	1.30	0.69	0.52	1.18
Aluminosilicate	16.02	16.98	10.57	3.62	14.58	12.42
Ca-aluminosilicate	2.07	1.23	3.69	5.23	1.86	3.57
Fe-aluminosilicate	0.52	0.05	0.42	1.64	0.69	1.35
K-aluminosilicate	39.20	40.45	40.08	26.46	39.43	38.46
Pyrite	1.14	0.51	0.00	0.00	0.00	0.03
Gypsum	0.70	0.42	0.14	1.31	0.38	0.15
Barite	0.00	0.00	0.03	0.04	0.00	0.05
Gypsum/Barite	0.00	0.02	0.00	0.00	0.00	0.00
Ca-Silicate	0.25	0.22	0.59	3.76	1.04	1.12
Aluminosil./Gypsum	0.67	0.12	0.50	0.02	0.00	0.00
Ca-Aluminate	0.00	0.00	0.00	0.01	0.00	0.00
Alumina	0.02	0.13	0.00	0.01	0.00	0.00
Calcite	0.00	0.00	0.00	0.04	0.00	0.03
Rutile	0.00	0.00	0.00	0.00	0.09	0.03
Pyrrhotite/Fe-Sulfate	0.13	0.00	0.08	0.01	0.00	0.00
Ca-Rich	0.00	0.00	0.05	0.01	0.00	0.01
Si-Rich	10.33	11.20	11.37	21.94	8.43	11.86
Unknown	13.26	5.80	7.59	12.15	7.31	7.82

TABLE 68

PARTICLE-SIZE DISTRIBUTION FOR INDIVIDUAL INORGANIC PHASES
IN SAN MIGUEL CHARS AT DIFFERENT RESIDENCE TIMES (MINERAL WEIGHT %)

A. San Miguel 0.05-Second Char
Particle-Size Categories (microns)

Mineral/Phase	1-2.2	2.2-4.6	4.6-10	10-22	22-46	>46	TOTAL WT%
Quartz	0.26	1.22	2.94	6.81	10.62	0.63	22.48
Iron Oxide	0.01	0.00	0.00	0.00	0.38	0.00	0.39
Aluminosilicate	0.06	0.32	0.79	1.96	9.96	3.90	16.98
Ca-aluminosilicate	0.18	0.45	0.30	0.31	0.00	0.00	1.23
Fe-aluminosilicate	0.01	0.00	0.00	0.04	0.00	0.00	0.05
K-aluminosilicate	0.20	0.90	5.42	1.91	22.43	0.58	40.45
Pyrite	0.00	0.00	0.08	0.00	0.44	0.00	0.51
Gypsum	0.00	0.01	0.00	0.12	0.28	0.00	0.42
Gypsum/Barite	0.00	0.02	0.00	0.00	0.00	0.00	0.02
Ca-Silicate	0.05	0.02	0.00	0.15	0.00	0.00	0.22
Aluminosil./Gypsum	0.06	0.06	0.00	0.00	0.00	0.00	0.12
Alumina	0.00	0.00	0.00	0.13	0.00	0.00	0.13
Si-Rich	0.28	1.11	2.01	2.86	3.06	1.90	11.20
Unknown	0.39	0.77	1.23	1.55	1.87	0.00	5.80
TOTAL (and PSD)	1.50	4.86	12.77	24.84	49.02	7.01	100.00

B. San Miguel 0.1-Second Char
Particle-Size Categories (microns)

Mineral/Phase	1-2.2	2.2-4.6	4.6-10	10-22	22-46	>46	TOTAL WT%
Quartz	0.52	1.70	2.66	3.99	13.04	1.70	23.59
Iron Oxide	0.01	0.02	0.00	0.11	1.16	0.00	1.30
Aluminosilicate	0.22	1.07	1.41	1.45	4.85	1.58	10.57
Ca-aluminosilicate	0.41	1.50	1.09	0.54	0.16	0.00	3.69
Fe-aluminosilicate	0.02	0.06	0.13	0.21	0.00	0.00	0.42
K-aluminosilicate	0.43	1.92	5.99	7.48	21.97	2.28	40.08
Gypsum	0.01	0.01	0.00	0.12	0.00	0.00	0.14
Barite	0.00	0.03	0.00	0.00	0.00	0.00	0.03
Ca-Silicate	0.20	0.27	0.04	0.07	0.00	0.00	0.59
Aluminosil./Gypsum	0.09	0.10	0.00	0.00	0.00	0.00	0.50
Pyrrhotite/Fe-Sulfate	0.00	0.00	0.00	0.00	0.00	0.00	0.08
Ca-Rich	0.00	0.05	0.00	0.00	0.00	0.00	0.05
Si-Rich	0.58	2.32	2.82	1.61	4.04	0.00	11.37
Unknown	0.65	1.20	1.48	1.13	3.14	0.00	7.59
TOTAL (and PSD)	3.14	10.24	15.63	16.77	48.66	5.56	100.00

continued . . .

TABLE 68 (Continued)

PARTICLE-SIZE DISTRIBUTION FOR INDIVIDUAL INORGANIC PHASES
IN SAN MIGUEL CHARS AT DIFFERENT RESIDENCE TIMES (MINERAL WEIGHT %)

C. San Miguel 0.2-Second Char
Particle-Size Categories (microns)

Mineral/Phase	1-2.2	2.2-4.6	4.6-10	10-22	22-46	>46	TOTAL WT%
Quartz	0.25	1.18	4.95	7.60	10.01	1.07	25.06
Iron Oxide	0.03	0.00	0.09	0.25	0.33	0.00	0.69
Aluminosilicate	0.17	0.83	2.19	0.24	0.20	0.00	3.62
Ca-aluminosilicate	0.31	1.30	2.06	0.58	0.99	0.00	5.23
Fe-aluminosilicate	0.02	0.07	0.00	0.60	0.95	0.00	1.64
K-aluminosilicate	0.31	1.58	8.05	5.43	8.02	1.07	24.46
Gypsum	0.00	0.01	0.05	0.30	0.49	0.46	1.31
Barite	0.00	0.00	0.00	0.04	0.00	0.00	0.04
Ca-Silicate	0.13	0.33	0.40	1.80	1.11	0.00	3.76
Aluminosil./Gypsum	0.00	0.00	0.00	0.02	0.00	0.00	0.02
Ca-Aluminate	0.00	0.01	0.00	0.00	0.00	0.00	0.01
Alumina	0.01	0.00	0.00	0.00	0.00	0.00	0.01
Calcite	0.00	0.00	0.00	0.04	0.00	0.00	0.04
Pyrrhotite/Fe-Sulfate	0.01	0.00	0.00	0.00	0.00	0.00	0.01
Ca-Rich	0.01	0.00	0.00	0.00	0.00	0.00	0.01
Si-Rich	0.25	1.27	2.05	7.90	9.87	0.61	21.94
Unknown	0.31	0.67	1.24	4.66	5.27	0.00	12.15
TOTAL (and PSD)	1.81	7.24	21.08	28.43	37.23	3.22	100.00

D. San Miguel 0.5-Second Char
Particle-Size Categories (microns)

Mineral/Phase	1-2.2	2.2-4.6	4.6-10	10-22	22-46	>46	TOTAL WT%
Quartz	0.14	0.63	1.73	4.31	15.48	3.38	25.67
Iron Oxide	0.01	0.02	0.00	0.00	0.00	0.50	0.52
Aluminosilicate	0.06	0.20	0.83	1.36	8.83	3.30	14.58
Ca-aluminosilicate	0.08	0.30	0.56	0.33	0.58	0.00	1.86
Fe-aluminosilicate	0.02	0.02	0.00	0.16	0.50	0.00	0.69
K-aluminosilicate	0.30	0.78	3.53	7.80	23.04	3.99	39.43
Gypsum	0.00	0.00	0.00	0.03	0.35	0.00	0.38
Ca-Silicate	0.05	0.10	0.25	0.03	0.61	0.00	1.04
Rutile	0.00	0.00	0.04	0.06	0.00	0.00	0.09
Si-Rich	0.08	0.59	0.90	1.99	4.69	0.18	8.43
Unknown	0.16	0.35	0.66	1.13	4.16	0.85	7.31
TOTAL (and PSD)	0.91	2.99	8.48	17.18	58.24	12.20	100.00

continued . . .

TABLE 68 (Continued)

PARTICLE-SIZE DISTRIBUTION FOR INDIVIDUAL INORGANIC PHASES
IN SAN MIGUEL CHARS AT DIFFERENT RESIDENCE TIMES (MINERAL WEIGHT %)

	E. San Miguel 0.8-Second Char Particle-Size Categories (microns)						
Mineral/Phase	1-2.2	2.2-4.6	4.6-10	10-22	22-46	>46	TOTAL WT%
Quartz	0.16	0.72	1.24	4.43	13.32	2.07	21.94
Iron Oxide	0.01	0.00	0.00	0.08	0.37	0.71	1.18
Aluminosilicate	0.07	0.36	1.06	2.24	7.59	1.10	12.42
Ca-aluminosilicate	0.14	0.53	0.58	0.61	1.29	0.43	3.57
Fe-aluminosilicate	0.01	0.05	0.00	0.09	0.46	0.74	1.35
K-aluminosilicate	0.26	1.17	3.47	6.57	22.84	3.14	38.46
Pyrite	0.00	0.03	0.00	0.00	0.00	0.00	0.03
Gypsum	0.00	0.00	0.00	0.03	0.12	0.00	0.15
Barite	0.00	0.00	0.00	0.05	0.00	0.00	0.05
Ca-Silicate	0.05	0.20	0.06	0.17	0.65	0.00	1.12
Calcite	0.00	0.00	0.00	0.03	0.00	0.00	0.03
Rutile	0.00	0.00	0.00	0.03	0.00	0.00	0.03
Ca-Rich	0.00	0.01	0.00	0.00	0.00	0.00	0.01
Si-Rich	0.17	0.85	2.00	1.90	6.26	0.67	11.86
Unknown	0.22	0.36	0.40	1.23	4.12	1.50	7.82
TOTAL (and PSD)	1.10	4.28	8.80	17.45	58.01	10.3	100.00

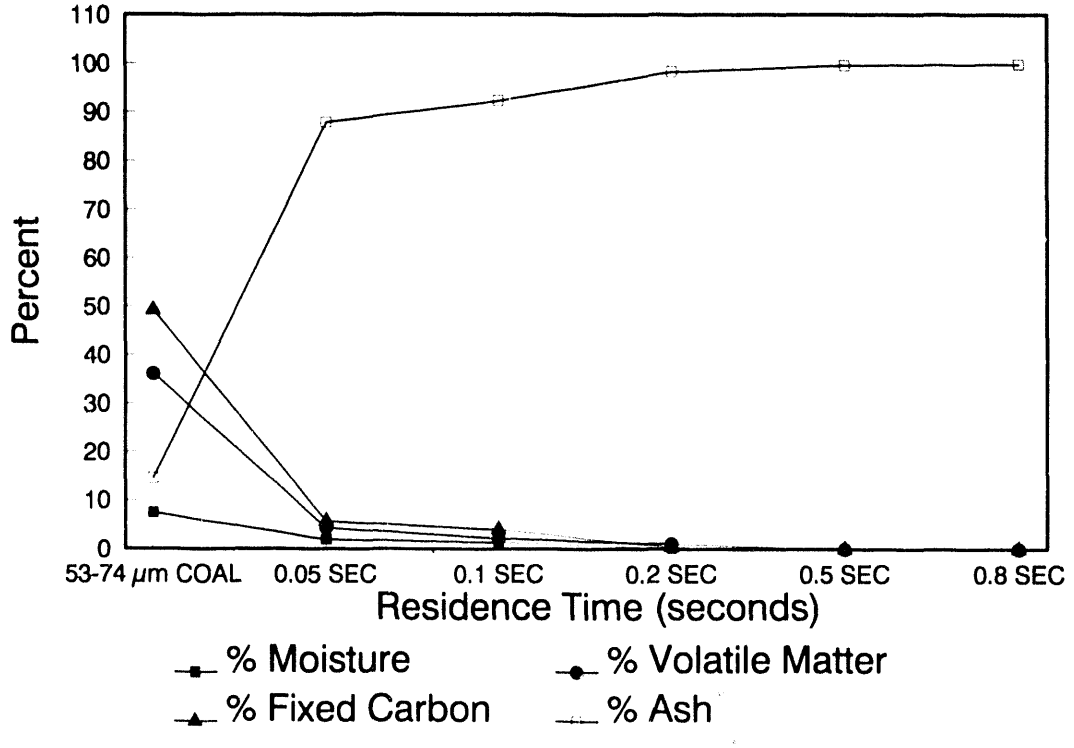

Figure 70. TGA analysis of San Miguel coal and chars.

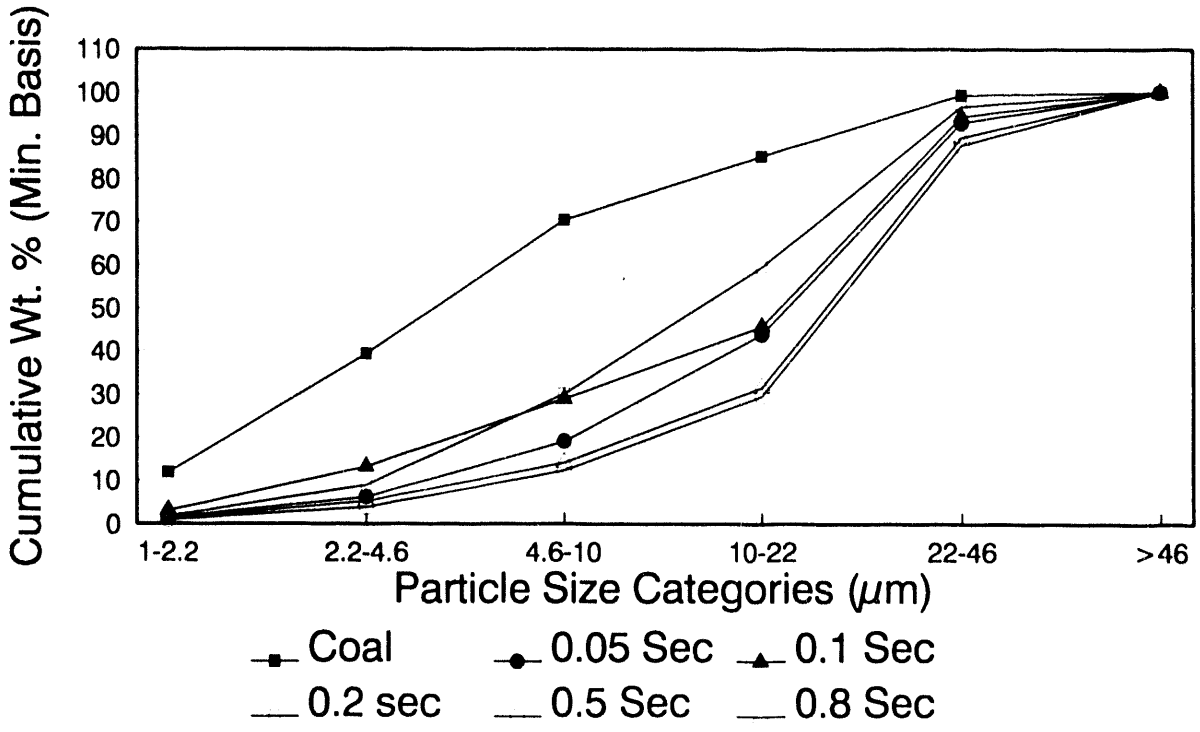

Figure 71. San Miguel coal and char mineral/phase particle-size distribution.

TABLE 69

COMPARISON MINERAL CONTENT FOR SAN MIGUEL COAL AND FLY ASH
(TOTAL WT% - CCSEM ANALYSIS)

	53-74 μm Coal Minerals	Unsized Coal Minerals	53-74 μm Fly Ash Minerals	Unsized Fly Ash Minerals
Quartz	15.47	16.27	14.42	18.67
Iron Oxide	0.22	0.12	0.94	0.07
Aluminosilicate	16.02	21.75	10.32	9.87
Ca-aluminosilicate	2.07	0.28	2.75	4.61
Fe-aluminosilicate	0.52	0.03	2.16	1.49
K-aluminosilicate	39.20	45.76	43.97	39.73
Pyrite	1.14	0.93	0.00	0.00
Gypsum	0.70	1.01	0.17	0.12
Barite	0.00	0.08	0.00	0.00
Ca-Silicate	0.25	0.02	0.85	1.08
Aluminosil./Gypsum	0.67	0.09	0.00	0.08
Alumina	0.02	0.00	0.00	0.00
Calcite	0.00	0.00	0.09	0.25
Rutile	0.00	0.05	0.00	0.00
Pyrrhotite/Fe-Sulfate	0.13	0.21	0.00	0.00
Si-Rich	10.33	5.83	14.17	14.41
Unknown	13.26	7.59	10.16	9.62

TABLE 70

PARTICLE-SIZE DISTRIBUTION IN SAN MIGUEL FLY ASH
FROM 53-74 μm AND UNSIZED COAL FRACTIONS
(WT% MINERAL BASIS)

	San Miguel Fly Ash from 53-74 μm Particle-Size Categories (μm)						
Mineral/Phase	1-2.2	2.2-4.6	4.6-10	10-22	22-46	>46	TOTAL WT%
Quartz	0.12	0.46	2.61	3.04	7.86	0.33	14.42
Iron Oxide	0.00	0.00	0.00	0.00	0.94	0.00	0.94
Aluminosilicate	0.00	0.00	0.00	3.22	6.34	0.76	10.32
Ca-aluminosilicate	0.03	0.00	0.19	0.69	1.44	0.40	2.75
Fe-aluminosilicate	0.03	0.05	0.72	0.46	0.56	0.34	2.16
K-aluminosilicate	0.10	0.51	1.76	7.67	25.25	8.67	43.97
Gypsum	0.01	0.06	0.00	0.02	0.09	0.00	0.17
Ca-Silicate	0.05	0.11	0.32	0.25	0.12	0.00	0.85
Calcite	0.00	0.00	0.00	0.09	0.00	0.00	0.09
Si-Rich	0.04	0.43	1.44	3.28	7.78	1.21	14.17
Unknown	0.28	0.63	2.30	1.46	4.46	1.03	10.16
TOTAL (and PSD)	0.65	2.24	9.33	20.17	54.84	12.76	100.00

	San Miguel Fly Ash From Unsized Coal Particle-Size Categories (μm)						
Mineral/Phase	1-2.2	2.2-4.6	4.6-10	10-22	22-46	>46	TOTAL WT%
Quartz	0.04	0.12	0.45	3.93	9.44	4.70	18.67
Iron Oxide	0.00	0.01	0.06	0.00	0.00	0.00	0.07
Aluminosilicate	0.02	0.15	0.44	1.43	3.47	4.35	9.87
Ca-aluminosilicate	0.08	0.48	0.64	0.87	2.27	0.29	4.61
Fe-aluminosilicate	0.00	0.01	0.00	0.39	0.44	0.64	1.49
K-aluminosilicate	0.12	0.52	1.72	7.70	21.58	8.10	39.73
Gypsum	0.00	0.00	0.01	0.03	0.08	0.00	0.12
Ca-Silicate	0.01	0.06	0.03	0.24	0.75	0.00	1.08
Aluminosil./Gypsum	0.00	0.00	0.00	0.00	0.08	0.00	0.08
Calcite	0.00	0.00	0.04	0.05	0.16	0.00	0.25
Si-Rich	0.05	0.38	0.78	2.56	6.35	4.30	14.41
Unknown	0.07	0.23	0.59	1.52	3.69	3.53	9.62
TOTAL (and PSD*)	0.38	1.96	4.75	18.71	48.30	25.90	100.00

* Particle-Size Distribution

Fly ash was also collected in the multicyclone, and the individual stages were analyzed using SEMPC. Table 71 gives the results from the SEMPC analysis. The major phases identified by molar ratios in the fly ash were quartz or silica, amorphous illite, and amorphous montmorillonite. The amorphous illite was actually the derivative of potassium-rich zeolites in the coal. Most of the fly ash mass (89%) was greater than 22 μm in average diameter. It was observed that SiO_2 and K_2O oxides increased with increasing fly ash particle size, corresponding to greater amounts of the amorphous illite-derived phase. The finer fly ash fraction had more CaO and Al_2O_3. The amorphous and bulk compositions of the ash were similar (Table 71).

4.6 Particle-Size Distribution of Kentucky #9 and San Miguel Fly Ash

Kentucky #9 and San Miguel coals were sized into three categories and combusted at 1300, 1400, and 1500°C. Each of the 18 samples were collected in both a five-stage multicyclone and a Mark V cascade impactor to gather particle-size data. The coal minerals from the 1500°C fly ash were analyzed with CCSEM. A bulk coal size was obtained using Malvern analysis. CCSEM was also run on a sample of the middle coal size at 1500°C to compare with the multicyclone and impactor data.

Figures 72-77 show the distribution of the three sizes of coal (38-53 μm, 53-74 μm, 74-106 μm) of Kentucky #9 combusted at 1300, 1400, and 1500°C as collected with the multicyclone. All six figures show no difference in particle distribution. The six figures are made of only nine actual distributions that, if all were placed on one graph, would constitute one solid line; thus no difference in particle-size distribution is evident in the Kentucky #9 at the parameters tested with the multicyclone.

Figures 78-83 show distributions of the Kentucky #9 fly ash at the same conditions as above, but collected with the cascade impactor. The data is very similar to that above with only one condition sticking out slightly. The 38-53-μm coal sample combusted at 1300°C has a slightly greater abundance of larger particles.

Figures 84-89 are the size distributions of the San Miguel fly ash at the nine different conditions as collected with the multicyclone. The only change in distributions occurred in the 75-106-μm micron coal size. The higher the temperature, the greater the particle-size distribution (i.e. more larger particles) was. This would possibly imply the occurrence of coalescence in this coal size only. The other two coal sizes show no substantial differences with temperature.

Figures 90-95 show the size distributions of the San Miguel as collected with the cascade impactor. The data shows that the smaller the initial coal size and the lower the temperature, the larger the particle sizes, with the exception of the 74-106-μm coal.

TABLE 71

COMPOSITION OF SAN MIGUEL FLY ASH UNDER SLAGGING CONDITIONS - SEMPC ANALYSIS (WEIGHT%)

%Mass	0.70	2.70	2.00	3.30	2.40	88.90	
Cutpoints	<2.1	2.1-5.3	5.3-8.4	8.4-14.0	14-16.6	>16.6	
Mean Diameter (μm)	0.9	2	4	6.6	9.3	21.3	
Phase Composition	FILTER	MC5	MC4	MC3	MC2	MC1	Weighted Average
Gehlenite	0.0	0.8	2.0	2.1	0.0	0.0	0.1
Anorthite	35.0	7.8	3,3	1.6	1.6	0.0	0.6
Albite	0.0	0.0	0.0	0.0	2.9	0.0	0.1
Quartz	0.0	0.0	2.5	4.5	5.3	5.3	5.0
Iron Oxide	0.0	0.0	0.0	0.0	0.0	0.8	0.7
Calcium Oxide	0.0	0.0	0.0	0.0	0.0	0.0	0.0
Calcium Silicate	0.0	0.4	1.2	0.0	0.0	0.0	0.0
Magnesium Oxide	0.0	0.0	0.0	0.0	0.0	0.0	0.0
Anhydrite	0.0	0.0	0.0	0.0	0.0	0.0	0.0
Pure Kaolinite (Amorp.)	0.0	0.4	0.4	0.4	1.2	0.8	0.8
Illite (Amorp.)	0.0	1.2	7.8	6.6	10.7	25.5	23.3
Montmorillonite (Amorp.)	60.1	14.4	22.1	12.3	6.6	4.1	5.5
Unclassified	4.9	74.5	60.2	72.4	71.6	63.4	63.7
Bulk Oxide Composition							
SiO_2	55.3	59.4	61.2	63.7	66.5	70.0	69.1
Al_2O_3	16.4	20.4	19.6	18.9	18.2	16.5	16.8
Fe_2O_3	3.0	2.3	2.3	2.8	1.4	2.9	2.8
TiO_2	3.0	2.2	1.9	1.7	1.3	1.1	1.2
P_2O_5	0.2	0.2	0.1	0.1	0.0	0.0	0.0
CaO	12.2	8.7	8.3	6.8	4.7	2.7	3.2
MgO	0.8	0.7	0.7	0.6	0.5	0.4	0.4
Na_2O	1.1	1.2	1.3	1.2	3.1	1.4	1.4
K_2O	1.7	1.8	1.8	1.9	2.0	2.4	2.3
SO_3	5.5	0.9	0.6	0.5	0.5	1.3	1.3
BaO	0.6	0.4	0.2	0.2	0.3	0.2	0.2
Mn_2O_7	0.2	0.2	0.2	0.2	0.2	0.2	0.2
ClO	0.0	1.5	1.7	1.4	1.3	0.8	0.9
Amorphous Oxide Composition							
SiO_2	59.2	61.3	63.9	65.0	66.5	70.7	69.9
Al_2O_3	17.7	21.1	21.0	20.3	19.8	18.3	18.5
Fe_2O_3	3.1	2.3	2.4	3.1	1.5	2.0	2.0
TiO_2	3.0	2.1	1.9	1.7	1.3	1.2	1.3
P_2O_5	0.2	0.1	0.1	0.0	0.0	0.0	0.0
CaO	12.0	8.7	6.1	5.4	4.4	2.6	3.0
MgO	0.8	0.7	0.7	0.6	0.6	0.5	0.5
Na_2O	1.2	1.2	1.5	1.3	3.2	1.6	1.6
K_2O	1.8	1.9	2.0	2.0	2.2	2.7	2.6
SO_3	0.0	0.0	0.0	0.0	0.0	0.0	0.0
BaO	0.7	0.3	0.2	0.2	0.3	0.2	0.2
Mn_2O_7	0.2	0.2	0.2	0.3	0.2	0.2	0.2
ClO	0.0	0.0	0.0	0.0	0.0	0.0	0.0

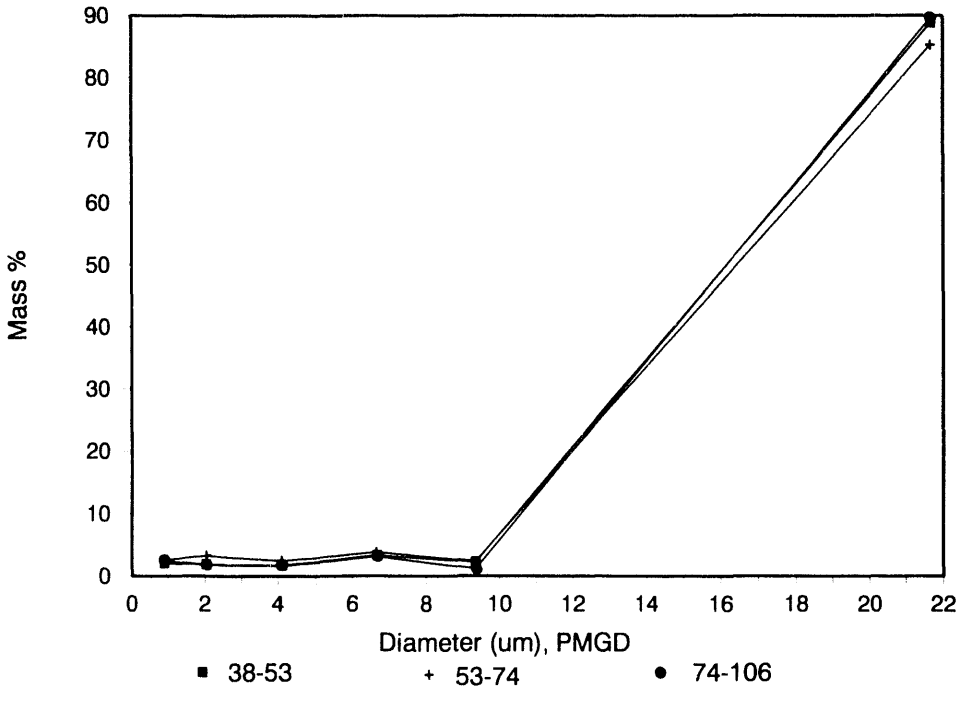

Figure 72. Kentucky #9 - multicyclone 1300°C, 3 coal sizes.

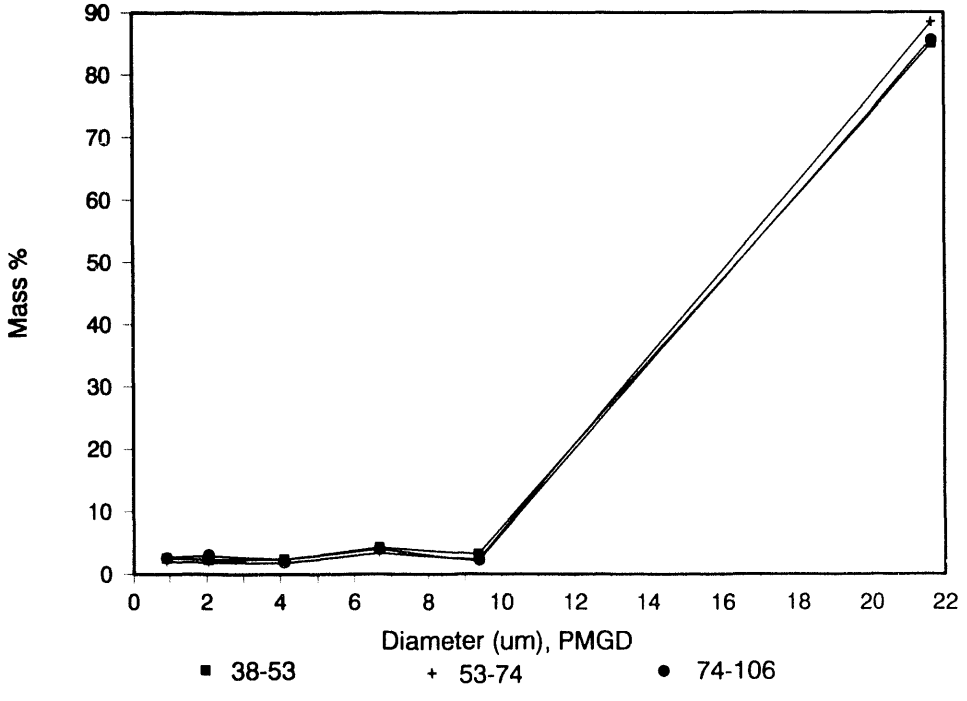

Figure 73. Kentucky #9 - multicyclone 1400°C, 3 coal sizes.

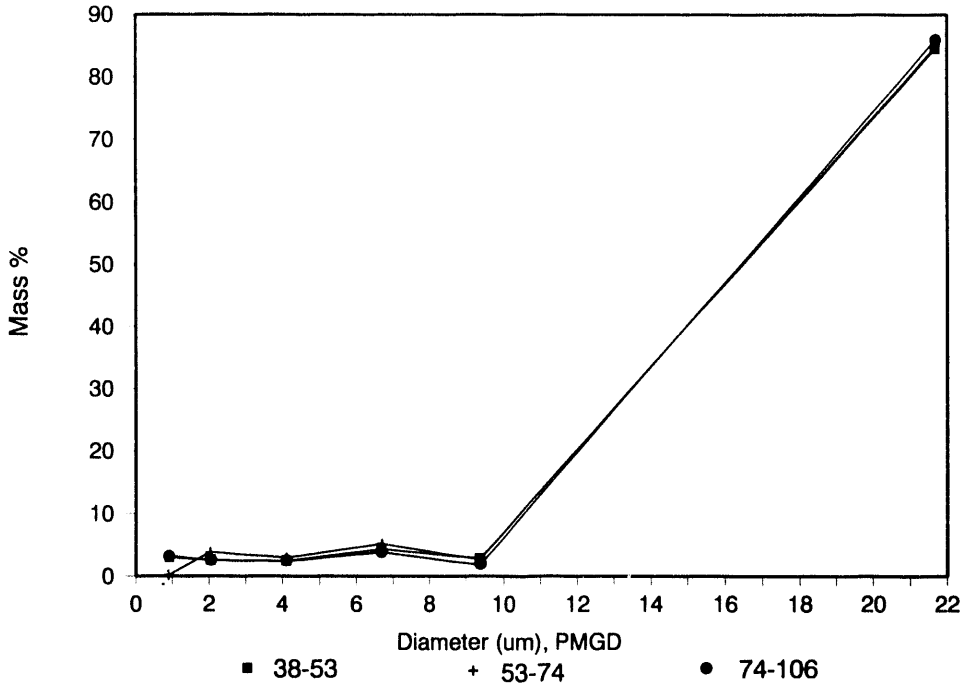

Figure 74. Kentucky #9 - multicyclone 1500°C, 3 coal sizes.

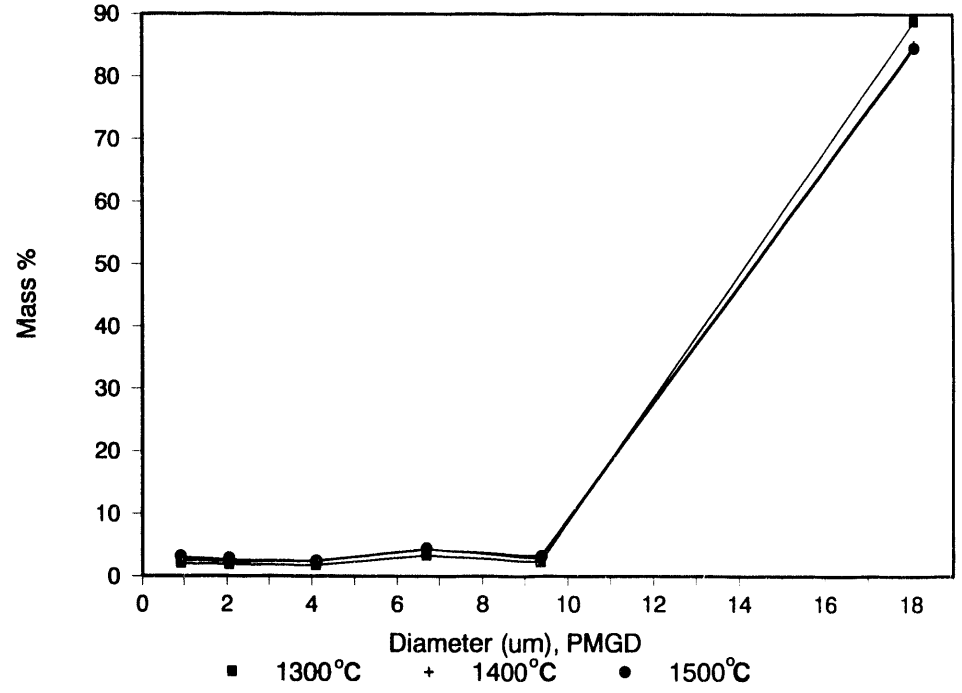

Figure 75. Kentucky #9 - multicyclone 38-53 μm, 3 temperatures.

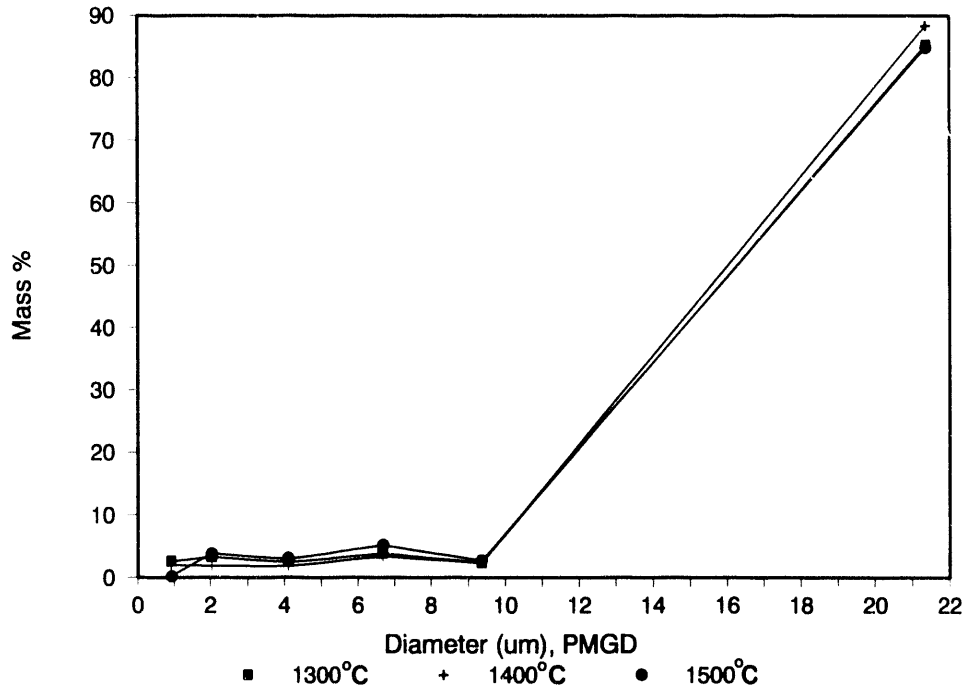

Figure 76. Kentucky #9 - multicyclone 53-74-μm coal, 3 temperatures.

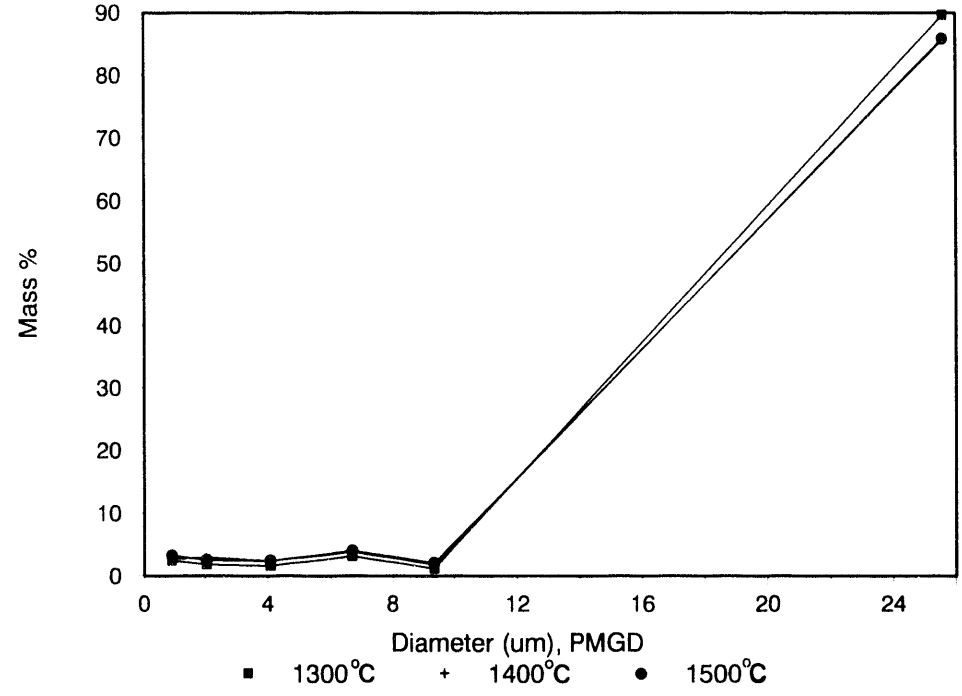

Figure 77. Kentucky #9 - multicyclone 74-106-μm coal, 3 temperatures.

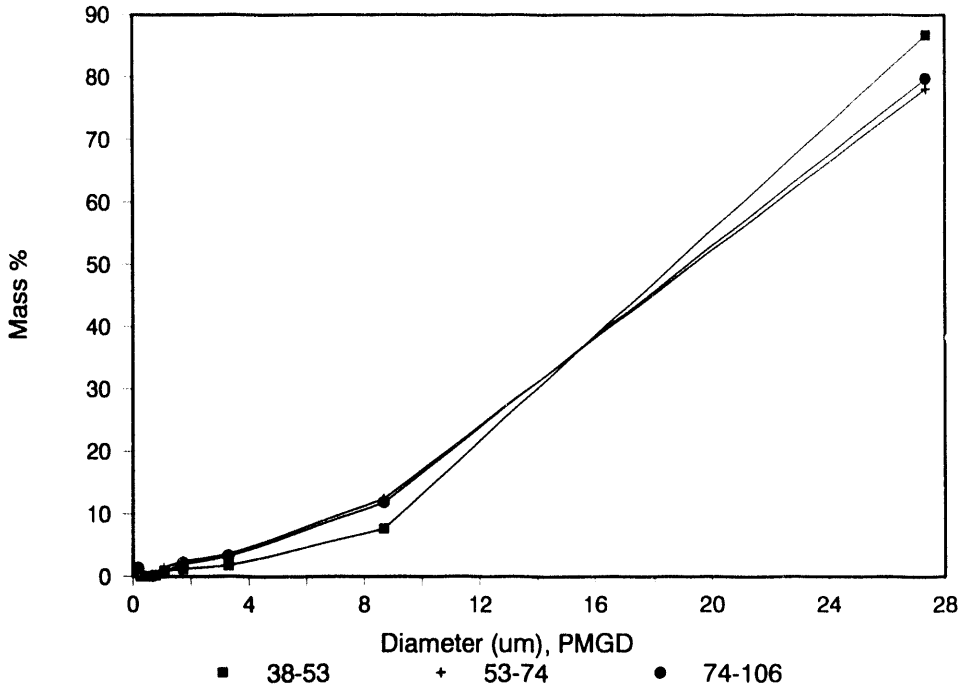

Figure 78. Kentucky #9 - impactor 1300°C, 3 coal sizes.

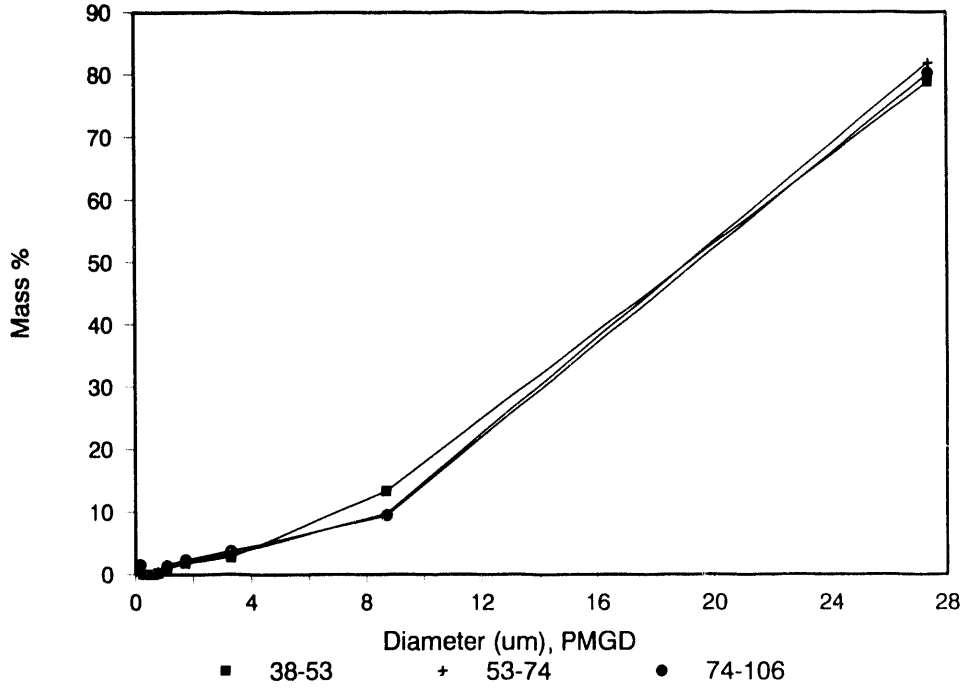

Figure 79. Kentucky #9 - impactor 1400°C, 3 coal sizes.

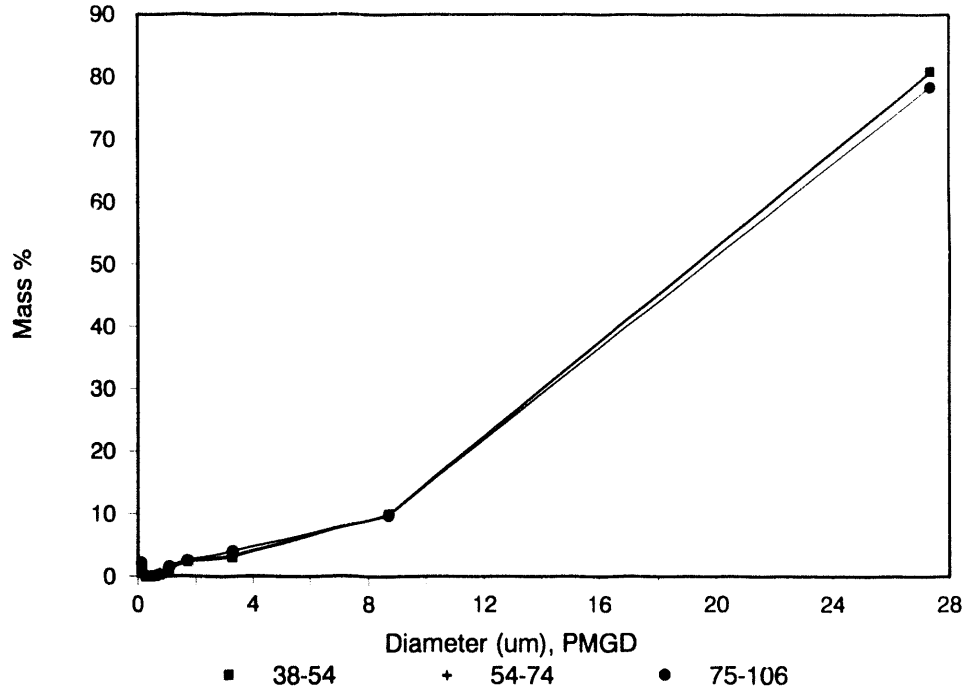

Figure 80. Kentucky #9 - impactor 1500°C, 3 coal sizes.

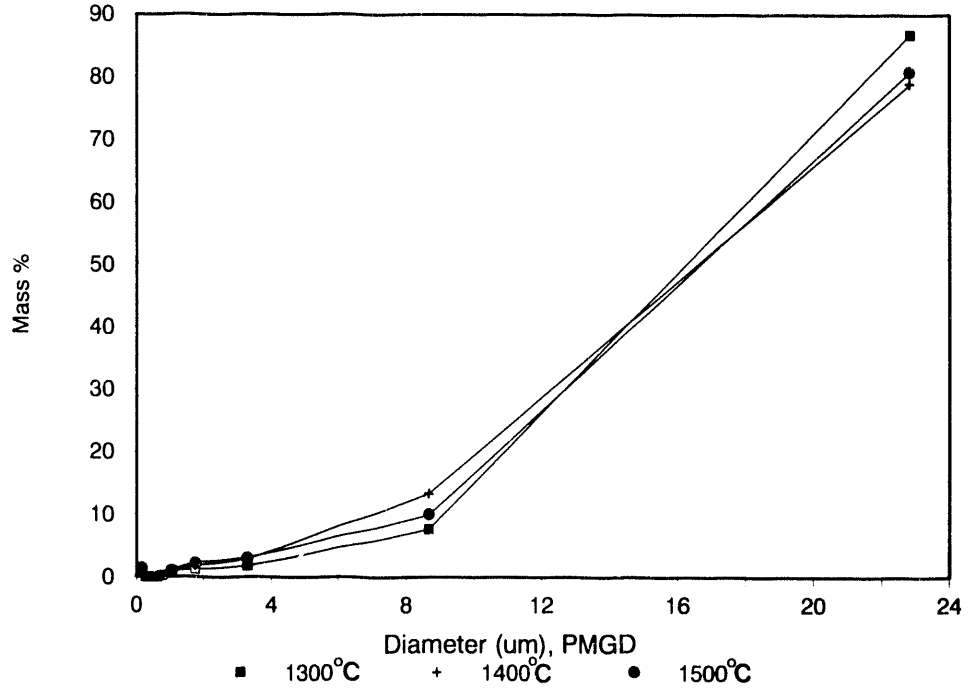

Figure 81. Kentucky #9 - impactor 38-54-μm coal, 3 temperatures.

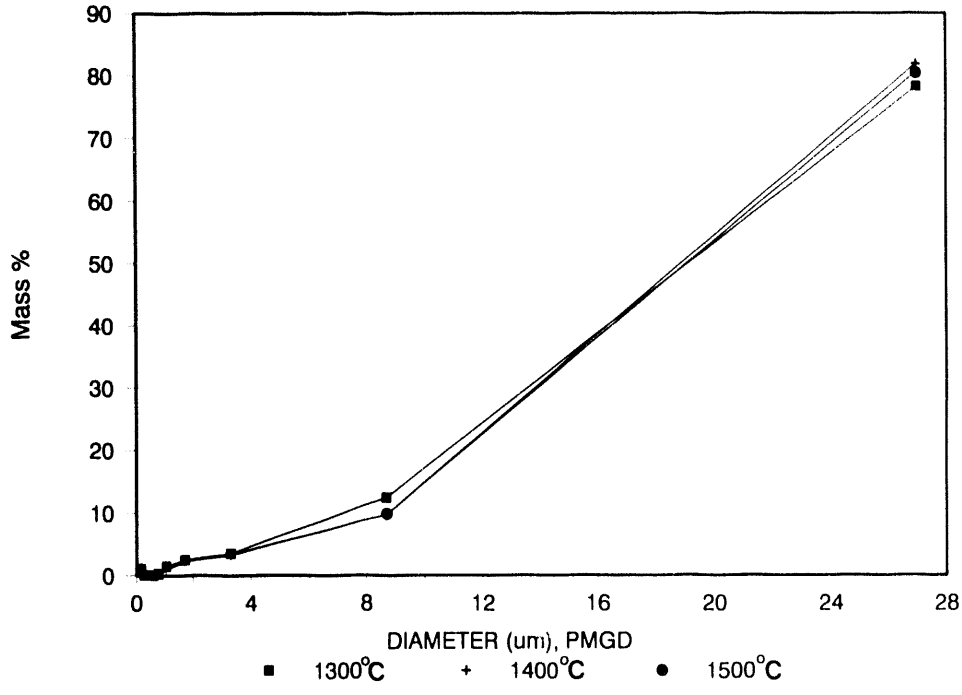

Figure 82. Kentucky #9 - impactor 53-74-μm coal, 3 temperatures.

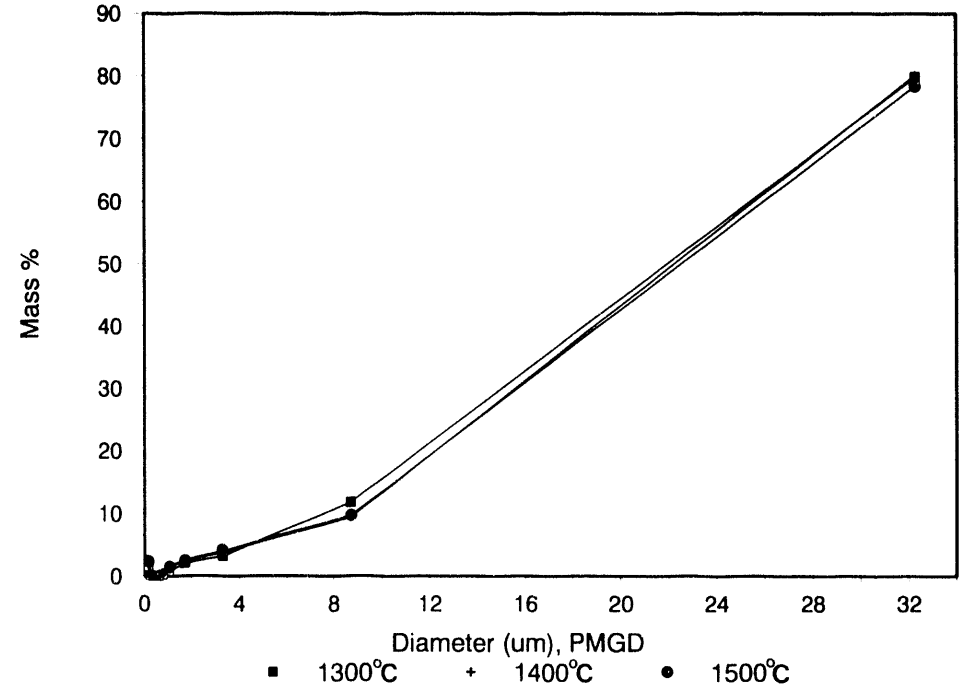

Figure 83. Kentucky #9 - impactor 74-106-μm coal, 3 temperatures.

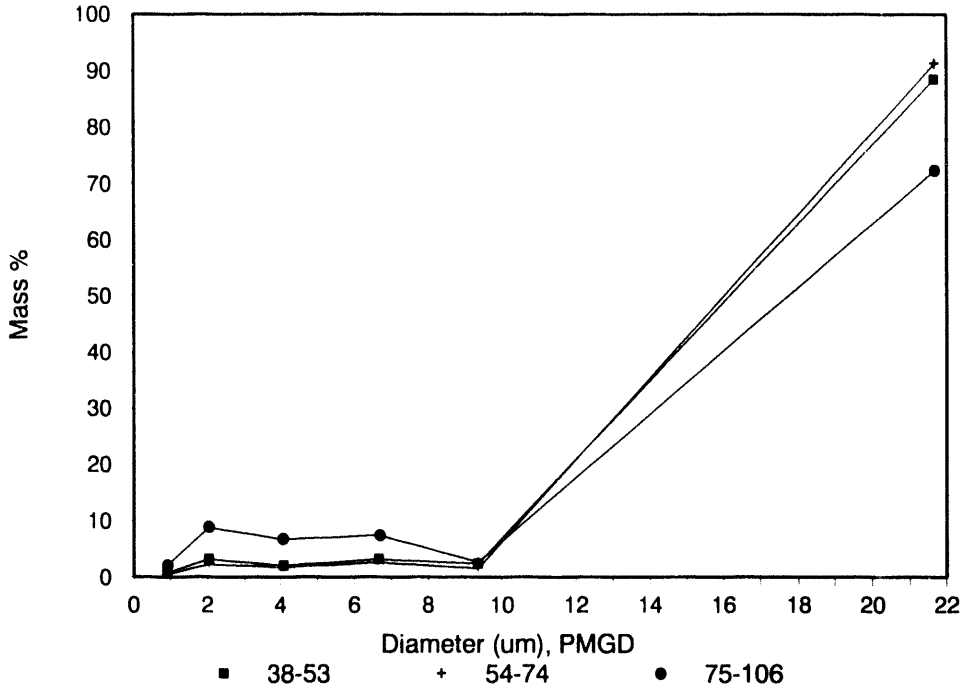

Figure 84. San Miguel - multicyclone 1300°C, 3 coal sizes.

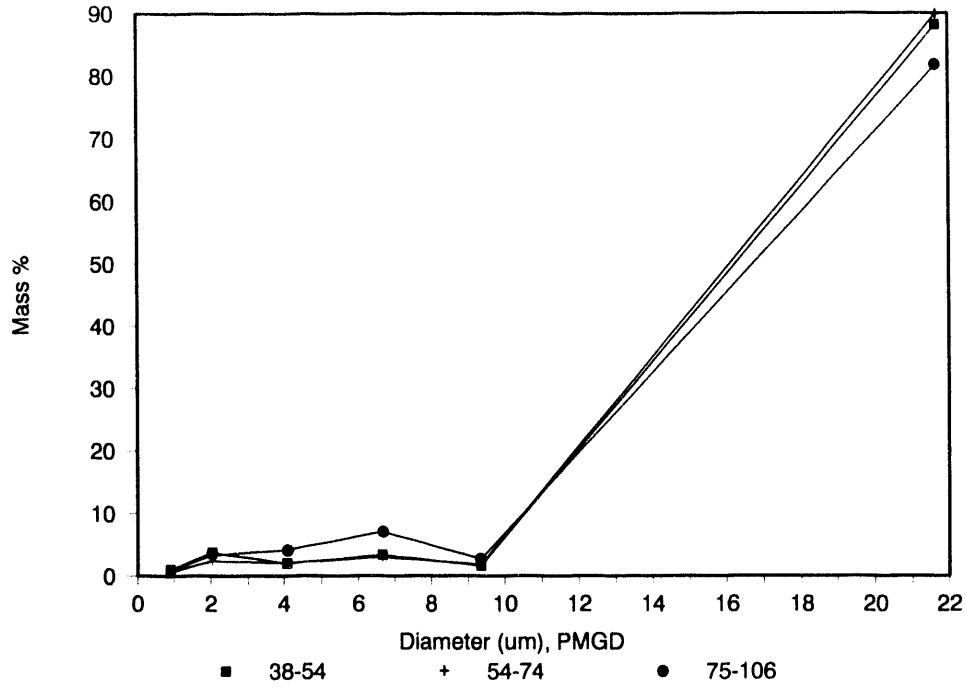

Figure 85. San Miguel - multicyclone 1400°C, 3 coal sizes.

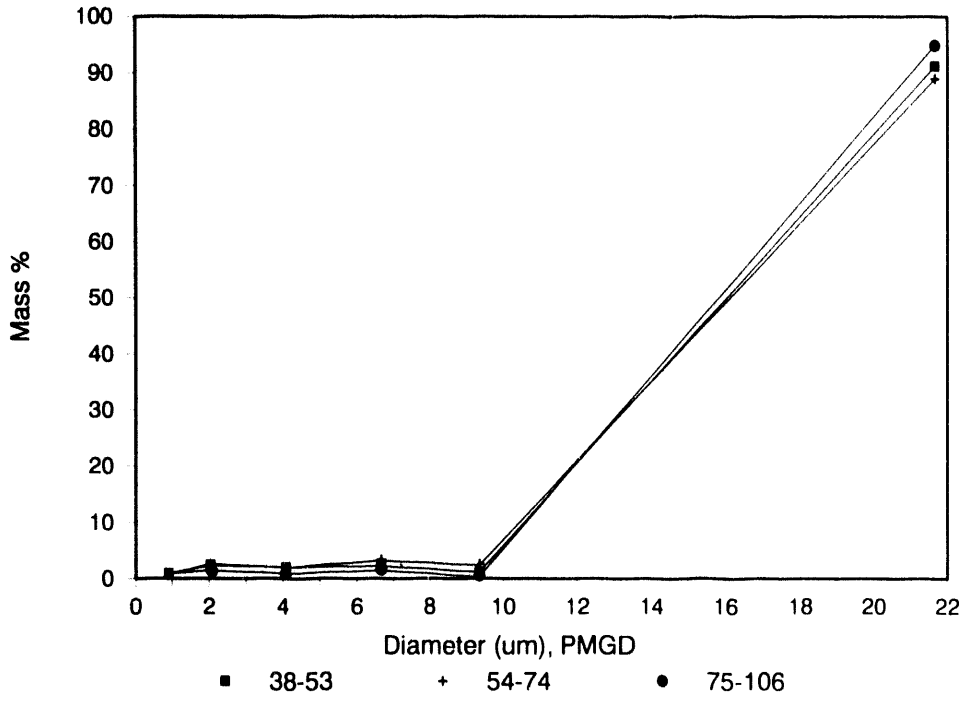

Figure 86. San Miguel - multicyclone 1500°C, 3 coal sizes.

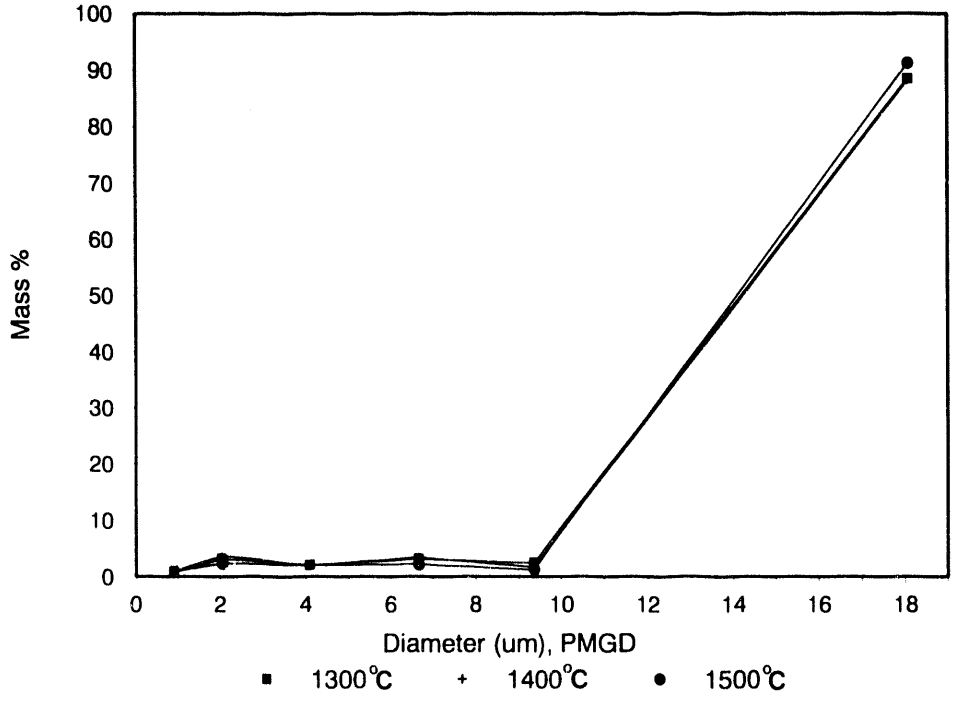

Figure 87. San Miguel - multicyclone 38-53-μm coal, 3 temperatures.

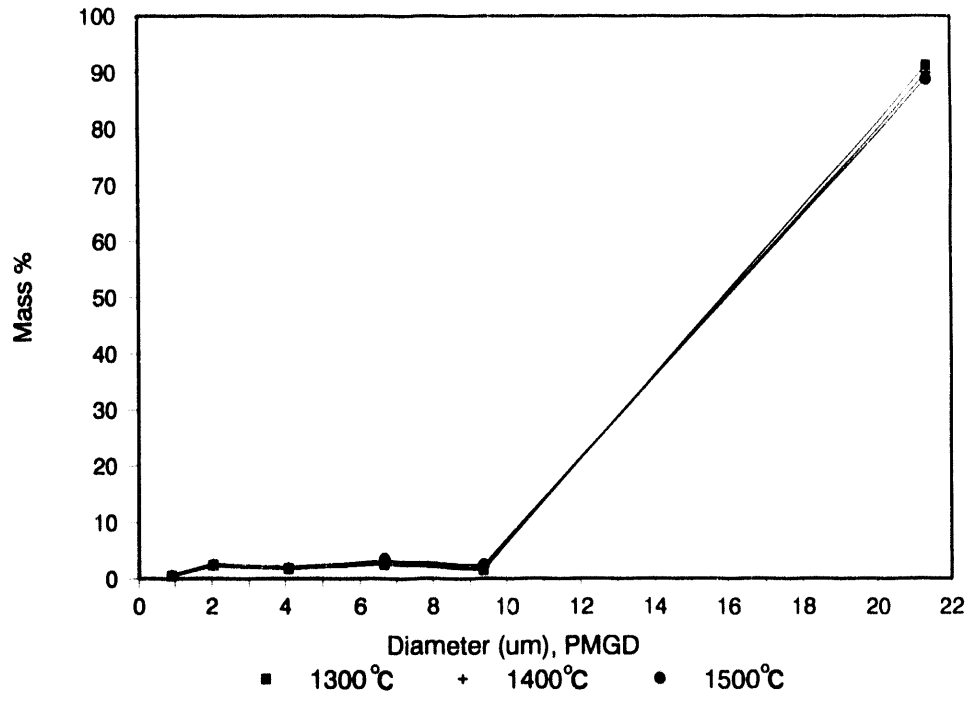

Figure 88. San Miguel - multicyclone 53-74-μm coal, 3 temperatures.

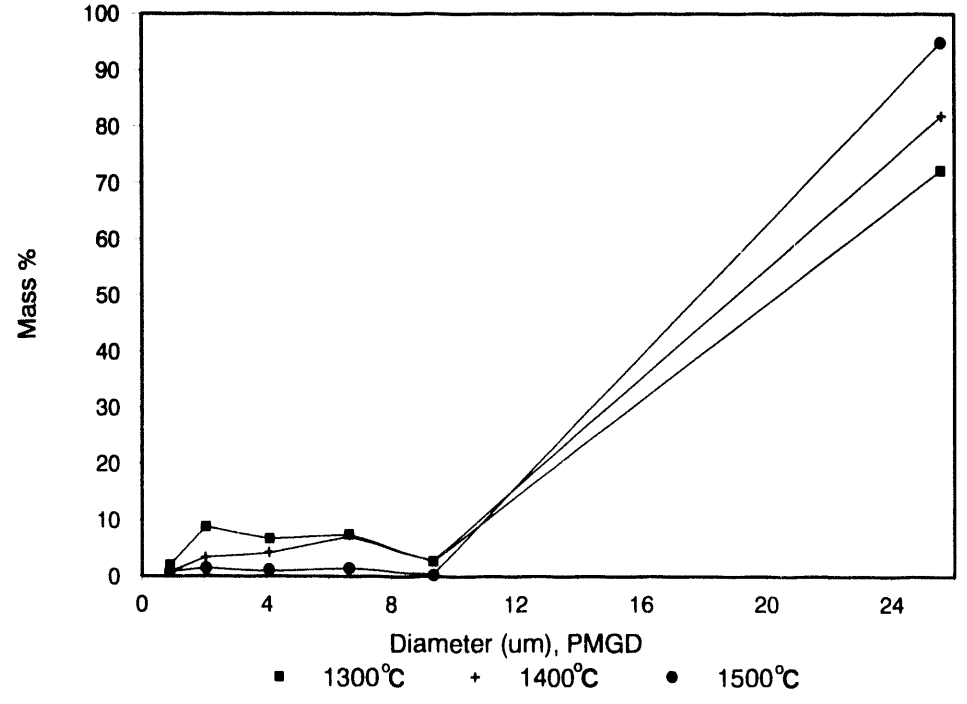

Figure 89. San Miguel - multicyclone 74-106-μm coal, 3 temperatures.

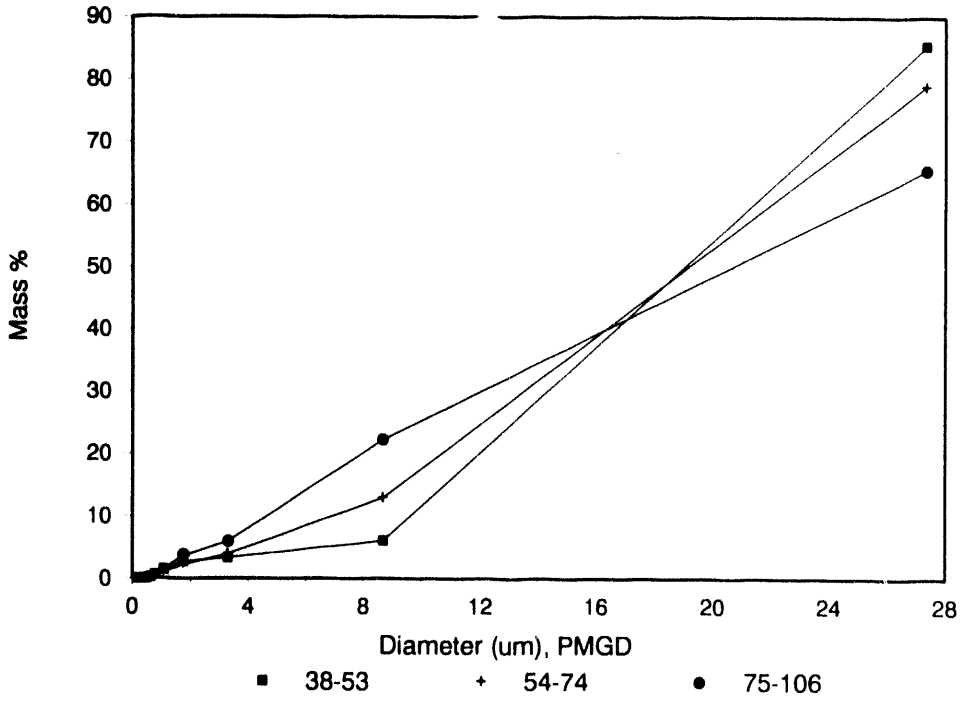

Figure 90. San Miguel - impactor 1300°C, 3 coal sizes.

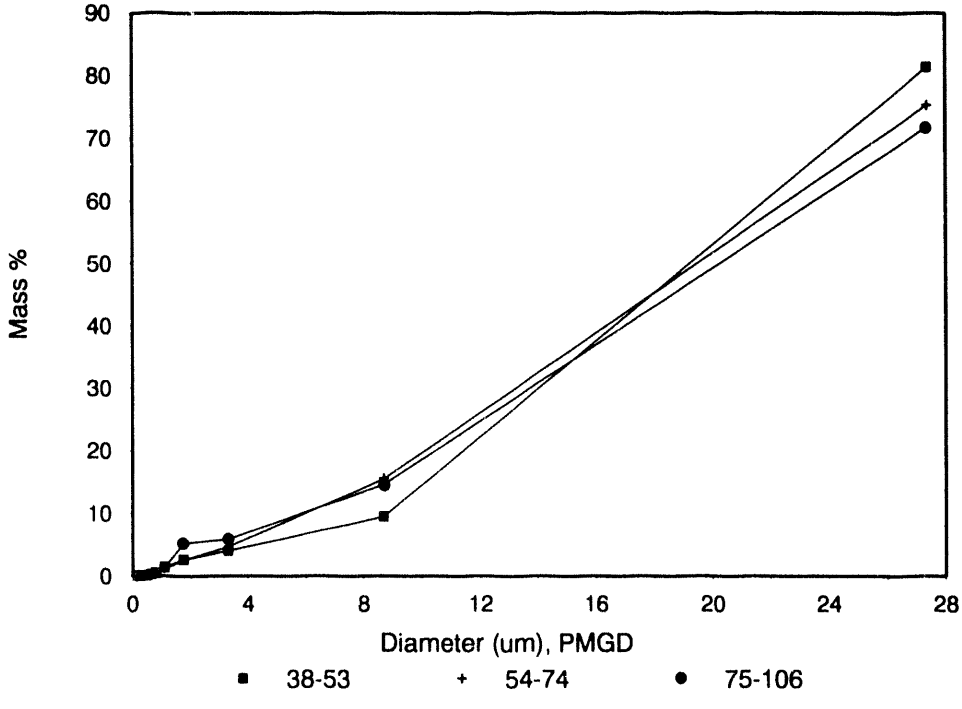

Figure 91. San Miguel - impactor 1400°C, 3 coal sizes.

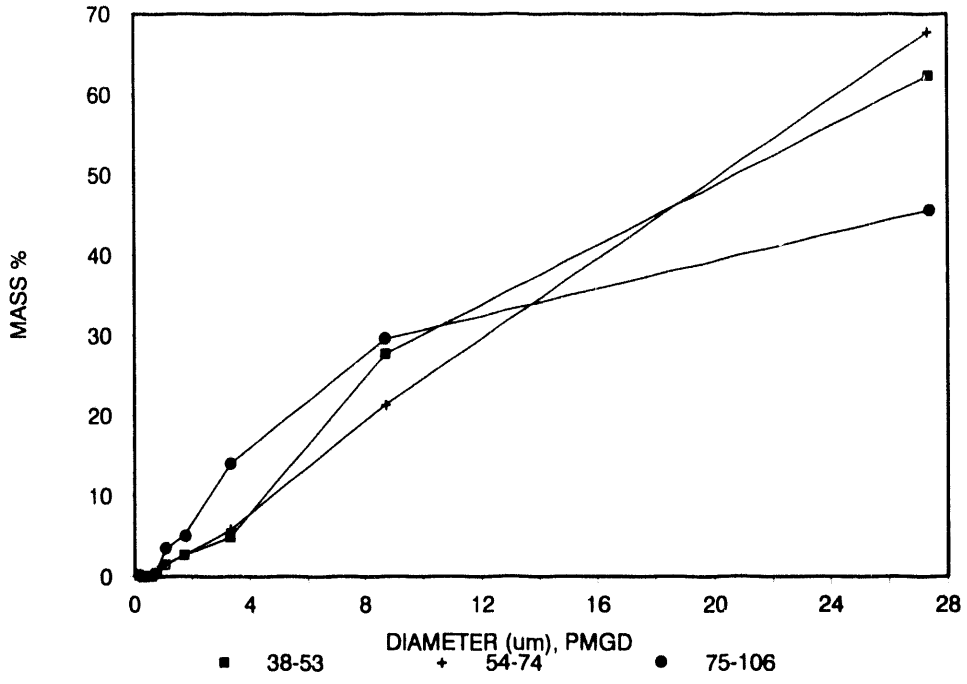

Figure 92. San Miguel - impactor 1500°C, 3 coal sizes.

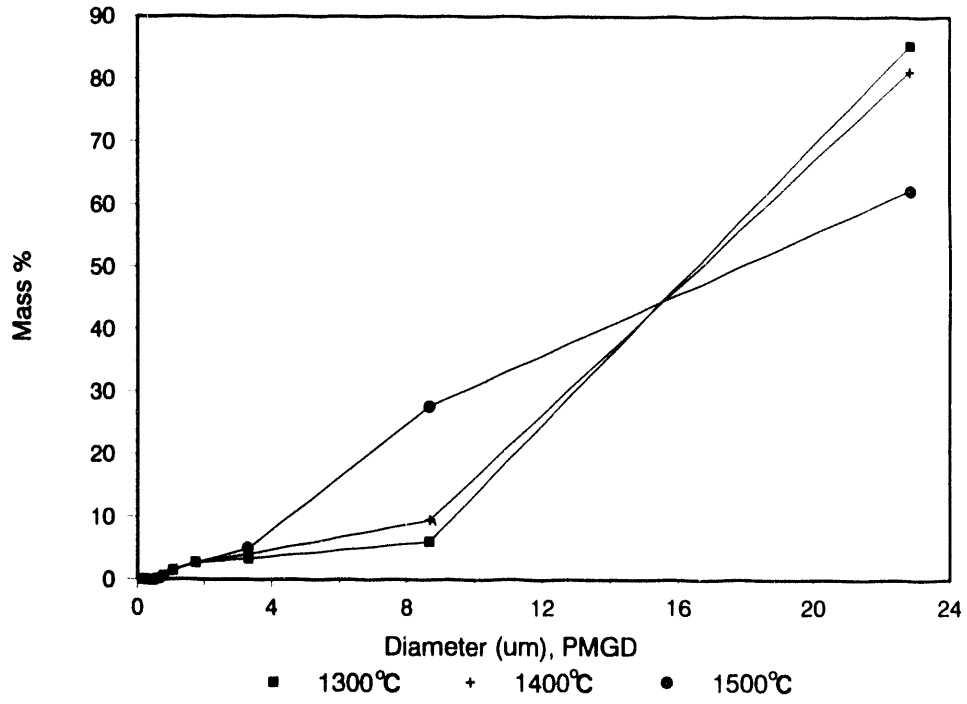

Figure 93. San Miguel - impactor 38-53-μm coal, 3 temperatures.

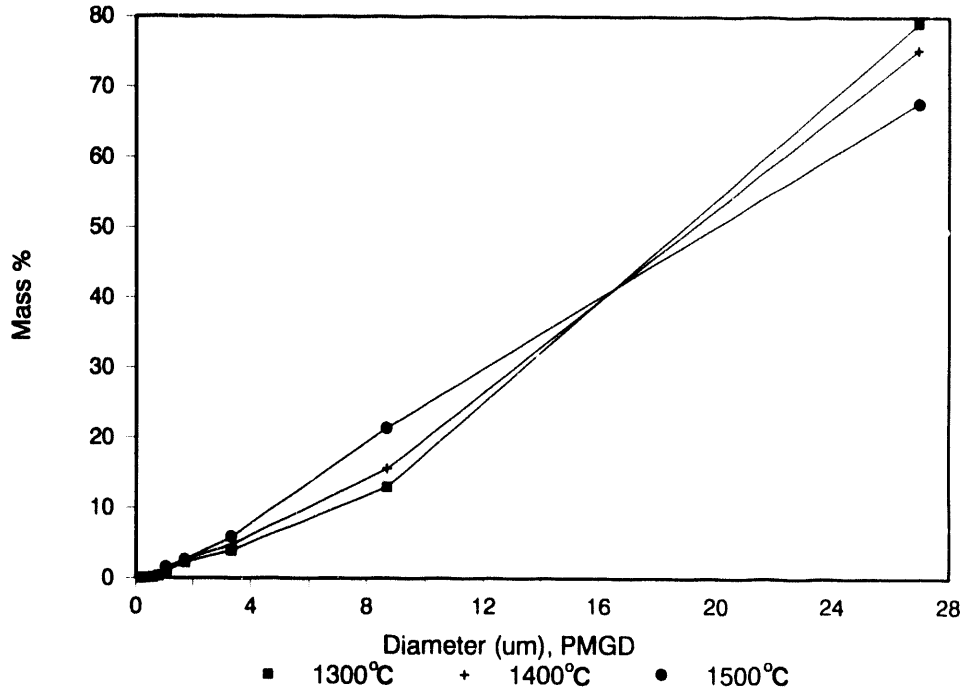

Figure 94. San Miguel - impactor 53-74-μm coal, 3 temperatures.

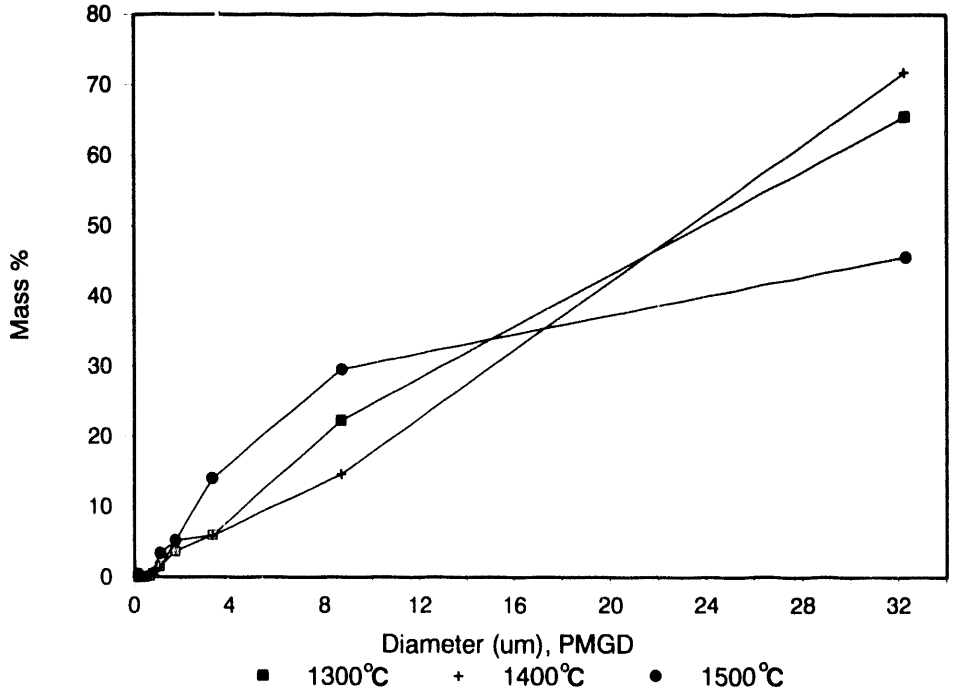

Figure 95. San Miguel - impactor 74-106-μm coal, 3 temperatures.

4.7 Synthetic Coal Combustion Testing

A synthetic coal was created by polymerizing furfuryl alcohol with p-toluenesulfonic acid (30, 31). During the polymerization of the alcohol, carbon black was added to increase the porosity of the sample. The synthetic coal (syncoal) was made to contain 10% by weight SiO_2, 5% Na, and 1% S. The SiO_2 (quartz) was sized to approximately 5 microns in diameter with a sonic sieve, the actual particle-size distribution can be seen in Figure 96 as determined by computer-controlled scanning electron microscopy (CCSEM). Quartz was added to the syncoal during the polymerization process; thus the quartz was bound as included mineral matter within the syncoal. The Na was added by dissolving sodium benzoate in ethyl alcohol, stirring the alcohol solution in with the syncoal and evaporating off the alcohol. This technique produced a sodium distribution similar to that of a Beulah lignite which is volatilized easily. The technique was studied by Mills (19). Sulfur was added extraneously to the sample by mixing sublimed sulfur with the syncoal. During polymerization, some sulfur was lost, leaving only 0.6% S in the syncoal. The actual inorganic compositions achieved were slightly different from those desired but are assumed, as previously mentioned, for the remainder of this discussion. The syncoal was then sized to 37-106 microns using a sonic sieve. The actual particle-size distribution of the syncoal is shown in Figure 97 as determined by Malvern analysis. The syncoal was combusted at 900, 1100, 1300, and 1500°C for approximately 1.4 seconds. The two temperature extremes were also run using particle residence times of 0.1 and 0.5 seconds.

Figures 98, 99, 100, and 101 are scanning electron microprobe (SEM) photographs of the ash produced at the four combustion temperatures: 900, 1100, 1300, and 1500°C, respectively. Note that all four photographs are at the same magnification. The particle size of the ash decreases with increasing combustion temperature. Table 72 shows the average particle size for each of the four samples. Figure 102 shows the particle-size distributions of the four ashes as measured manually with a Tracor Northern 8500 image analyzer. Also included in Figure 102 are the two expected extremes during combustion: 1) 100% fragmentation - assuming each mineral forms a fly ash particle, 2) 100% coalescence - assuming that the mineral matter in each coal particle forms one fly ash particle (the minerals were also assumed to be homogeneously dispersed in the syncoal). The four ash size distributions are inside the two expected extremes. The higher combustion temperatures shift the distributions towards the fragmentation curve, while the lower temperatures shift it towards the coalescence curve.

The surface characteristics of the two temperature extreme samples were studied by SEM techniques. The 900 and 1500°C samples have similar surface characteristics. The samples contain white moieties on the larger fly ash samples. The particles, as stated earlier, get smaller with increasing temperature and so do their accompanying white moieties. The approximate size of the moieties at 900°C is 0.5 to 2 microns, where at 1500°C they are about half that size. The abundance of the moieties also diminishes with combustion temperature. The surface compositions of the two temperature extreme samples in Table 73 were determined in the following three categories: 1) bulk composition, 2) grey area composition (larger particles), and 3) white moiety composition. It is noted that when analyzing the white moieties, the electron

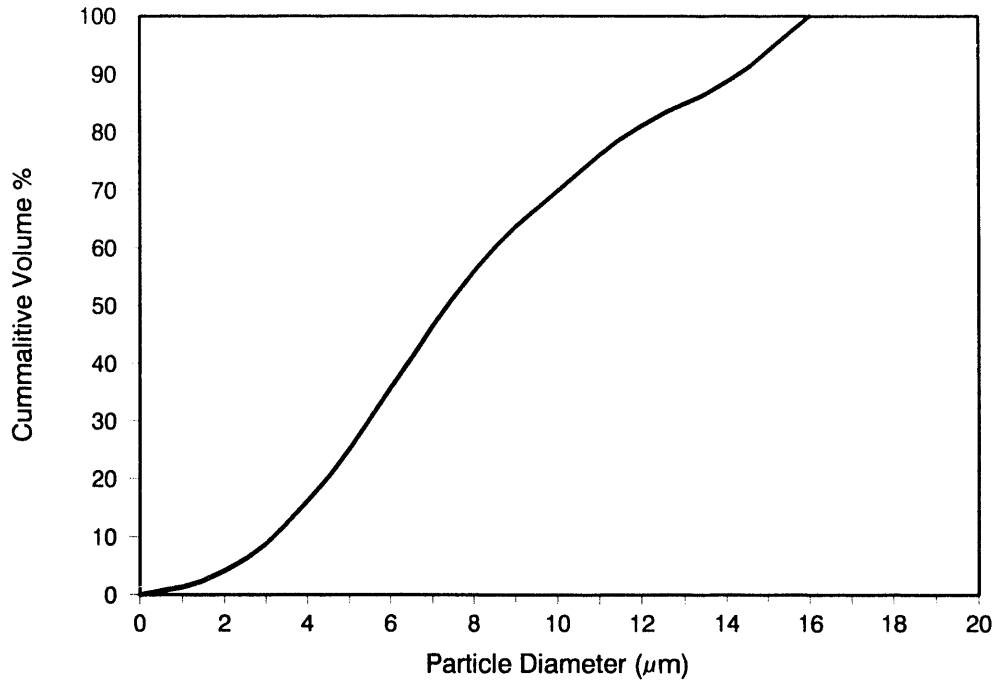

Figure 96. Particle-size distribution of quartz in synthetic coal as determined by CCSEM.

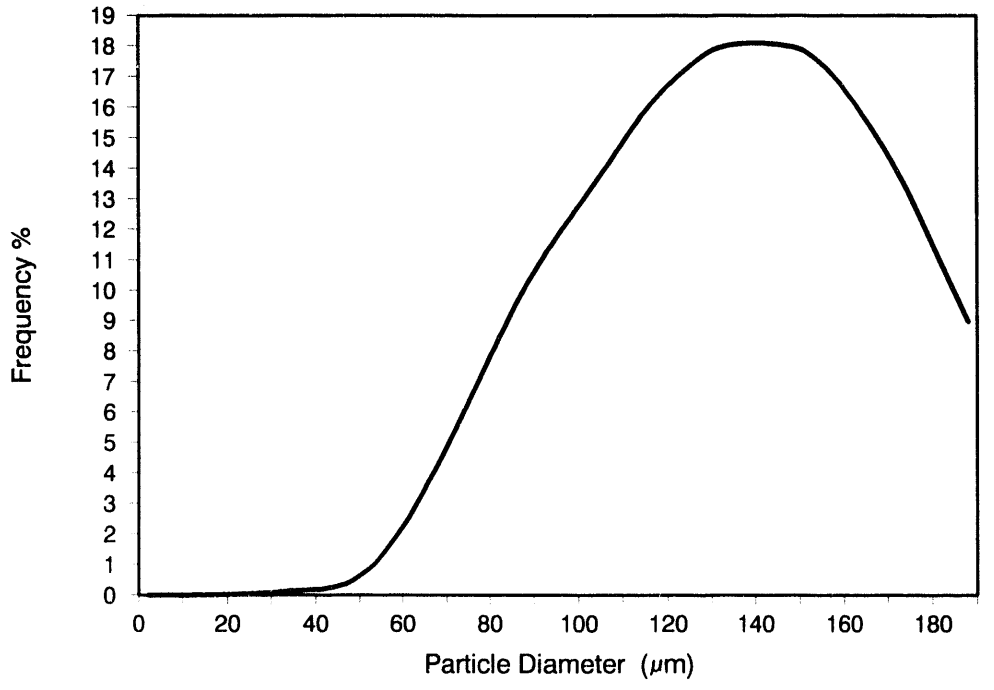

Figure 97. Particle-size distribution of syncoal prior to combustion testing (Malvern).

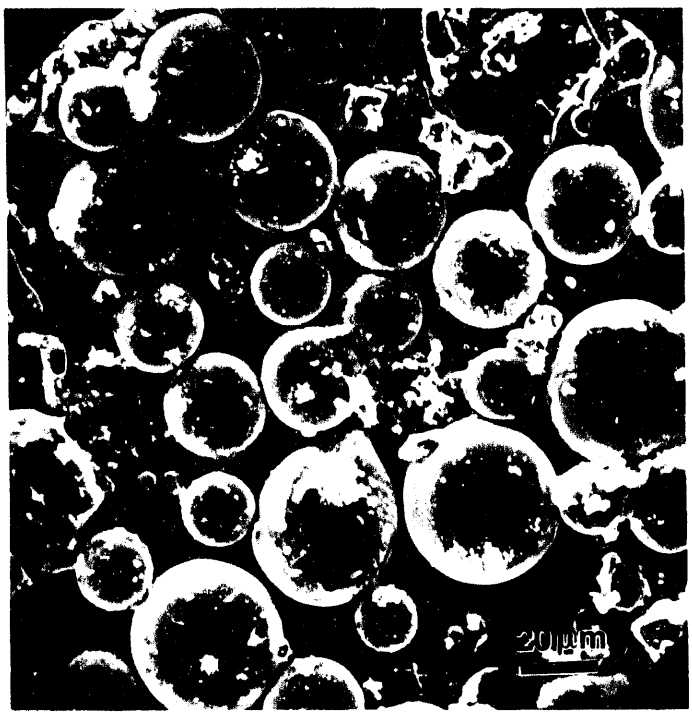

Figure 98. Scanning electron micrograph of syncoal fly ash generated at 900°C (500x).

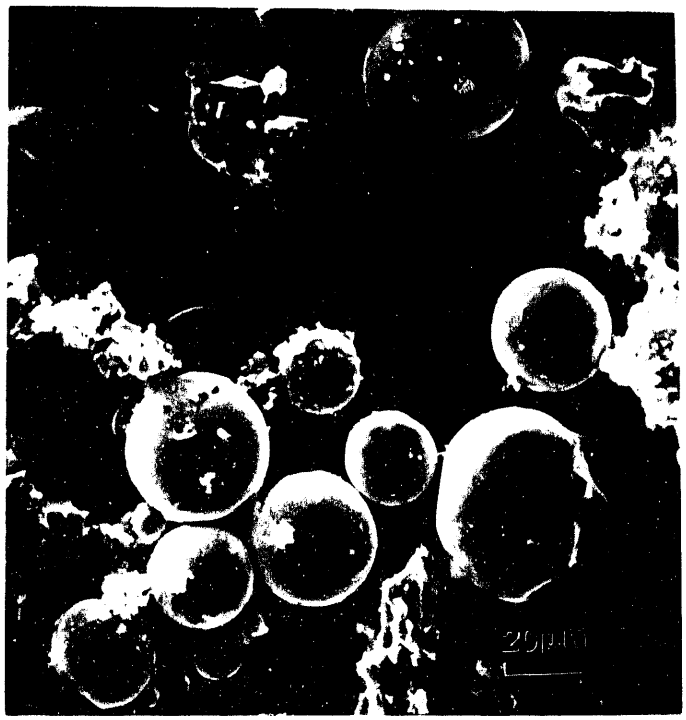

Figure 99. Scanning electron micrograph of syncoal fly ash generated at 1100°C (500x).

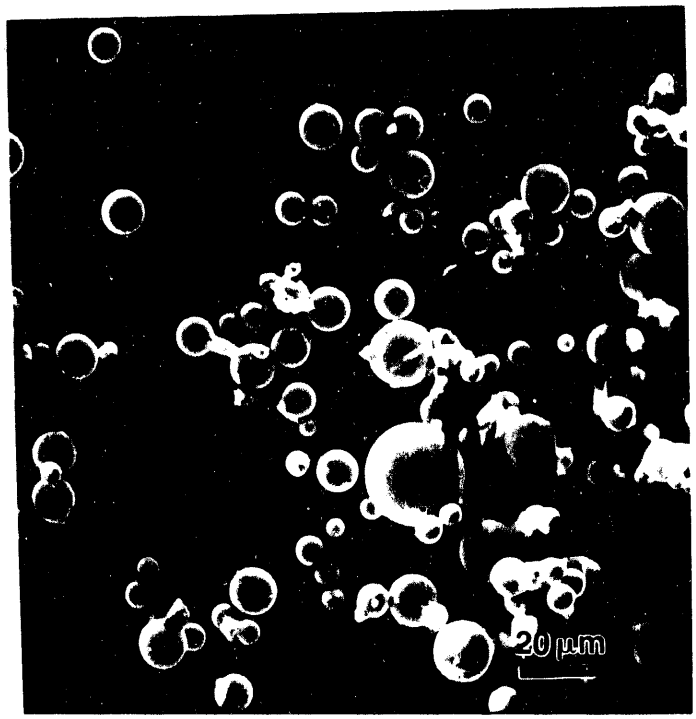

Figure 100. Scanning electron micrograph of syncoal fly ash generated at 1300°C (500x).

Figure 101. Scanning electron micrograph of syncoal fly ash generated at 1500°C (500x).

TABLE 72

PARTICLE DIAMETERS (SPHERICAL)

Temperature	# of Particles Analyzed	Average Particle Size
900°C	124	27.0 μm
1100°C	114	27.7 μm
1300°C	117	17.6 μm
1500°C	120	8.5 μm

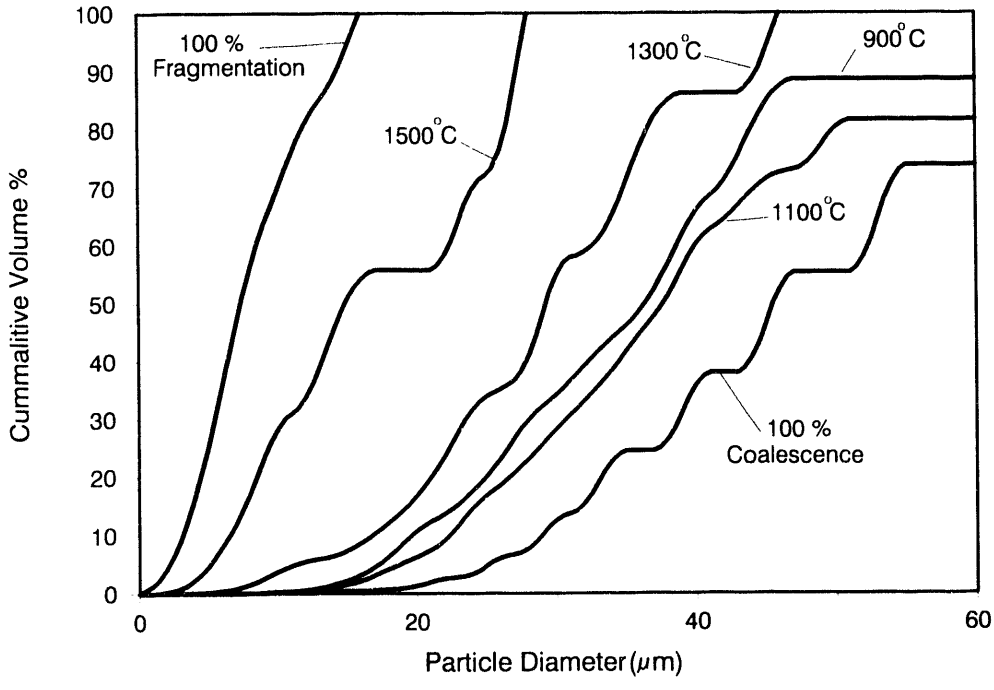

Figure 102. Particle-size distributions of syncoal fly ash generated at 900, 1100, 1300, and 1500°C and also size distributions for complete fragmentation and coalescence.

TABLE 73

PARTICLE SURFACE COMPOSITION

Temperature	Bulk Composition			Grey Area Composition			White Moiety Composition		
(°C)	Na	S	Si	Na	S	Si	Na	S	Si
900	24	5	61	19	1	80	39	18	43
1500	80	1	19	5	0	95	6	1	93

beam penetrates through them because of their small size and thus some signal from the sample behind them is received. From the data it appears that the larger particles (grey area) are comprised of sodium and silica, with sodium sulfate particles (white moieties) sticking on the outside.

Two residence times were studied at the two temperature extremes (900 and 1500°C). All four samples were analyzed by CCSEM, and the summary of those results along with the CCSEM of the raw coal are found in Table 74. The average particle size for the four samples was similar with the 1500°C. The 0.1-second sample was slightly larger, possibly attributed to sampling variability. The average sizes of all four samples are similar to the average particle size of the raw coal, which implies that no appreciable coalescence of the minerals has taken place in this amount of time. The area percent of sodium silicates present in the samples is also shown in Table 74. These are categorized as having a composition of at least 5% Na and a sulfur content less than 5%. The higher temperatures and longer residence times demonstrate a higher interaction between the sodium and quartz. A major assumption that must be made is that the sodium is volatilized immediately at both temperature extremes. No appreciable formation of sodium sulfates was evident. The CCSEM method (in the manner it was used) only analyzes particles greater than 1 μm, which will exclude most sodium sulfate particles that may have formed during the early stages of combustion.

The sample that was generated at 900°C and 0.1-second residence time appears to have a bimodal distribution of char. The large particles are about 100 μm in size, and the smaller particles are about 20 μm in size. It appears that the smaller particles are fragments from the larger particles since no appreciable amount of the fine particles was evident in the raw coal. Some (5-10%) of the larger particles have cracks in them, suggesting the occurrence of fragmentation. A sample of the same synthetic coal was run at 1500°C for 1.4 seconds under a nitrogen atmosphere, and no molten quartz particles were evident, although molten quartz particles were noted using the oxygen atmosphere. Mineral particles elsewhere remained jagged and apparently unaffected. There was very little evidence of coalescence at this temperature and residence time.

TABLE 74

CCSEM RESULTS OF SHORT RESIDENCE TIME RUNS

Temperature	Residence Time	Avg. Diameter	Area % Na-Si
900°C	0.1 sec	4.04 μm	1.2
1100°C	0.5 sec	4.06 μm	18.9
1300°C	0.1 sec	5.06 μm	1.0
1500°C	0.5 sec	4.20 μm	45.4
Raw Coal -		3.84 μm	

At 900°C and 0.5-seconds residence time the char particles were much smaller and more homogeneous in size than the shorter residence time sample. They had an average particle size of about 20 μm. The char samples would be expected to be smaller, but not this small at this early of a stage of combustion which would imply that fragmentation has occurred. There is a larger extent of coalescence of the minerals (quartz) than at the shorter residence times. The coalescence evident is not enough to increase the ash particle size at this stage.

The 1500°C-0.1 second sample showed a similar bimodal size distribution as did the 900°C-0.1 second sample. The two major differences are that the higher temperature sample has a greater degree of carbon burnout and coalescence. A larger amount of sodium than the previous samples is found on the surface of the char particles, but it is not found appreciably in conjunction with the quartz particles. Sulfur is also found and is concentrated along with the sodium on the surface of the unburned carbon. This may demonstrate the early formation of sodium sulfates, but their actual presence is hard to verify visually.

For the 1500°C-0.5 second sample, the amount of carbon remaining has decreased substantially. The ash particles formed are as large as 30 μm which is larger than the ash after 1.4 seconds of combustion which may demonstrate the formation of cenospheres during the early states of combustion. The size of the particles also demonstrates an early stage of coalescence. The quartz particles have a small amount of sodium associated with them (5%). There is also a small amount of sulfur present with the unburned carbon, but no sodium is present along with it. There appears to be some submicron particles found on the quartz particles, but they do not show the presence of sodium or sulfur when analyzed.

4.8 Conclusions

Kentucky #9 coal contained about 15% ash and had high iron (20%) and moderate calcium (3.4%) and potassium (3%) contents on a normalized oxide basis. The most abundant minerals were quartz, aluminosilicate (degraded illite or mixed clay), illite, pyrite, and for the 74-106 μm and unsized fraction, siderite. Ash content decreased with increasing coal size, but minerals sizes increased. Variability in mineral content was noted for these different coal sizes analyzed by CCSEM. An increase in pyrite with coal size corresponded with an increase in iron oxide in the coal ash.

Kentucky #9 fly ash showed interaction between iron in the pyrite with aluminosilicate to form Fe-aluminosilicates. Pyrite transformation was evidenced by reduction from 28% to 0%, and iron oxide was increased from 8% to 22% of the minerals using CCSEM analysis. Kentucky #9 minerals that were <10 μm underwent coalescence to a size range mostly between 22-46 μm, while the largest Kentucky #9 minerals (>46 μm), which include pyrite and illite, underwent fragmentation. Time-resolved studies showed that k-aluminosilicate and iron oxide increased with time. Quartz remained fairly constant in quantity from coal to 0.8-seconds residence time char. The finest fraction of the Kentucky #9 size segregated fly ash was enriched in CaO, SO_3, and TiO_2.

San Miguel lignite had about 53% ash on a dry basis and was very low in iron (1.9%) and calcium (3.5%). Sodium content was moderately low at 2.5% of the ash. Sodium and calcium were 65% and 72% organically bound, respectively. The major minerals in the San Miguel lignite as determined by CCSEM were quartz, clinoptilolite, and an unknown aluminosilicate that was probably mixed clay or montmorillonite. Mineralogic compositions on a mineral basis were similar for 38-53, 53-74, and 74-106-μm coal fractions; however, larger minerals were observed with increased coal size. The total ash contents and elemental oxide chemistry were similar for the different coal size fractions.

Analysis of San Miguel short residence time char revealed that quartz and K-aluminosilicate contents remained fairly constant through the combustion process, relative to their abundance in the original coal. Aluminosilicate was slightly reduced, and Fe-aluminosilicate and calcium silicate were slightly increased. The particle-size distributions of the char inorganic phases showed coalescence with increased residence time. Smaller minerals between 1 and 10 μm decreased in abundance, and large inorganic phases 22-46 μm increased in abundance progressively until 0.5 seconds into combustion. The 0.5 and 0.8 second chars were nearly identical in particle size and composition. This is the result of near 100% carbon burnout by 0.5 seconds of combustion.

Fly ash was produced using a residence time of about 2.6 seconds and collected on bulk filters for the San Miguel 53-74 μm and unsized coals. In general, these San Miguel fly ashes were similarly composed. Aluminosilicate and K-aluminosilicate decreased with combustion, probably through interaction with the other mineral components. SEMPC analysis of the size-segregated fly ash from the multicyclone showed the major phases of quartz or silica, amorphous illite, and amorphous montmorillonite. The amorphous illite was actually the derivative of potassium-rich zeolites in the coal. Most of the fly ash mass (89%) was greater than 22 μm in average diameter. It was observed

that SiO_2 and K_2O oxides increased with increasing fly ash particle size, corresponding to greater amounts of the amorphous illite-derived phase. The finer fly ash fraction had more CaO and Al_2O_3.

The Kentucky #9 shows no change in particle-size distribution change for a change in starting coal size or combustion temperature. Neither the multicyclone or the cascade impactor showed any difference. The San Miguel size distributions change with both temperature and initial coal size. The impactor data, and some of the multicyclone data, show that the lower the temperature and the smaller the initial coal size, the larger the particle-size distribution. This implies that coalescence may dominate at the lower temperatures and coal sizes and fragmentation at the higher temperatures and larger coal sizes.

The formation of sodium silicates during coal combustion is favored by longer residence times and higher temperatures. The formation of sodium sulfates do not interfere to any large degree with the formation of sodium silicates due to the high temperature of combustion taking place within the burning coal environment. The formation of fly ash at the four temperatures appears to be governed by different mechanisms. At the lower temperatures, coalescence is dominating, while at the higher temperatures, fragmentation and shedding dominate. The formation of cenospheres at the lower temperatures may also effect the particle-size results. The exothermic reaction temperature of a burning piece of synthetic coal appears higher than that of coal, which may sway results towards the higher temperature regimes, but overall results of the synthetic coal appear good.

5.0 FUTURE WORK

The next year of work includes an exciting agenda of CCSEM development, coal and ash characterization of one new coal, formulation of new synthetic coal mixtures doped with quartz, aluminosilicate, and Ca, and development of a mathematical model to predict fly ash particle size and composition from initial raw coal data. Additional combustion testing will be done on the sodium sulfur, the silica synthetic coal, and on the unsized Beulah, Upper Freeport, and Eagle Butte coals.

6.0 REFERENCES

1. Kalmanovitch, D.P.; Frank, M. "An Effective Model of Viscosity for Ash Deposition Phenomena," Presented at the Conference on Mineral Matter and Ash Deposition from Coal, The Engineering Foundation, Santa Barbara, CA, February 21-26, 1988.

2. Ramanathan, M.; Kalmanovitch, D.P.; Ness, S. "New Techniques for Thermochemical Phase Equilibria Prediction in Coal Ash Systems II: High-Temperature Materials Chemistry, 89," Sixth International Conference on High Temperatures, Chemistry of Inorganic Materials, Gaithersburg, MD, April 3-7, 1989.

3. Zygarlicke, C.J.; Benson, S.A.; Hurley, J.P.; Steadman, E.N. "Combustion Inorganic Transformations," Fifteenth Quarterly Technical Progress Report; U.S. Department of Energy; October through December 1989; DE-FC21-86MC10637.

4. Zygarlicke, C.J.; Benson, S.A.; Hurley, J.P.; Steadman, E.N.; Brekke, D.W. "Combustion Inorganic Transformations," Fourteenth Quarterly Technical Progress Report; U.S. Department of Energy; July through September 1989; DE-FC21-86MC10637.

5. Zygarlicke, C.J.; Benson, S.A.; Toman, D.L.; Steadman, E.N.; Brekke, D.W. "Combustion Inorganic Transformations," Sixteenth Quarterly Technical Progress Report; U.S. Department of Energy; January through March 1990; DE-FC2186MC10637.

6. Boni, A.A. "Transformations of Inorganic Coal Constituents in Combustion Systems," Quarterly Report No. 6 for Period January to March 1988, DE-AC22-86PC90751.

7. Hilliard, J.E. "Measurement of Volume in Volume," in Quantitative Microscopy Materials Science and Engineering Series; Dehoff, R. and Rhines, F., Eds., McGraw Hill, 1968.

8. Zygarlicke, C.J.; Steadman, E.N. "Advanced SEM Techniques to Characterize Coal Minerals," Scanning Microsc. Int. **1990**, 4, (3), 579-589.

9. Kalmanovitch, D.P.; Montgomery, G.G.; Steadman, E.N. ASME Paper Number 87-JPGC-FACT-4, 1987.

10. Howard, J.B. "Mechanism of Ignition and Combustion in Flames of Pulverized Bituminous Coal," Ph.D. Thesis, Pennsylvania State University, 1965.

11. Kinneman, W.P. "A Study of Slag Initiation Using Controlled Surface Temperature Probes in a 15 Lb/Hr Pulverized Coal Test Furnace," M.S. Thesis, Pennsylvania State University, 1983.

12. Jenkins, R.; Walker, P. "Analysis of Mineral Matter in Coal," In Analytical Methods for Coal and Coal Products; Academic Press: NY, 1978, Vol. 2, pp 265-292.

13. Huggins, F.E.; Kosmack, D.A.; Huffman, G.P.; Lee, R.J. Scanning Electron Microscopy **1980**, 1, 531-540.

14. Newbury, D.E.; et al. Advanced Scanning Electron Microscopy and X-ray Microanalysis; Plenum Press: New York, 1986; p 258.

15. Field, M.A.; et al. Combustion of Pulverized Coal BCURA, Cheney and Sons, Ltd.: Banbury, England, 1967.

16. Beer, J.M.; Chigier, N.A. Combustion Aerodynamics; Halsted Press Division, John Wiley and Sons, Inc.: New York, 1972; p 214-232.

17. Bird, R.B.; et al. Transport Phenomena; John Wiley and Sons Inc.: New York, 1960; p 47.

18. Scaroni, A.W.; Khan, M.R.; Eser, S.; Radovic, L.R. "Coal Pyrolysis," Ullmann's Encyclopedia of Industrial Chemistry; Fifth Edition, VCH Verlagsgesellschaft mbH: Weinheim, FRG, 1986.

19. Zygarlicke, C.J.; Benson, S.A.; Abrahamson, H.B.; Mills, M.E. "Combustion Inorganic Transformations," Final Technical Report; U.S. Department of Energy; April 1988 through June 1989; DE-FC21-86MC10637.

20. Hyam, E.D.; Nutting, J. "The Tempering of Plain Carbon Steels," Journal of the Iron Steel Institute **1956**, 184, 148-165.

21. DeHoff, R.T.; Rhines, F.N. Quantitative Microscopy Materials Science and Engineering Series; McGraw Hill Book Company, 1968.

22. Friel, J.J.; Mehta, S.; Mitchell, G.D.; Karpinski, J.M. "Direct Observation of the Mesophase in Coal," Fuel **1980**, 59, 610-616.

23. Allen, R.M.; VanderSande, J.B. "Analysis of Submicron Mineral Matter in Coal Via Scanning Transmission Electron Microscopy," Fuel **1984**, Vol. 63, pp. 24-29.

24. Hsieh, K.C. "Transmission Electron Microscopy (TEM) Study of Minerals in Coal," Ph.D. Thesis, University of Illinois at Urbana-Champaign, 1982.

25. Srinivasachar, S.; Boni, A.A. "A Kinetic Model for Pyrite Transformations in a Combustion Environment," Fuel **1989**, 68, 829.

26. Helble, J.J.; Srinivasachar, S.; Boni, A.A.; Karg, S.G.; Sarofim, A.F.; Beer, J.M.; Gallagher, N.; Bool, L; Peterson, T.W.; Wendt, J.O.L.; Shah, N.; Huggins, F.E.; and Huffman, G.P. "Effects of Combustion Scale on Fundamental Mineral Transformations for Selected U.S. Coals," In Proceedings of the Sixth Annual International Pittsburgh Coal Conference; 1989, Vol. 1, pp 81-90.

27. Miller, S.F.; Schobert, H.H.; Scaroni, A.W. "A Study of Ash Formation During the Combustion of Pulverized Coal," ACS Div. Fuel Chem Preprints of Papers **1990**, 35, (3), 637-644.

28. Boni, A.A. "Program Plan for Transformations of Inorganic Coal Constituents in Combustion Systems," Prepared by A.A. Boni, Physical Sciences, Inc., DE-AC22-86PC90751, 1986.

29. Benson, S.A.; Holm, P.L. Ind. Eng. Chem. Prod. Res. Dev. **1985**, 24, 145.

30. Erickson, T.A. "The Fate of Flame Volatilized Sodium During the Combustion of Pulverized Coal in Reaction with Silica and Sulfur (Studied with the Aid of a Synthetic Coal)," Masters Thesis, University of North Dakota, 1990.

31. Senior, C.L. "Submicron Aerosol Production During Combustion of Pulverized Coal," Ph.D. Thesis, California Institute of Technology, 1984.

3.4 Liquefaction Reactivity of Low-Rank Coals

LIQUEFACTION REACTIVITY OF LOW-RANK COALS

Annual Technical Project Report
for the Period July 1, 1989 through June 30, 1990

Including

the Quarterly Technical Progress Report
for the Period April through June 1990

by

Edwin S. Olson, Research Supervisor &
Ramesh K. Sharma, Research Associate
Energy & Environmental Research Center
University of North Dakota
P.O. Box 8213, University Station
Grand Forks, ND 58202

Contracting Officer's Technical Representative: Udaya Rao

for

U.S. Department of Energy
Pittsburgh Energy Technology Center
Pittsburgh, Pennsylvania 15236

July 1990

Work Performed Under Cooperative Agreement No. DE-FC21-86MC10637

TABLE OF CONTENTS

LIST OF TABLES

LIST OF FIGURES

LIQUEFACTION REACTIVITY OF LOW-RANK COALS

1.0 EXECUTIVE SUMMARY

In the preceding decade, molten zinc chloride was demonstrated to be an effective catalyst for the production of clean gasoline fuels; however, some disadvantages relating to its corrosiveness and loss during regeneration were noted. During the last year we have extensively investigated supported forms of zinc chloride which may overcome these problems. Silica gel-supported zinc chloride was shown to be an effective catalyst for hydrotreating first-stage coal liquefaction products to a distillate fuel containing no sulfur. Higher conversions (53-68%) were obtained with this catalyst than that with a commercially available Ni-Mo catalyst (35%). Extensive studies with model compounds were carried out with the objective of achieving a better understanding of the chemistry of hydrotreating coal liquids with solid strong-acid catalysts. These studies showed that the silica gel-supported zinc chloride catalyst cleaves aryl sulfides, ethers, phenols, nitrogen heterocyclics, and alkylaromatic compounds. Alkyl transfer reactions also occur very readily. Molecular hydrogen is not utilized directly in the cleavage reaction, but it is needed to prevent coking and condensation reactions and is indirectly incorporated into products. Products are consistent with a mechanism involving formation of carbonium ion intermediates which are converted to products via hydride abstraction. The sources of the hydride ions apparently are various aromatic condensation intermediates. Tertiary alkanes are not effective hydride donors. Polynuclear aromatics are hydrogenated but single ring aromatics are not.

Characterization of the silica gel-zinc chloride catalyst was carried out to provide further information on the nature of the zinc chloride in the catalyst. The acidic properties of the SZC catalyst were determined by several methods. Hammett acidities obtained by titrations with various weak bases demonstrated that the catalyst contained a relatively large number of highly acidic sites. Total acidities (Bronsted and Lewis) were determined by thermogravimetric pyridine adsorption-desorption experiments. Infrared studies of the pyridine adsorbed catalyst also gave relative amounts of Bronsted and Lewis acid sites. Elemental analysis showed that very little of the chloride was lost in the preparation of the catalyst. SEM/EDA studies showed that the zinc chloride is evenly distributed over the surface of the silica gel support. X-ray diffraction indicated that recovered catalysts from hydrotreating tests had incorporated part of the sulfur released from the substrates as zinc sulfide (the rest becomes hydrogen sulfide). The zinc sulfide must be microcrystalline since it appeared in SEM/EDA maps to be evenly distributed on the surface of the silica gel support, rather than as crystals.

The optimum loading of zinc chloride on the silica gel support was investigated. Results for hydrotreating tests with loadings of 5%, 16%, and 50% zinc chloride by weight on the silica gel indicated that the 16% and 50% catalysts had essentially the same activity, whereas the activity on the 5% catalyst was substantially less. The 16% composition may represent close exhaustive surface coverage by the zinc chloride. Because of the slow rates for some of the hydrotreating reactions at temperatures less than 400°C, a catalyst to substrate of 0.5 was found to give decent conversions in a reasonable time

period. Carbon tetrachloride has been found to be a better solvent than water for the preparation of the silica gel-supported catalyst.

A catalyst was prepared by supporting zinc chloride on montmorillonite clay. This catalyst was effective in cleaving sulfides and alkylbenzenes; however, condensation reactions to oligomeric products were more extensive with a low-severity liquefaction product from Wyodak subbituminous coal which gave conversion of 53%, 57%, and 62% to distillable liquids. Pumice-supported zinc chloride was a considerably less effective catalyst than the silica gel-supported catalyst.

A pillared clay-supported metal sulfide catalyst was prepared and tested for hydrotreatment of first-stage coal liquefaction products. This catalyst was based on the concept that the pillared clay will allow large micropore volumes for accommodation of the very large coal macromolecules at the active metal sulfide sites in the catalyst. A chromia-pillared was prepared and nickel and molybdenum were dispersed in the interlayer spaces. After sulfiding, the catalyst was tested in hydrotreating reactions with model compounds and low-severity product. This catalyst gave very high conversions in cleavage of alkylbenzenes and sulfides (98-99%) and in hydrogenation of aromatic compounds without condensation to larger molecules or coking. Conversion of the Wyodak low-severity product to distillate was 47%, which was higher than that obtained with commercial catalyst. Removal of sulfur from the distillate was complete, and 75% was removed from the vacuum bottoms.

Total acidity and type of acidity of the pillared clay-supported metal sulfide catalyst were determined and compared with the pillared clay. Infrared spectroscopy and thermogravimetric analysis of the pyridine-adsorbed catalyst showed that these materials contain significant numbers of highly acidic sites, the metal-loaded pillared clay containing fewer sites than the pillared clay. The number of Lewis acid sites are almost twice the Bronsted acid sites.

Hydrotalcites were also investigated as supports for metal sulfide catalysts, and as catalysts themselves. Both the pillared hydrotalcites and molybdenum-loaded pillar hydrotalcites were ineffective in hydrocracking alkylbenzenes. However, both catalysts were highly effective for hydrodesulfurization of aryl sulfides and benzothiophenes. Hydrotalcite and pillared hydrotalcite gave benzene as the major product, whereas the molybdenum-loaded hydrotalcite gave cyclohexane in addition to benzene. Promising results were also obtained for hydrodeoxygenation of aryl ethers to benzene and hydrodenitrification of quinoline to various products.

2.0 GOALS AND OBJECTIVES

The efficient production of environmentally acceptable distillate fuels requires catalysts for hydrogenation and cleavage of the coal macromolecules and removal of oxygen, nitrogen, and sulfur heteroatoms. Currently, two stage processes for coal conversion are under development. The first stage converts coal to a soluble form with minimal cracking and hydrogenation. This process presently involves no catalyst other than the coal mineral matter, but a promoter, hydrogen sulfide, is added, which may have a catalytic effect. The

second stage involves hydrogenation upgrading of the first-stage product to distillates with fixed or ebullated bed catalysts.

The catalysts currently used in the coal liquefaction are the same as those used in conventional petroleum refining; however, this application has not been very successful. Improvements in upgrading efficiency could be obtained if catalysts with longer life and better activity and selectivity were available. Rapid deactivation of the conventional Co-Mo and Ni-Mo catalysts on an alumina support have been attributed to coke formation (1), metals deposition (2), and inhibition of active center by chemisorbed compounds (3). The objectives of this research project are to develop and test novel heterogeneous catalysts for hydrotreatment upgrading of first stage coal liquefaction products. The new hydrogenation catalysts are based on pillared clays and hydrotalcites, which have very large micropore dimensions which can accommodate the coal macromolecules, but do not possess strong acidities which lead to coking at high temperatures. A second objective is to develop a solid acid catalyst for depolymerization of coal macromolecules. The acid catalysis process for coal liquefaction is believed to operate by ionic mechanisms. Some molten acids have successfully depolymerized coal, but the poor efficiencies of catalyst recovery and the corrosive nature of the catalyst make the process uneconomical. Stable solid acid catalysts will be developed which will avoid these difficulties. These catalysts are also based on pillared clays as well as silica bases.

3.0 ACCOMPLISHMENTS

3.1 Introduction

The development of new heterogeneous catalysts for hydrotreating was continued. The synthesis of several new catalysts was accomplished. The new catalysts are basically of three types: hydrotalcites, sulfided metal hydrogenation catalysts, and solid acid ionic hydrogenation catalysts. These are discussed separately below.

3.1.1 Metal Hydrogenation Catalysts on Pillared Smectite Support

Acid smectite clays are used as catalysts in petroleum-cracking and various other reactions. Unfortunately, they dehydrate and collapse at temperatures above 200°C. Acid zeolites are more stable at high temperatures; however, the pores are too narrow to be useful for coal macromolecules, and they are not effective in upgrading as compared with conventional Ni-Mo or Co-Mo catalysts. In the pillared clays, intercalation of hydroxylated or complexed metal cations maintains the clay layer structure after loss of water and generates large pores. These structures are stable to 450° or 500°C. The alumina cluster pillared clays are effective catalysts for petroleum catalysis. Chromia pillared clays with even larger pore spacings have considerable potential for upgrading. A new catalyst has been prepared by dispersing/exchanging active metals (Ni and Mo) into chromia pillared clay, and tested for hydrocracking and hydrodesulfurization. This catalyst gave almost quantitative conversion of diphenylsulfide into benzene, and unwanted side reactions such as coking and oligomer formation were prevented.

3.1.2. Solid Acid-Catalyzed Hydrocracking

Acid-catalyzed coal conversion has been thoroughly investigated; however, the efficiencies of catalyst recovery are not high enough or the catalyst is consumed, resulting in high cost. Another disadvantage is the corrosive nature of the catalyst. A stable solid acid catalyst may have more potential in recovery schemes. Acid zeolites can be used at high temperatures, but have pore sizes too small for the large coal macromolecules. Thermally stable pillared clay catalysts with large interlayer pores are more attractive for acid-catalyzed depolymerization of coal macromolecules. Chromium and aluminum cluster-pillared smectites are being tested both in the Bronsted and Lewis acid form, the latter being formed from reactions with metal chlorides. The liquefaction reactivity of Wyodak coal which has been in-situ pillared with polyoxy chromium ions or metal(s) supported will be compared with other solid acid catalysts, such as Drago aluminum chloride-silica complex and similar zinc chloride complex. Reactions of supported zinc(II) chloride catalysts as a function of amount of zinc chloride loading (5 or 16 wt%), solvent for catalyst preparation (carbontetrachloride or water), supporting material(silica gel or pumice powder), and the catalyst amount (10 or 50 wt%) will be compared with silica gel-zinc chloride catalyst.

3.1.3 Metal Hydrogenation Catalysts on Hydrotalcite Supports

The hydrotalcites are bimetallic hydroxides with cationic layers separated by exchangeable anions which have been applied to the catalysis of polymerization and carbon monoxide reduction. A pair of di- and trivalent metal ions such as magnesium, aluminum or zinc, and chromium are used in generating the cationic layers. The cationic layer is then pillared with a bulky inorganic or organic anion to create a gallery space when water is driven out.

Reichle (4) has provided an account of the anionic hydrotalcite clays. These anionic clays are easily synthesized, and a variety of compositions are readily prepared. Thus the potential to design a clay-like material to hydrotalcite-like compositions has been described (5-7).

The catalytic capabilities of these materials have been investigated to some extent by Reichle and other workers (7-12). To be useful as hydrotreating catalysts, the introduction of a metal sulfide or other transition metal complex catalysts into the interlayer is required. Our interest has been in exploring the possibility of initially placing a molybdenum-containing ion in the space between the hydrotalcite-like layers and examining the catalytic activity related to the hydrogenation of compounds which model those found in liquefaction products of coal.

3.2 Experimental

3.2.1 Catalyst Preparation

3.2.1.1 Preparation of Zinc Chloride supported catalysts

Silica gel-zinc chloride catalysts were prepared by loading 5 and 16 wt.% of anhydrous zinc chloride on silica gel in carbon tetrachloride using same

procedure as described for the preparation of silica gel-zinc chloride in our previous quarterly report (13). Pumice powder was also loaded with 16 wt.% of zinc chloride in carbon tetrachloride using the same general procedure.

In a separate experiment 5.0 g silica gel was added to a solution of 1.0 g of zinc chloride in 50 ml water, and stirred overnight. The solvent was removed by evaporation, and residue dried at 200°C.

3.2.1.2 Preparation of metal supported hydrotalcites

Hydrotalcites and molybdenum exchanged hydrotalcites were prepared as described earlier (14). Instead of ammonium molybdate, ammonium tetrathiomolybdate was exchanged into hydrotalcite.

3.2.2 Elemental Analysis

Total sulfur determination was done with a LECO model 532 sulfur analyzer using the ASTM D1551 method. The method of Vogel (15) was used for chlorine analysis. Carbon, hydrogen, and nitrogen analyses were performed on a Control Equipment Corporation Model 240XA Elemental Analyzer.

Proton and ^{13}C NMR spectra were obtained in dichloromethane-d_2 with TMS standard on a Varian XL200 NMR spectrometer. Infrared spectra were obtained in KBr on either a Perkin Elmer Model 283 spectrometer or a Nicolet 20SXB FTIR spectrometer equipped with a mercury cadmium telluride (MCTA) detector, and a Nicolet 1280 computer with a fast Fourier transform coprocessor.

Quantitative GC/FID analyses were performed with a Hewlett Packard 5880A gas chromatograph equipped with a J&W 60 m x 0.25 mm (i.d.), 1.0 micron DB-1701 capillary column. n-Octadecane was the internal standard. Isotope dilution GC/MS was performed on a Finnigan 800 ITD ion trap detector with an HP 5890A gas chromatograph and a J&W 30 m x 0.32 mm (i.d.), 1.0 micron film of DB-5. Phenol, naphthalene, and tetralin were determined with per-deutrated analogs as the respective internal standards. A 15 m x 0.25 mm (i.d.), 0.25 micron DB-5 film capillary column was used for the analysis of high boiling point components.

3.2.3 Characterization of Solid Acid Catalysts

3.2.3.1 Acidity Measurements

The acidities of the solid acid catalysts, chromia pillared clay and chromia pillared clay supported Ni-Mo were determined by the pyridine adsorption and desorption method using FTIR and the Thermogravimetric (TGA) method.

3.2.3.2 Infrared Method

A small amount of sample (100 mg) was placed in a glass chamber attached to a vacuum pump, gas inlet, and a gas outlet. The chamber was evacuated, and argon saturated with pyridine was introduced into the chamber until the weight increase ceased. At this stage the chamber was evacuated until the physisorbed pyridine was removed, as indicated by the constant weight of the base absorbed sample. The infrared spectra of the pyridine-absorbed catalyst was obtained on the

Nicolet FTIR spectrometer with the diffuse reflectance cell. Infrared spectral data are presented in Tables 3 and 4.

3.2.3.3 Thermogravimetric method

Total acidity of the catalyst was determined from chemisorption of pyridine on the catalyst surface using a thermogravimetric analysis (TGA) technique.

Approximately 20 mg of catalyst were placed on the sample pan of the DuPont 951 thermogravimetric balance module, which was interfaced with a DuPont 1090 Thermoanalyzer (controller and data station). The sample was purged with argon at ambient temperature until constant weight was achieved (several minutes). The argon flow was then stopped and the sample chamber was evacuated. The vacuum pump continued to hold the partial vacuum until constant weight was once again achieved. The pump was turned off and a flow of pyridine-saturated argon at ambient temperature was introduced into the sample chamber. The pyridine-argon flow continued for 180 minutes, at which time the weight gained by the sample had nearly ceased. The chamber was again evacuated, still at ambient temperature, and held under partial vacuum for 40 minutes. When constant weight was achieved, the temperature was increased at a rate of 20°C/min to 105°C, where it was held for 30 minutes. The temperature was then increased at a rate of 2°C/min to 202°C and held there for 30 minutes, followed by a temperature increase at a rate of 20°C/min to 300°C, where it was held for 60 minutes. The experiment was terminated when constant temperature was achieved.

The 1090 Thermoanalyzer records time, temperature and weight during the experiment. On reducing the data, dw/dt is calculated and the data are reported on a plot of wt% and dw/dt vs time, wt% and dw/dt vs temperature or in tabular form.

3.3 Results and Discussion

3.3.1 Zinc chloride-Supported catalysts

3.3.1.1 Characterization of Catalysts

Mixtures of silica gel and pumice powder with zinc chloride were characterized by elemental analysis, infrared spectroscopy, and thermogravimetric methods.

3.3.1.1.1 Elemental analysis

Elemental analyses of the zinc(II) chloride mixtures with silica gel and pumice powder, both obtained from the reaction in carbon tetrachloride, indicated that no loss of chloride occurred during the heating procedure. Thus, most of the zinc is present as $ZnCl_2$, part of which is complexed with silica hydroxyls.

3.3.1.2 Testing of Supported Zinc Chloride Catalysts

3.3.1.2.1 Catalytic Hydrotreating of Bibenzyl

Bibenzyl was used as a test compound to investigate catalytic activity of supported zinc chloride catalysts. The reactions were carried out by heating bibenzyl and the catalyst in the presence of 1000 psig of molecular hydrogen (if needed) at 350°C for 3 hours. The effects of zinc chloride loading, support material, solvent used for catalyst preparation, and the ratio of catalyst to substrate on the catalytic activity of zinc chloride supported catalysts were investigated. The roles of hydrogen, hydrogen transfer, and hydrogen donor solvent in the hydrotreating were also investigated. Relevant physical and analytical data are given in Table 1.

In a typical run, 1.0 g of bibenzyl, and 0.5 g of desired catalyst, and hydrogen donor solvent (if needed) were placed in a tubing bomb (12 ml microreactor). The microreactor was evacuated, pressurized with 1000 psig of hydrogen or deuterium (if needed), and placed in a rocking autoclave heated to 350°C. At the end of the reaction period, the microreactor was cooled to room temperature, degassed and opened. The desired amount of the internal standard was added to the product slurry, the product slurry was transferred into a centrifugation tube by washing with methylene chloride, and the solid catalyst was removed by centrifugation. The liquid sample was analyzed by GC/FID and GC/FTIR/MS.

The chlorine analysis of the recovered catalyst did not indicate any loss of chlorine during reaction. Detailed characterization of the recovered catalyst to determine the possible loss of catalytic activity is in progress.

TABLE 1

CATALYTIC HYDROCRACKING OF BIBENZYL
(REACTION TEMP. = 350°C, REACTION TIME = 3 HRS)

Catalyst (g)	Substrate (mmol)	Reductant	Conversion (%)	Major Products
SG (0.25)	5.49	1000 units	2	Benzene (tr.) Ethylbenzene (tr.) Toluene (tr.)
ZC-melt (0.25)	5.62	1000 units	13	Benzene (0.08) Ethylbenzene (0.04)

TABLE 1 (CONTINUED)

CATALYTIC HYDROCRACKING OF BIBENZYL
(REACTION TEMP. = 350°C, REACTION TIME = 3 HRS)

Catalyst (g)	Substrate (mmol)	Reductant	Conversion (%)	Major Products
				Toluene (0.02)
SZC (0%)	5.49	1000 units	80	Benzene (3.54) Toluene (0.15) Ethylbenzene (1.35) Cond. Prod. (18%) Coke 0%
SZC (0.1)	5.50	1000 units	18.5	Benzene (0.35) Ethylbenzene (0.24)
SZC-5 (0.5)	5.52	1000 units	39.9	Benzene (1.0) Toluene (0.1) Ethylbenzene (0.4)
SZC-16 (0.5)	5.63	1000 units	74.6	Benzene (3.12) Toluene (0.2) Ethylbenzene (0.9)
SZC-16A (0.5)	5.51	1000 units	64	Benzene (2.2) Toluene (0.2) Ethylbenzene (0.5)
PZC-16 (0.5)	5.62	1000 units	3	Benzene (0.03) Toluene (0.05) Ethylbenzene (0.04)
SZC (0.5)	5.49	None	83	Benzene (3.2) Toluene (0.2) Ethylbenzene (0.8) Cond. Prod. = 27% Coke =7%
SZC (0.5)	5.53	Deuterium (1000 units)	64	Benzene (2.6) Toluene (0.1) Ethylbenzene (1.1 Cond. Prod. = 24% Coke = 0%

TABLE 1 (CONTINUED)

CATALYTIC HYDROCRACKING OF BIBENZYL
(REACTION TEMP. = 350°C, REACTION TIME = 3 HRS)

Catalyst (g)	Substrate (mmol)	Reductant	Conversion (%)	Major Products
SZC (0.5)	5.52	Isopentane (0.2 units)	76	Benzene (2.73) Toluene (0.2) Ethylbenzene (0.75) Cond. Prod. = 29% Coke = 6%

SG = Silica gel
ZC-melt = Molten zinc chloride
SZC = Silica gel-zinc chloride (50% zinc chloride)
SZC-5 = Silica gel-zinc chloride (5% zinc chloride)
SZC-16 = Silica gel-zinc chloride (16% zinc chloride)
SZC-16A = Silica gel-zinc chloride (16% zinc chloride, water solvent
PZC-16 = Pumice powder-zinc chloride (16% zinc chloride)
tr = trace

The reaction of bibenzyl with unsupported silica gel in hydrogen gave very small conversion of bibenzyl into products, mainly benzene, toluene, and ethylbenzene. Similarly with molten zinc chloride, the conversion was only 13%, and benzene and ethylbenzene were major products. A small amount of toluene was also formed. However, when the same reaction was carried out with silica gel-zinc chloride (50% zinc chloride) catalyst, 85% of bibenzyl was converted into the products benzene and ethylbenzene, with a small amount of toluene. The ratio of benzene to ethylbenzene was 3. In addition, 18% of the starting product was converted into oligomers. No coke formation occurred under these conditions. When the ratio of silica gel-zinc chloride / bibenzyl was reduced to 0.1 the percent conversion dropped from 85 to 18.5. The product distribution was the same as in the previous reaction. These reactions indicate that the combination of zinc chloride with silica gel generates the highly acidic sites needed for hydrocracking reactions. A considerable amount of the catalyst is necessary to get a reasonable amount of reaction to occur under the conditions used.

The effect of percentage of zinc chloride on the catalytic activity of silica gel-zinc chloride was investigated by comparing the results using zinc chloride loadings of 50%, 16%, and 5%. The reaction with 5% zinc chloridion silica gel (SZC-5) gave only 39.9% conversion of bibenzyl into products. However, the conversion of bibenzyl with SZC-16 was comparable with that obtained from SZC. The product distributions from the reactions of SZC-5 and SZC-16 were same as that obtained from the reaction of bibenzyl with SZC. These results

that direct deuterium addition to the 2-phenylethyl carbonium ion was not a major pathway.

In another reaction, molecular hydrogen was replaced with isopentane as a hydrogen donor solvent. Isopentane is a good hydride donor in reactions in superacid media. This reaction resulted in almost the same conversion and product distribution as in the reaction without hydrogen. As before, a significant fraction of the substrate was converted into coke and condensation products. A quantitative amount of isopentane was recovered at the end of the reaction. These results show that isopentane does not directly transfer hydride to the fragments formed from the cracking of bibenzyl with the solid acid catalyst. It also does not reduce the condensation products or indirectly transfer hydrogen to the products.

3.3.1.2.2 Catalytic Hydrotreating of 1-Methylnaphthalene

In continuation with our studies of the relative kinetics of the hydrotreating reactions of polynuclear aromatics with solid acid catalysts (Silica gel-zinc chloride), the effects of hydrogen and hydrogen donor solvent on the hydrotreating of methylnaphthalene were examined during this quarter. The

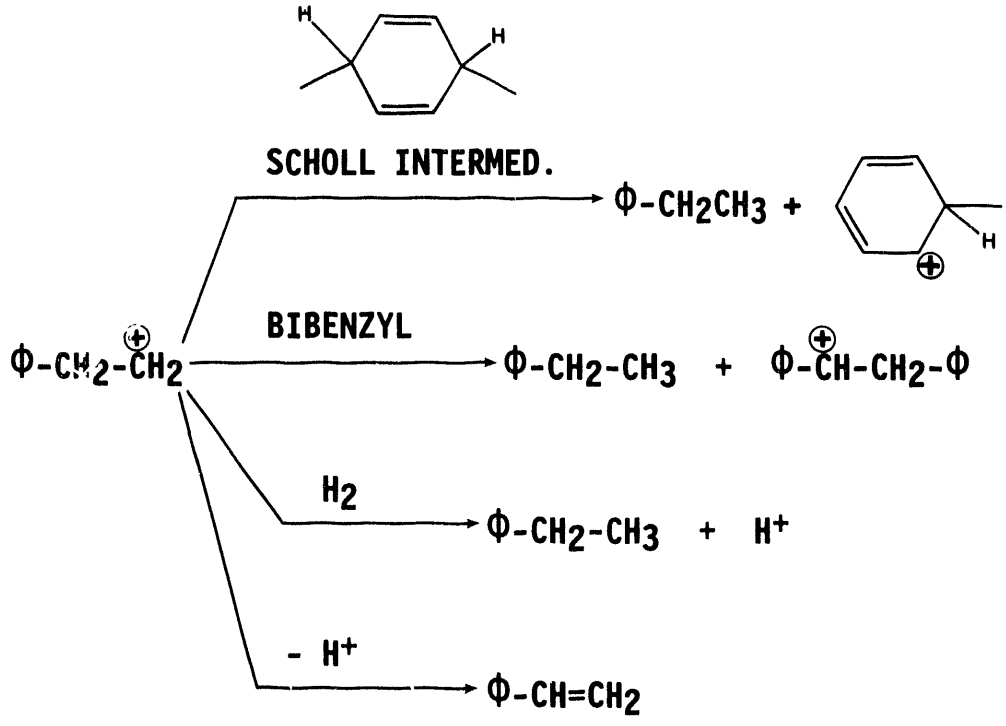

Figure 1. Reactions of phenylethylcarbonium ion.